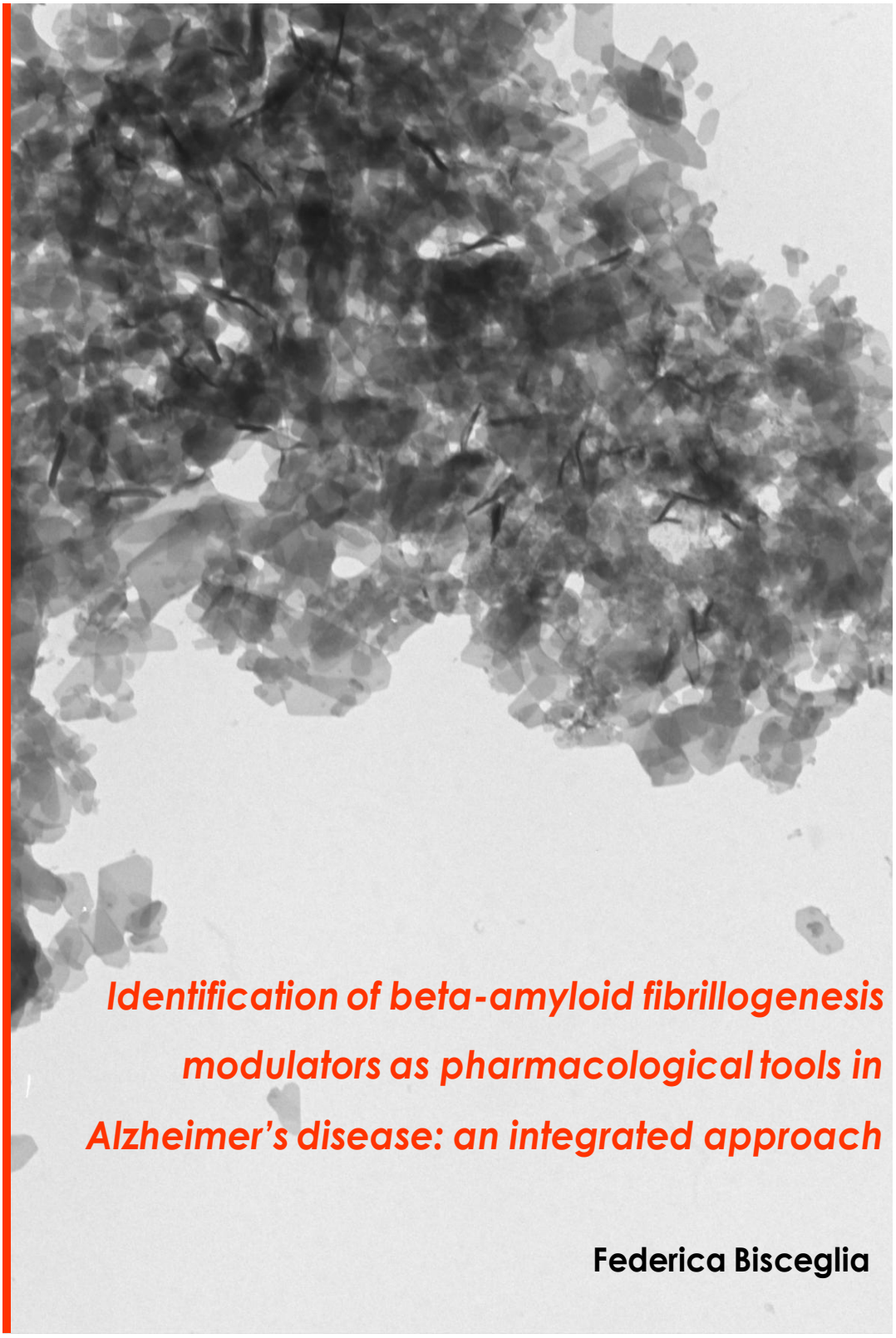

Identification of beta-amyloid fibrillogenesis modulators as pharmacological tools in Alzheimer's disease: an integrated approach

Federica Bisceglia

UNIVERSITÀ DEGLI STUDI DI PAVIA

DOTTORATO IN SCIENZE CHIMICHE E FARMACEUTICHE

XXX CICLO

Coordinatore: Chiar.mo Prof. Mauro Freccero

IDENTIFICATION OF BETA-AMYLOID FIBRILLOGENESIS MODULATORS AS PHARMACOLOGICAL TOOLS IN ALZHEIMER'S DISEASE: AN INTEGRATED APPROACH

Tutore

Chiar.ma Prof.ssa Ersilia De Lorenzi

Tesi di Dottorato di

FEDERICA BISCEGLIA

2014-2017

Identification of beta-amyloid fibrillogenesis modulators as pharmacological tools in Alzheimer's disease: an integrated approach

Federica Bisceglia

Table of contents

Abbreviation list

aa	Amino acid
ACh	Acetylcholine
AChE	Acetylcholinesterase
ACN	Acetonitrile
AD	Alzheimer's disease
ADME	Adsorption, distribution, metabolism, excretion
AFM	Atomic force microscopy
AIMOP	Antimicrobial immunomodulatory peptides
AMP	Antimicrobial peptides
ANS	Autonomic nervous system
ApoE	Apolipoprotein E
APP	Amyloid precursor protein
Aß	Amyloid beta
Aß*56	56 kDa soluble Aß assemblies
ATR	Attenuated total reflection
BACE-1	ß-site amyloid precursor protein cleaving enzyme 1
BBB	Blood-brain barrier
BGE	Background electrolyte
CCD	Charge-coupled device
CD	Circular dichroism
CE	Capillary electrophoresis
CJD	Creutzfeldt-Jakob disease
CNS	Central nervous system
CRDB	Curcumin resource database
DLS	Dynamic light scattering
DMSO	Dimethyl sulphoxide
ELISA	Enzyme-linked immunosorbent assay
EM	Electron microscopy
EOF	Electroosmotic flow
ESI-IT	Electrospray ionization-ion trap
FBS	Foetal bovine serum
FCS	Fluorescence correlation spectroscopy
FPRL1	Formyl-like peptide receptor
FTIR	Fourier transform infrared spectroscopy
GPCR	G-protein coupled receptor
GSK-3ß	Glycogen synthase kinase 3ß
GSS	Gerstmann-Straüssler-Scheinker
HDL	High density lipoprotein
HDX	Hydrogen-deuterium exchange
HFIP	1,1,1,3,3,3, hexafluoro-2-propanol
HMW	High molecular weight

HTS	High throughput screening
IL-6 and IL-1ß	Interleukins 6 and 1ß
IM-MS	Ion mobility mass spectrometry
INF-γ	Interferon γ
LDL	Low density lipoprotein
LMW	Low molecular weight
LPS	Lipopolysaccharide
MALDI	Matrix-assisted laser desorption/ionization
MALS	Multi angle light scattering
MD	Molecular dynamics
MRI	Magnetic resonance imaging
MS	Mass spectrometry
MW	Molecular weight
NF-κß	Nuclear factor κß
NGM	Nematode growth medium
NPs	Natural products
PET	Positron emission tomography
Phe	Phenylalanine
PICUP	Photo-induced cross-linking of unmodified proteins
PNS	Peripheral nervous system
PS-1 and PS-2	Presenilin 1 and presenilin 2
Q-TOF	Quadrupole time of flight
ROS	Reactive oxygen species
SAR	Structure-activity relationship
SDS-PAGE	Sodium dodecyl sulphate-polyacrylamide gel electrophoresis
SEC	Size exclusion chromatography
SEM	Scanning electron microscopy
SPR	Surface plasmon resonance
SPRi	Surface plasmon resonance imaging
ssNMR	Solid state nuclear magnetic resonance
TEM	Transmission electron microscopy
ThT	Thioflavin T
TNF-α	Tumor necrosis factor α
TOF	Time of flight
UF	Ultrafiltration
WB	Western Blot

Amyloidosis

Proteins are complex biopolymers of amino acids characterized by an array of functions in living systems.
The primary amino acid sequence is encoded by relative genes and drives processes that ultimately lead to the unique protein's three dimensional structure, essential for its biological activities.
The establishment of thousands of intra and intermolecular interactions between the side chains of amino acids triggers the reorganization of the linear polypeptide chain. The folding process is very fast and proceeds through the formation of unfolded and partially folded states before reaching the structure with the free energy minimum [1].
Because only proteins in their native conformation are soluble and functional, cells have developed mechanisms to protect themselves from modifications of the three-dimensional structure. Generally, the folding process is assisted by molecular chaperones that isolate the polypeptide chain by avoiding any contact with the forming protein and the solvent or other biomolecules that could interfere with the folding. The unfolded protein response system recognizes and destroys proteins with a structure which is different from the native one [2]. In addition to these cell-autonomous controls, the loss of folding should be intrinsically avoided by the primary sequence resulting from a selection by evolution, to promote folding into a compact stable structure.
Nevertheless, misfolded or partially folded proteins can elude these defensive systems and cause aberrant events that in some cases ultimately lead to pathological conditions known as ***protein misfolding diseases or amyloidoses***.

Approximately 50 human diseases including Alzheimer's and Parkison's disease have been classified as amyloidoses, since the common hallmark is the presence in tissues of insoluble amyloid fibrils due to aggregation and deposition of misfolded proteins [1,2].

To date, 37 peptides or proteins have been found to form amyloid deposits in human pathologies (**Table 1**). There are no evident similarities among amyloidogenic proteins in terms of sequence, structure or function: most of them are small, whereas 5 have more than 400 residues; some reach the native folding, some are intrinsically disordered and some others contain globular and disordered portions [3].

	Precursor protein	Systemic and/ or localized	Acquired or hereditary	Target organs
AL	Immunoglobulin light chain	S, L	A, H	All organs, usually except CNS
AH	Immunoglobulin heavy chain	S, L	A	All organs except CNS
AA	(Apo) Serum amyloid A	S	A	All organs except CNS
ATTR	Transthyretin, wild type	S	A	Heart mainly in males, ligaments, tenosynovium
	Transthyretin, variants	S	H	PNS, ANS, heart, eye, leptomeninges
Aß2M	ß2-Microglobulin, wild type	S	A	Musculoskeletal system
	ß2-Microglobulin, variants	S	H	ASN
AApoAI	Apolipoprotein A I, variants	S	H	Heart, liver, kidney, PNS, testis,larynx (C-terminal variants), skin (C-terminal variants)
AApoAII	Apolipoprotein A II, variants	S	H	Kidney
AApoAIV	Apolipoprotein A IV, wild type	S	A	Kidney medulla and systemic
AApoCII	Apolipoprotein C II, variants	S	H	Kidney
AApoCIII	Apolipoprotein C III, variants	S	H	Kidney
AGel	Gelsolin, variants	S	H	PNS, cornea
Alys	Lysozyme, variants	S	H	Kidney
ALECT2	Leukocyte chemotactic factor-2	S	A	Kidney, primarily
ACys	Cystatin C, variants	S	H	PNS, skin
ABri	ABriPP, variants	S	H	CNS
AFib	Fibrinogen α, variants	S	H	Kidney, primarily
ADan*	ADanPP, variants	L	H	CNS
Aß	Aß protein precursor, wild type	L	A	CNS
	Aß protein precursor, variant	L	H	CNS
AαSyn	α-Synuclein	L	A	CNS
ATau	Tau	L	A	CNS
APrP	Prion protein, wild type	L	A	CJD, fatal insomnia
	Prion protein variants	L	H	CJD, GSS syndrome, fatal insomnia
	Prion protein variant	S	H	PNS
ACal	(Pro)calcitonin	L	A	C-cell thyroid tumors
AIAPP	Islet amyloid polypeptide**	L	A	insulinomas
AANF	Atrial natriuretic factor	L	A	Cardiac atria
APro	Prolactin	L	A	Pituitary prolactinomas, aging pituitary
AIns	Insulin	L	A	Iatrogenic, local injection
ASPC***	Lung surfactant protein	L	A	Lung
AGal7	Galectin 7	L	A	Skin
ACor	Corneodesmosin	L	A	Cornified epithelia, hair follicles
AMed	Lactadherin	L	A	Senile aortic, media
AKer	Kerato-epithelin	L	A	Cornea, hereditary
ALac	Lactoferrin	L	A	Cornea
AOAAP	Odontogenic ameloblast-associated protein	L	A	Odontogenic tumors
ASem1	Semenogelin 1	L	A	Vesicula seminalis
AEnf	Enfurvitide	L	A	Iatrogenic

Table 1. Amyloid fibril proteins and their precursors in humans (*ADan is the product of the same gene as ABri, **also called amylin, ***not proven by amino acid sequence analysis) [3].

Since the pathogenesis of amyloid deposits remains unknown, several mechanisms of toxicity have been proposed [4]:

- amyloid fibrils destroy the architecture and compromise tissue functions by accumulation in the extracellular space of organs;
- prefibrillar species could be toxic and damage cellular membranes;
- proteins, essential for the cellular homeostasis, could be trapped into amyloid deposits which could also incorporate redox metals with subsequent production of toxic reactive oxygen species (ROS).

Despite the great variability of the proteins of origin, resulting amyloid fibrils possess a common structure and share some biophysical properties.
The utilization of different microscopic techniques, such as transmission electron, atomic force and cryo-electron microscopy (TEM, AFM, Cryo-EM), X-ray crystallography, hydrogen/deuterium exchange (HDX), solid state nuclear magnetic resonance (ssNMR), circular dichroism (CD) and Fourier transform infrared spectroscopy (FTIR), discloses the structure and physicochemical properties of fibrils [1-3].
Mature fibrils are unbranched linear structures with a diameter of 7-13 nm and a length in the range of 0,1-10 μm. In the cross-ß architecture, ß-strands are perpendicular to fibril axis and form continuous hydrogen bonded ß-sheets that run along the length of the fibril.
This conserved unique structure allows the regular intercalation of dyes, such as Thioflavin–T (ThT) and Congo red, which confer to fibrils the typical apple-green birefringence under polarized light microscopy [1,2,5-7] (**Figure 1**).

a)

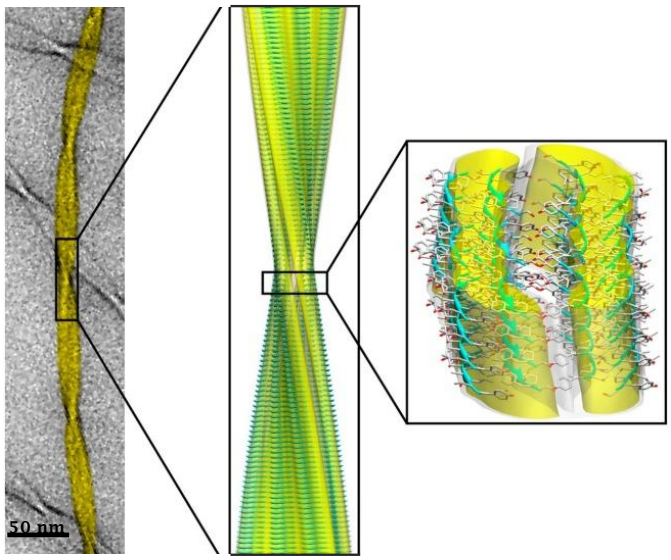

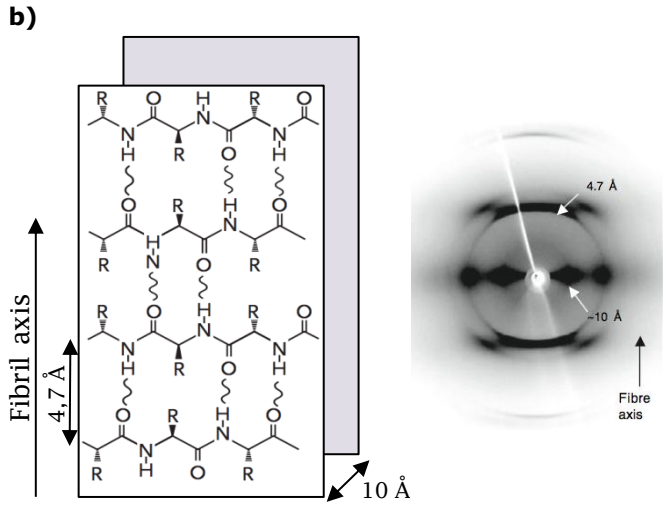

Figure 1. Structure of amyloid fibrils: **a)** cryo-EM imaging, atomic level structure obtained by ssNMR and a more detailed view of the hierarchical organization of pairs of ß-sheets in pairs of cross-ß protofilaments, which in turn form mature fibrils [6]. **b)** cross-ß sheet structure characterized by a typical X-ray diffraction pattern with interstrand and intersheet distances of 4,7 and 10 Å [1,7].

Data obtained by these techniques have shed light on the common mechanism of fibril formation (**Figure 2**).

The nucleation-elongation process is divided into three phases in which different microscopic mechanisms occur [2,5]. During the lag phase, unfolded or partially folded monomers generate nuclei or seeds which are considered to be the smallest species able to trigger fibril growth. Since they are assembled via a thermodynamically unfavourable process, their formation is the rate-limiting step of the entire fibrillation process. In fact, if preformed seeds are added, the lag phase is totally or mostly abolished (**Figure 2 a)**).

Once formed, nuclei and monomers rapidly assemble with each other by leading to fibrils in a thermodynamic favourable growth phase. When monomers are mostly incorporated into fibrils, the growth rate decelerates and a plateau or stationary phase represents the end-point of the reaction, as shown in **Figure 2 b)**.

However, it is increasingly accepted that the complex growth of amyloid fibrils results from the contribution of several mechanisms (**Figure 2 b)**). Initially, both primary and secondary nucleation pathways can lead to nuclei. These two complementary mechanisms form new aggregates at a rate which is dependent on the concentration of monomers present in solution (primary process) or on the presence of pre-existing fibrils (secondary nucleation). If in the secondary process the rate depends only on fibrils already formed, the process is defined as monomer-independent or fragmentation; on the other hand, in the

monomer-dependent process the surface of pre-existing fibrils acts as a catalytic point for the addition of further monomers and both concentration of monomers and fibrils affect the rate of nucleation [2,5,6,8,9].

a)

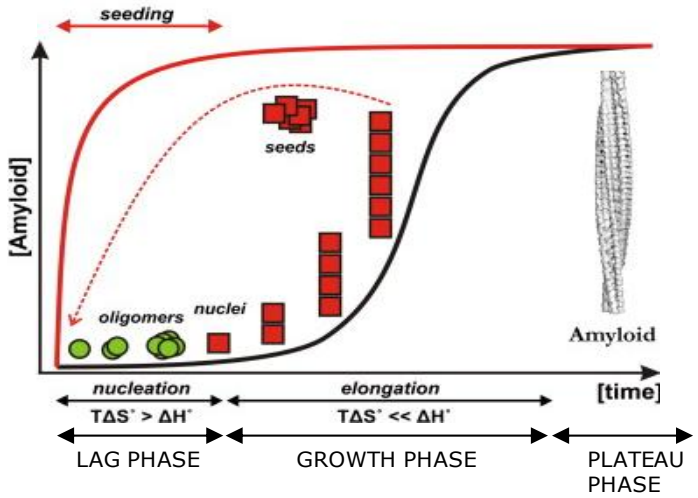

b)

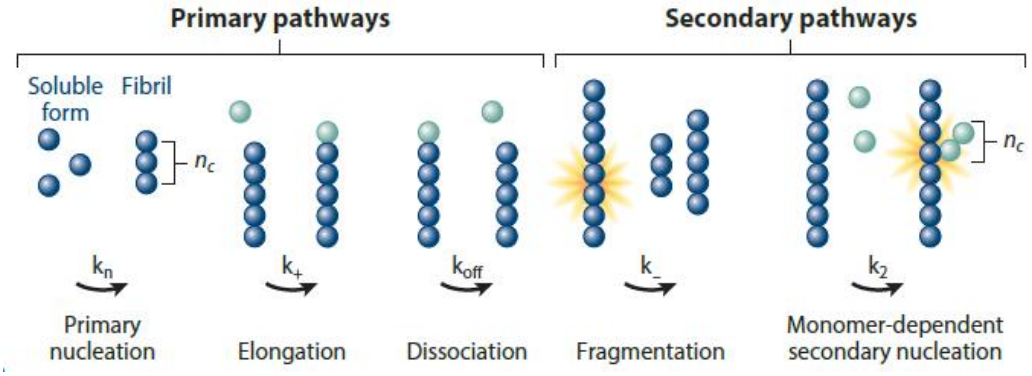

Figure 2. Formation of amyloid fibrils. **a)** Kinetics of amyloidogenesis (black line) and effect of the addition of preformed seeds (red line) [9]. **b)** primary and secondary nucleation processes [2].

Amyloidoses are also defined conformational diseases, since amyloidogenic proteins can not adopt or maintain their native functional folding by assuming a partially disordered state.

Among different amyloidoses, folding loss can be due to several causes [1]:

- an intrinsic propensity of the protein to assume the pathological conformation (e.g. wild-type transthyretin);
- a persistent high concentration in biological fluids (e.g. wild-type $ß_2$-microglobulin);

- mutations in the protein sequence can affect the aggregation tendency of the mutated protein in respect to the wild-type (e.g. immunoglobulin light chains);
- the proteolitic cleavage of a non amyloidogenic precursor protein can release amyloidogenic degradation products (e.g. amyloid ß peptides involved in Alzheimer's disease).

According to the "folding energy landscape theory" (**Figure 3**), high values of free energy (ΔG°) suggest high instability of unstructured monomers. To reach the most stable conformation, a polypeptide chain can assume a large number of possible conformations (>10^{30} for a 100-aa protein) with progressively lower free energies up to adopt the native folding.

However, the free-energy landscape is not linear and therefore a protein could remain in a partially folded state because of the difficulty in overcoming an energy barrier toward the thermodynamically favourable native state.

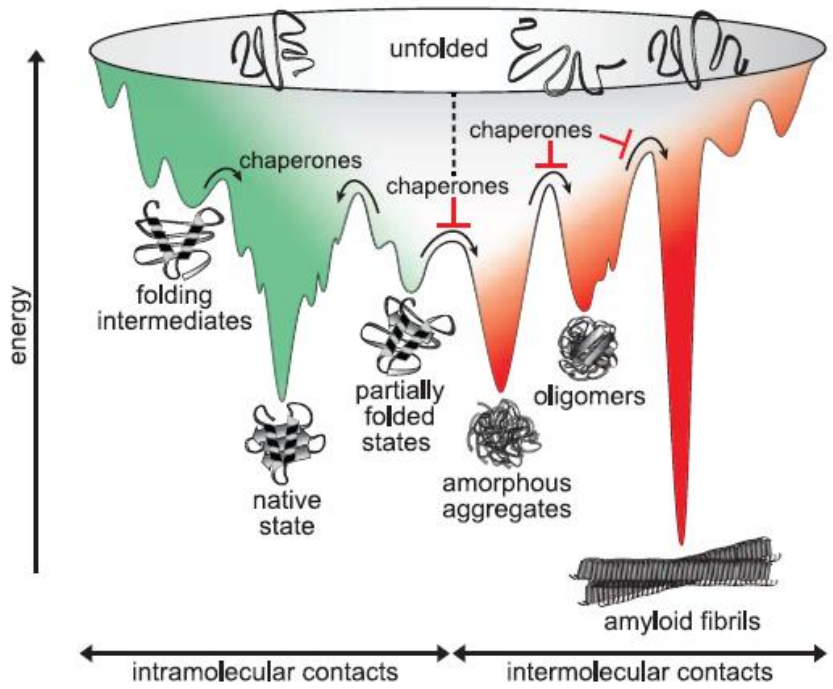

Figure 3. Protein folding and aggregation: two processes in competition [10].

This means that the folding is a inherently error-prone process. Since misfolding and aggregation are collateral effects of the folding process, folding errors, namely destabilized native proteins, are the driving force in protein aggregation.
In fact the exposure of segments, normally buried into the core of proteins, permits the establishment of hydrogen bonds between protein backbones as

well as of weak interactions among side chains of amino acidic residues of the same chain and/or of different polypeptides. As shown in **Figure 3**, the interaction among unfolded monomers progressively first leads to small oligomeric species, then to larger aggregates (protofilaments) which in turn associate into mature insoluble fibrils [5,10].

Recently, the role of charged residues [1] and of distal protein regions (N and C-termini) [11] in modulating the aggregation tendency, has emerged.

However, primary and secondary structures of proteins are important but not sufficient alone to trigger aggregation. Chemical modifications, proteolytic cleavage and physical effects of the cellular environment are some of the numerous events which could contribute and be essential in the adoption of an aggregation-prone conformation that ultimately leads to pathological conditions [11].

Alzheimer's disease

Dementia is the fifth-biggest cause of death in developed countries and it represents the most expensive disease to manage, since patients' care is costly and constant for years.
Alzheimer's disease (AD) is the most common form of dementia accounting for 50-70% of cases. To date, this devastating malady has been diagnosed in about 30 million people worldwide. However, the numbers are going to increase; in fact, by 2050 more than 130 million could be diagnosed AD [12].
People over 65 years of age are more affected by the disease and after this age the incidence doubles ever 5 years, because increasing age is one of the principal risk factors for AD [13].
Impairment in recent memory is the initial symptom of AD. With the progression of the disease, neurons die and the brain starts to shrink by causing other symptoms such as: more serious deficits in memory, disorientation, behavioural changes, difficulties in swallowing, speaking and moving. Patients progressively lose their independence and this has a great social impact.
Therefore, it is imperative to hinder the unabated progression of Alzheimer's disease, although for over a century no disease-modifying treatments have been available.

In the early 1900s, Alois Alzheimer had encountered a patient with a clinical picture characterized by memory loss and changes in personality.
Fascinated by these peculiar symptoms, Alzheimer followed over time the patient by systematically interviewing her and recorded her answers in detailed protocols. At her death, together with Franz Nissl, Gaetano Perusini and Francesco Bonfiglio, Alzheimer meticulously examined the histological sections of the patient's brain.
They observed and described what today are known as the two hallmarks of Alzheimer's disease: neurofibrillary tangles and amyloid plaques [14] (**Figure 4**).

a)

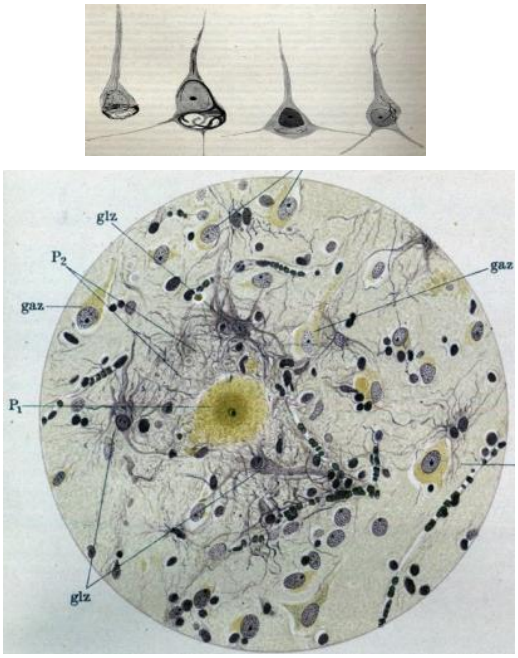

b)

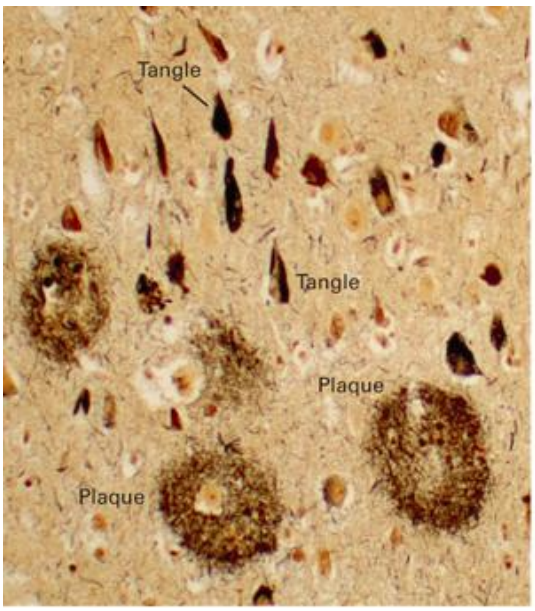

Figure 4. **a)** original illustrations of Alois Alzheimer of the brain patient section: neurofibrillary tangles (top part), plaques indicated in the drawing with "P1 and P2", nerve cells indicated with "gaz" and glial cells "glz" (bottom part) [14]. **b)** senile plaques and neurofibrillary tangles in AD brain revealed by Bielschowsky silver stain [15].

These two typical lesions are due to the aggregation and deposition of two amyloidogenic proteins: tau protein and amyloid-ß peptides (**Table 1**). Indeed, Alzheimer's disease belongs to the category of neurodegenerative amyloidosis [1-3].
In normal conditions, tau protein drives the formation of neuronal microtubules by binding tubulin. In pathological conditions, tau hyperphosphorilation disrupts its molecular interactions with tubulin and this increases its aggregation propensity [11].
Amyloid plaques are spherical structures of about 0,1 mm which are interspersed among atrophic neurons. These plaques are primarily constituted of insoluble amyloid fibrils resulting from aggregation of amyloid-ß (Aß) peptides [12,15].

Despite impressive efforts, the aetiology and pathogenesis of AD are still unclear and undefined. Indeed, the neurodegeneration can be induced by several factors and through different molecular pathways still opened to debate. This represents a huge obstacle in the elucidation of the basis of the disease and consequently in the finding of effective treatments [16,17].

It is also known that AD arises from the contribution of genetic, epigenetic and environmental factors, as well as from complex interactions of molecular systems.

Genetic factors: about 2% of all patients have autosomal dominant familial forms of AD caused by mutations in genes involved in the production of Aß peptides that determine the early-onset of the disease. More than 200 mutations have been identified in genes encoding for APP and for presenilins (PS-1 and PS-2). Amyloid precursor protein (APP) is a membrane glycoprotein expressed in all tissues; its metabolism is performed by two enzymes (γ and ß-secretases) which release Aß peptides. PS-1 and PS-2 are catalytic subunits of γ-secretase with aspartyl-protease activity [13,17,18].

The rest of 98% of AD are classified as sporadic AD with late-onset.

APOE is the only gene with susceptibility in sporadic forms of AD. It was discovered in 1993 and it is associated with high concentrations of LDL cholesterol. In particular *APOEε4* allel is a risk factor for AD, since more than 50% of AD patients are homozygous carriers. It has been demonstrated that APOE increases the activity of glycogen synthase 3ß (GSK-3ß), a kinase responsible for tau hyperphosphorilation. Conversely, *APOEε2* is a protective factor that reduces the risk of AD.
Nevertheless, the inheritance of *APOEε4* increases the risk of the onset of AD, but it is not sufficient to develop the disorder. This is consistent with a semi-dominant inheritance of a moderately penetrant gene [12].

Epigenetic modifications in neurons could also be starting points for neurodegeneration, such as DNA methylation and histone acetylation.

Moreover, hypertension, high blood cholesterol concentrations, repeated head traumas, obesity, diabetes, homocysteinemia, smoking and diet are some important environmental factors that increase the risk of AD in the population [13].

Molecular pathways

Other events have been also identified as important molecular actors in the onset of AD: apart from the aggregated forms of Aß peptides and tau protein, also mitochondria dysfunction, neuroinflammation, oxidative stress and neurovascular damage are involved in neurodegeneration. As shown in **Figure 5**, these phenomena are strictly interconnected and can directly or indirectly induce neuronal damage and death in differentiated neurons [12,19,20]. Notably, the aggregation of Aß and its toxicity are enhanced by the interaction of Aß with acetylcholinesterase (AChE), also because the complex Aß-AChE with metal ions (like Fe^{2+} or Cu^{2+}) leads to the production of reactive oxygen species (ROS) [21]. In turn, ROS could damage the cellular membrane, which results in an uncontrolled flux of ions, membrane depolarization and eventually apoptosis.

a)

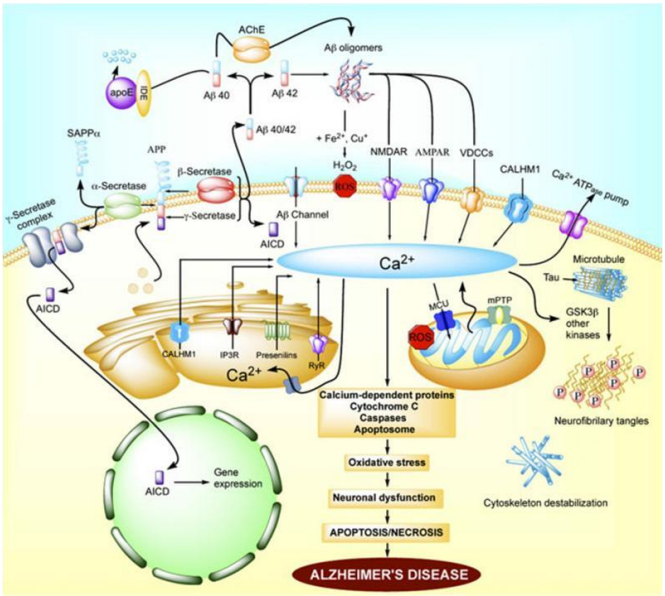

b)

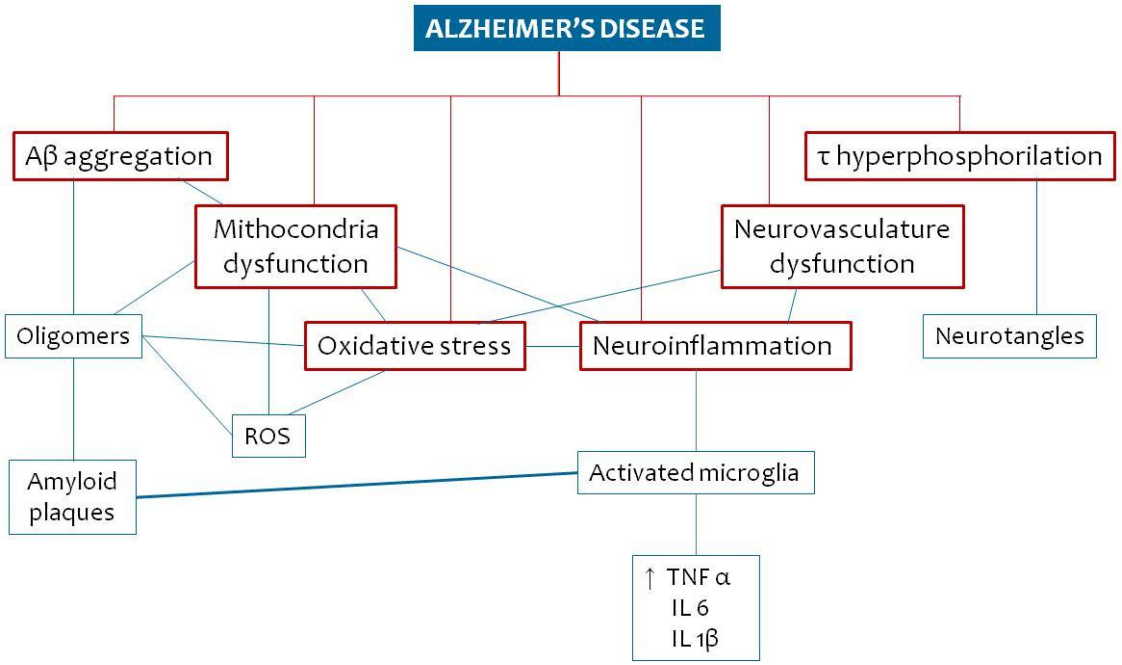

Figure 5. Interconnected molecular pathways involved in AD [16].

The membrane depolarization induced by ROS, by some products of lipid peroxidation and by Aß aggregates can affect the function of those receptors and voltage-dependent channels that are important for the regulation of intracellular Ca^{2+} concentrations. Alterations in Ca^{2+} homeostasis have crucial multiple effects: i) on the mentioned binding equilibrium between tau protein and tubulin, as cells can lose their structural stability and apoptotic pathways are activated; ii) on the activity of kinases involved in this equilibrium such as GSK-3ß; iii) on the production of ROS [22].
Further, mitochondria dysfunction can lead to the release of Ca^{2+} and to the overproduction of ROS [23].
All steps of this complex network intensify neuroinflammation by increasing the release of proinflammatory cytokines (e.g. TNFα, IL-1ß, IL-6, IL-10, INF-γ). In turn these cytokines can determine an increase of Aß production by modulating the expression and the activity of ß-secreatse (BACE1) whose transcription also is upregulated by TNFα-activated nuclear factor kappa B (NF-κB) [24].
Activated microglia and astrocytes exert a direct neurotoxic effect, can promote Aß deposition and can cause death in adjacent neuronal cells through the production of ROS, nitric oxide (NO) and the activation of the complement system [25].

Scientific evidences, collected over decades of research, strongly indicate that Aß peptides play a crucial role in AD.

Initially, as for other amyloidoses, the Aß-mediated neurotoxicity was conferred to plaques formed by amyloid fibrils. However, in the last 25 years, the attention has been shifted on soluble pre-fibrillar forms of Aß peptides [26,27].

Aß peptides

In 1992, John Hardy and Gerald Higgins formulated the "amyloid cascade hypotesis". According to this hypothesis, the Aß peptides that constitute amyloid plaques are among the causative agents of Alzheimer's pathology [28].

For long times, the amyloid plaques were considered the principal neurotoxic mediators in AD. Imaging techniques (positron emission tomography, PET, and magnetic resonance imaging, MRI) have demonstrated that fibrillar deposits are formed decades before the onset of clinical signs of AD. Moreover, it is well known that the number of plaques does not correlate with the severity of the dementia [29,30].

Numerous evidences have shown a strong correlation between Aß oligomers and cognitive impairments [31]. For example, Shankar et al. in 2008 have demonstrated that soluble oligomers isolated from AD brain can affect, in a dose-concentration manner, synaptic function, structure and memory of healthy adult rats [32].
Therefore, in the last two decades there was a paradigm shift from amyloid fibrils to soluble pre-fibrillar species of Aß peptides as toxic agents. In fact, the predominant working hypothesis of AD aetiology now is focused on Aß oligomers. [12,26,29,30].

Aß peptides are a class of peptides with different lengths which are produced from the metabolism of APP [19].

The gene *APP* is localized on the long arm of chromosome 21 and encodes for the transmembrane glycoprotein APP. APP undergoes a process of alternative splicing that produces three main isoforms: APP751 and APP770 are ubiquitously expressed and APP695, constituted by 695 amino acidic residues, is the isoform highly expressed in neurons and occurs at very low abundance in other cells [33].

Two different types of metabolism are possible for APP: the non amyloidogenic and the amyloidogenic one (**Figure 6**).

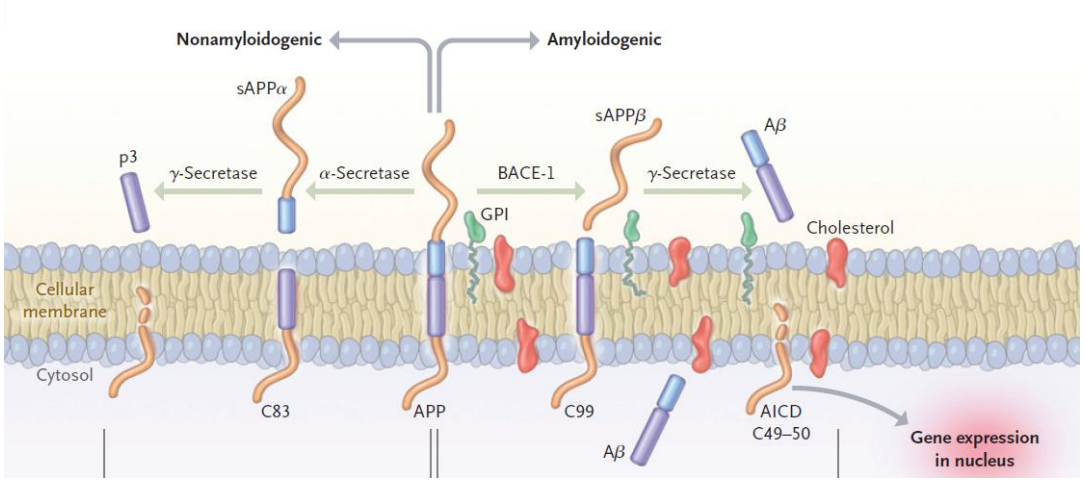

Figure 6. The metabolism of APP [19].

The α-secretase starts the non amyloidogenic process: the soluble ectodomain (sAPPα) is released in the extracellular milieu by proteolytic cleavage. The residual portion (C83) is then split by γ-secretase liberating the extracellular peptide p3 and the amyloid intracellular domain (AICD).

In the amyloidogenic pathway, the first cleavage of APP is performed by the ß-site APP-cleaving enzyme or ß-secretase (BACE). Contrary to α-secretase, this enzyme catalyzes a cleavage at a different position and a peptide shorter than sAPPα, named sAPPß, is released in the extracellular site. At this point, γ-secretase, together with presenilins, carries out the second enzymatic cut on the fragment C99 that leads to AICD and to Aß peptides [19].

According to the cleavage site of C99, a population of Aß peptides ranging from 36 to 43 amino acids can be produced. Among these, Aß40 and Aß42 (with 40 and 42 residues, respectively) and their oligomers are considered crucial in the development of AD. Therefore they may represent the key point for the comprehension of the aetiology of the disease [19].

Aß are natively disordered peptides and as a result they are prone to aggregate. Folded or partially folded monomers are not toxic, however when aggregation occurs the resulting soluble oligomers are toxic for neurons at different levels [34].

Aß40 is the most abundant peptide, whereas Aß42 is the most amylodogenic one, as it is endowed with highest aggregation propensity and toxicity.

Toxicity of Aß peptides

From *in vitro* and *in vivo* studies on animal models of AD, it is clear that Aß oligomers directly and indirectly affect numerous cellular systems through different molecular mechanisms, in an non specific fashion [27,35,36].

In physiological conditions, Aß is a neuromodulator of the cholinergic system and very high concentrations of Aß compromise the muscarinic receptors-mediated response. As a result, the release of both γ-aminobutyric acid (GABA) in the prefrontal cortex and of the neurotransmitter acetylcholine (ACh) at the synaptic terminations are altered.

Aß, and in particular Aß42, is able to interact with the receptors of the glutamatergic system involved in the generation of long term potentiation (LTP) and long term depression (LTD). These two events are forms of synaptic plasticity and they are considered the keystone of the memory formation [19]. These alterations, together with the fact that Aß can cause the down-regulation of factors essential for the neuronal survival (e.g. brain-derived neurotrophic factor, BDNF, and nerve growth factor, NGF), induce synaptic loss which correlates best with the most common cognitive impairments observed in AD [19].

Age-related dysfunctions like mitochondria dysfunction and oxidative stress, are exacerbated also by Aß oligomers. Indeed, aggregated forms of Aß can inhibit mitochondrial enzymes with consequent inhibition of ATP production, cytochrome *c* release [37], caspase activation, transition pore opening and increase of ROS production, with overall detrimental effects on the cellular homeostasis [36].

The receptor for advanced glycation end products (RAGE) mediates the pro-oxidant effect of Aß on neuronal, microglia and vascular cells, by enhancing oxidative stress and neuroinflammation [24,25].

The disruption of cellular membranes mediated by Aß oligomers seems to be a key mechanism of Aß toxicity, since it can trigger the vast majority of the neurodegeneration events (**Figure 7**) [38].

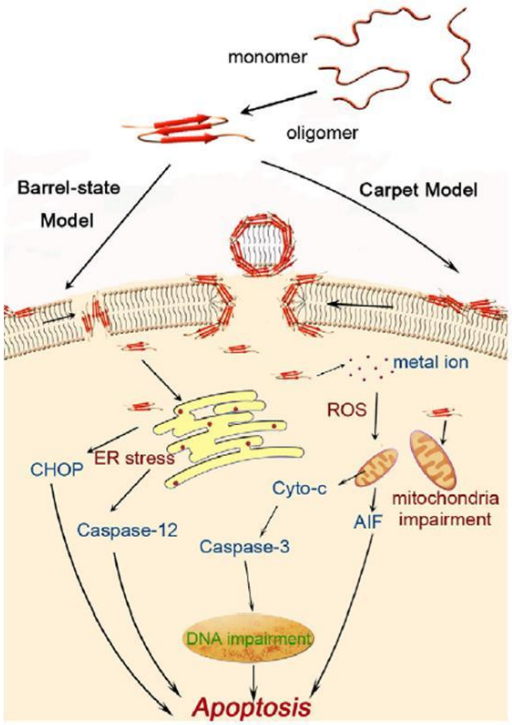

Figure 7. Proposed models of lipids permeabilization: the "barrel-stave" and the "carpet model", and events triggered by membrane disruption [38].

Two different models have been proposed and both lead to membrane permeabilization. According to the "barrel-stave model", oligomers or monomers, which in turn can recruit other monomers, are able to penetrate into the hydrophobic core of membranes and form pores. Conversely, if Aß interacts first with charged phospholipid head groups, oligomers lay on the surface and form a carpet, following the "carpet model". When it reaches a critical monomer concentration, the layer induces membrane disintegration in a detergent-like manner [38].

Since the aggregation of Aß peptides is of increasing importance, the literature regarding this topic is vast and also controversial.

The core of the so called "oligomer question" is that different oligomers are present at dynamic equilibrium inside or outside the cell. Particular oligomeric populations can exert specific toxic mechanisms and therefore it is crucial to identify all oligomers and their associated detrimental effects on the brain. However, because of their peculiar nature, this goal is far to be reached [30,39].

Clinical trials

To date there are not disease-modifying treatments available for Alzheimer's disease [12,40].

Contrary to other diseases, the drug discovery and development process for Alzheimer's disease is characterized by an impressively high rate of failures (>95%) even in advanced phases (i.e. phase III) and this results in time and money loss. Few pharmaceutical companies are willing to support such expensive investigations [12,41].

Despite huge investments, at present only four drugs (Donepezil, Rivastigmine, Galantamine and Memantine) are marketed for AD. As they hit the cholinergic and glutamatergic systems, these molecules serve only as symptomatic treatments [40].

Many reasons could explain this situation: above all the aetiology of the disease it not yet clarified. In addition, recent increasing evidences on the peculiar multifactorial nature of AD may suggest that the focus on a single target could not be a successful strategy.

Starting from the late 90s, the attention was shifted on treatments which could remove plaques and/or oligomers of Aß peptides.
With this goal, several trials have been carried out and nevertheless they failed, because of serious adverse effects or because of the inefficacy of the treatment [41].

This could be a strong evidence that aggregated forms of Aß peptides are not good targets. However, one explanation for these failures that has been recently reported [42] it is that these studies have involved patients who were already 20 years or more into the pathological process, when neurodegeneration was too advanced to be stopped or reverted or to rescue the compromised brain.

Therefore, it is necessary treat AD before brain pathology develops (**Figure 8**). Some of the current clinical trials recruit people with increased risk of AD, as emerged by genetics or brain scan tests and investigations are focused on drugs designed to treat AD before brain pathology or cognitive symptoms develop.

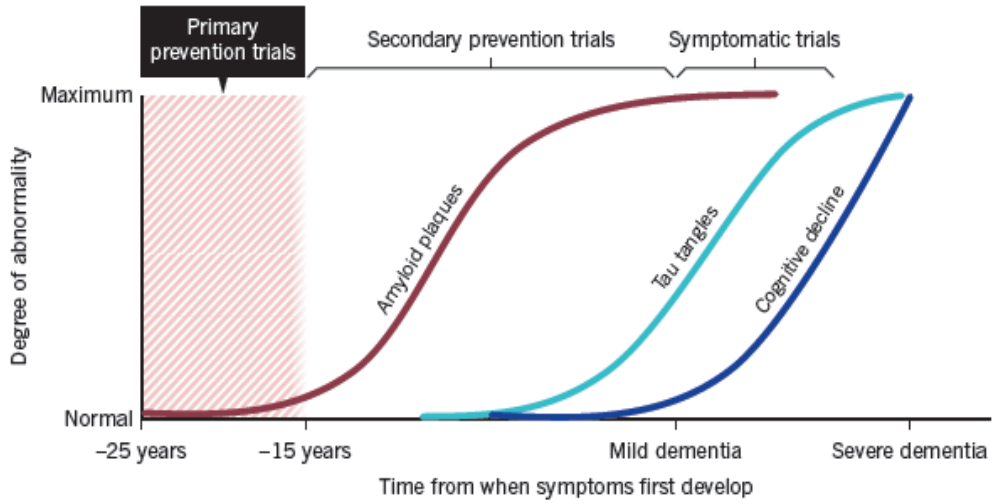

Figure 8. Time course development of brain pathology (Aß plaques and tau tangles) and of cognitive impairments. Types of clinical trials: primary and secondary prevention and symptomatic trials [42].

According to the time lapse in which the potential treatment should be active, it is possible distinguish three different types of clinical trials: primary prevention, secondary prevention and symptomatic trials (**Figure 8**). Clearly, a primary prevention treatment should be the most desirable strategy [41].

Nowadays, among the potential anti amyloidogenic therapeutics studied, some are in different phases of clinical trials. They hit the amyloid cascade by different mechanisms [43].
It has been demonstrated that proteoglycans are able to bind Aß and this can accelerate the conversion of unfolded monomers to ß-sheet structure that is characteristic of Aß aggregates. As Tramiprosate is a glycosaminoglycan mimetic, its binding to Aß would inhibit amyloid aggregation. Nevertheless, data supporting this effect were weak and not replicated by other laboratories.
Another target in the amyloid cascade could be the enzymes that yield to Aß peptides. Tarenflurbil, an anti-inflammatory agent, has been tested as γ-secretase modulator, with the ultimate aim of reducing Aß42 production in favour of shorter forms of Aß. This drug was not found to penetrate the brain at a sufficient concentration to mediate its pharmacological effect. Semagacestat is a classical non competitive inhibitor of γ-secretase; however, during phase III the clinical trial was stopped because of an increase of incidence of skin cancer, infections and haematological alterations.

Biopharmaceuticals have been developed as potential AD treatments. Bapineuzumab is a humanized antibody which recognizes the first 5 amino acids of Aß; the hypothesis was that it would promote the amyloid plaque clearance through the activation of microglia. However, during the phase III two out of four clinical trials were terminated due to the lack of clinical benefit.

Gammagard is an intravenous preparation of Immunoglobuiln G (IVIg) obtained from B cells of AD patients and immortalized with Epstein-Barr virus. IVIg are directed against the N-terminus of Aß peptides. In phase III Gammagard failed to reach its coprimary outcomes.

Very recently Sevigny *et al*. have reported the results obtained in a double-blind, placebo-controlled randomized trial. The trial was designed to verify the safety and the efficacy of a monthly treatment of AD patients with aducanumab.

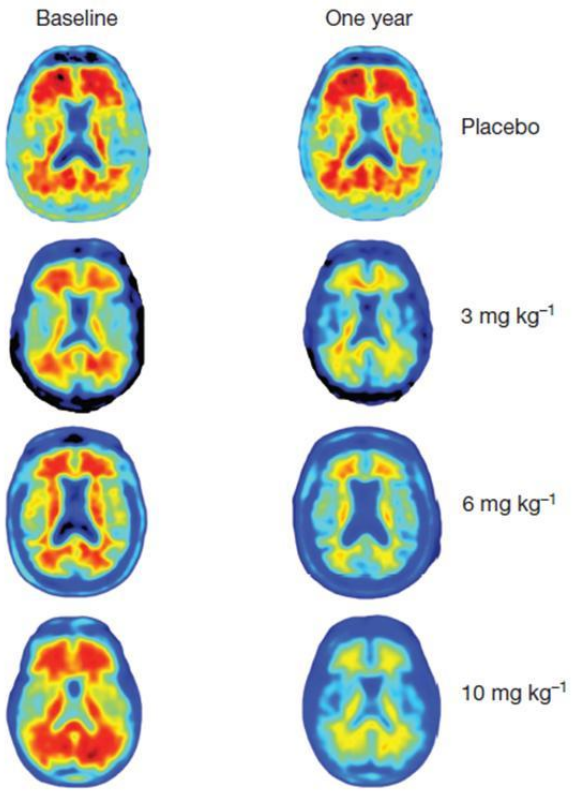

Figure 9. Effect of aducanumab on amyloid plaques. PET images of AD brains of patients treated with placebo or increasing concentrations of aducanumab. Amyloid plaques are revealed in red [44].

They observed that this antibody robustly removed amyloid plaques after 1 year (**Figure 9**) of treatment and that the apparent clinical benefits observed may be due to the reduction of oligomeric forms of Aß [44]. Therefore, aducanumab reaches the brain at concentrations sufficient to exert its activity. Notably, the antibody can trigger the clearance of pre-existing Aß amyloid plaques and prevent the formation of new deposits.

Even though this latter example is encouraging, it is just one recent exception among so many drug development failures.

All these findings confirm that the stakes are extraordinarily high, on the other hand, they have allowed to head the research toward more promising strategies.

In order to develop efficient disease-modifying treatments, it seems to be imperative to deeper understand all the alterations involved in neurodegeneration, by paying particular attention to soluble oligomers of Aß peptides. Moreover, increasingly evidences suggest that the paradigm "one protein-one target-one drug" is not applicable for Alzheimer's disease, so that a multitarget-directed approach should be undertaken [16].

Scope and outline of the work

The main scope of this research work is the set up of an analytical platform that allows the identification of new Aß fibrillogenesis modulators by focusing on soluble oligomers of Aß42 as protein targets.
The idea behind this work is to fill the gap that still exists on the availability of suitable *in vitro* methods to reach this end.
Despite the great interest in these targets, the fact that the oligomeric state of the peptide is not due to covalent binding, therefore transitory in nature, poses a number of challenges. These include, among others, the set up of Aß42 sample preparation protocols to tune the formation of different oligomeric species; the monitoring of oligomer formation, possibly in free solution, until fibril precipitation; the identification and characterization of the formed oligomers; the independent evaluation of their neurotoxicity.
Further, Aß42 peptide is very prone to aggregation into insoluble fibrils, thus the formed oligomers have to be kept in solution over a suitable time window, in order to appreciate the potential activity of the selected fibrillogenesis modulators.

Bearing these premises in mind, the content of the chapters is outlined below:

Chapter I

In this chapter the most important analytical challenges faced in *in vitro* studies on Aß42 soluble oligomers are addressed, namely identification and characterization.
Oligomers obtained from different solubilization protocols are analytically separated by capillary electrophoresis (CE) until precipitation into fibrils, whose presence is confirmed by transmission electron microscopy (TEM).
CE represents the analytical nucleus of the proposed platform. By working in free solution, it allows to preserve the non-covalent oligomeric structure of Aß assemblies. Notably, the comparison of results obtained by CE and SDS-PAGE reveals the intrinsic bias associated to the data obtained by the latter technique. Therefore, CE can play an alternative and unique role in the studies on the Aß aggregation process.
The assignment of a molecular weight range to the separated oligomeric populations is carried out by ultrafiltration (UF). UF affords the physical isolation of the aggregates formed in solution. In this way, it is possible to independently assess the neurotoxicity induced by small oligomers and that induced by large aggregates.
Further, a characterization of the secondary structure of the aggregates is evaluated by Attenuated Total Reflectance-Fourier Transform infrared spectroscopy (ATR-FTIR).

Chapter II

One important application of the platform set up as reported in Chapter I, is the possibility to discriminate whether an inhibitor of the fibrillogenesis may act on oligomer formation kinetics or on formed fibrils or on both.
Thus, in Chapter II the analytical platform has been exploited to test two sets (SET1 and SET2) of curcumin-based analogues synthesized by two different groups at the University of Bologna. The chemical modifications applied to both sets are intended to improve the biological profile of curcumin, as well as to transfer to the curcumin scaffold additional activities, in the context of a multitarget-directed approach [16]. The activity of curcumin, taken as a reference compound, is examined and compared to that of curcumin-based analogues.
As far as SET1 [45], the less toxic molecules were selected on the basis of toxicity data and anti-inflammatory activity that were assessed on microglia cells by the University of Padua.
Anti-oligomeric and anti-fibrillogenic activities of curcumin and of curcumin-based analogues belonging to SET1 are investigated at decreasing concentrations by CE analysis and by TEM. Moreover, to approach a structure-activity relationship (SAR) study, the curcumin pharmacophore was dissected by modifying the functional groups involved in these activities.
Because of promising findings, the best compounds in terms of anti-amyloid activity are tested *in vivo* on CL2120 (Aß3-42) *C. elegans*. This invertebrate animal model of AD has recently emerged as a useful tool to screen compound activity.

Preliminary results on the anti-oligomeric activity as assessed by CE studies is also reported for two molecules belonging to SET2. The set has already been described in literature [46] and two compounds have been singled out to be tested in this work, on the basis of their known activity: the first compound is a potent inhibitor of the Aß aggregation and the second has shown anti-oxidant activity.

Chapter III

In Chapter III the binding, *in vitro,* between Aß42 and the human innate immune peptide LL-37 together with its effects on the amyloid aggregation process are demonstrated.
To this end, a multifaceted approach is set up, by using different analytical and spectroscopic techniques namely surface plasmon resonance imaging (SPRi), CE, circular dichroism (CD), and TEM.
From these studies, it emerges that LL-37 binds Aß peptides and exerts a neuroprotective effect against microglia-mediated Aß42 toxicity on SH-SY5Y neuroblastoma cells. These *in vitro* data constitute a step forward in the identification of physiologically relevant binding partners of Aß that could

modulate fibril formation *in vivo* and therefore might yield new insights into the causes of AD.

References

1 Merlini, G. and Bellotti, V. (2003) Molecular mechanisms of amyloidosis. *N Engl J Med* 349 (6), 583-596

2 Chiti, F. and Dobson, C.M. (2017) Protein Misfolding, Amyloid Formation, and Human Disease: A Summary of Progress Over the Last Decade. *Annu Rev Biochem* 86, 35.1-35.42

3 Sipe, J.D. et al. (2016) Amyloid fibril proteins and amyloidosis: chemical identification and clinical classification International Society of Amyloidosis 2016 Nomenclature Guidelines. *Amyloid* 23 (4), 209-213

4 Eisenberg, D. and Jucker, M. (2012) The amyloid state of proteins in human diseases. *Cell* 148 (6), 1188-1203

5 Gillam, J.E. and MacPhee, C.E. (2013) Modelling amyloid fibril formation kinetics: mechanisms of nucleation and growth. *J Phys Condens Matter* 25 (37), 373101

6 Knowles, T.P. et al. (2014) The amyloid state and its association with protein misfolding diseases. *Nat Rev Mol Cell Biol* 15 (6), 384-396

7 Makin, O.S. and Serpell, L.C. (2005) Structures for amyloid fibrils. In *FEBS J* 272, 5950-5961

8 Cohen, S.I. et al. (2013) Proliferation of amyloid-beta42 aggregates occurs through a secondary nucleation mechanism. *Proc Natl Acad Sci U S A* 110 (24), 9758-9763

9 Eichner, T. and Radford, S.E. (2011) A diversity of assembly mechanisms of a generic amyloid fold. *Mol Cell* 43, 8-18

10 Balchin, D. et al. (2016) In vivo aspects of protein folding and quality control. *Science* 353, pp. aac4354-1-aac4354-12

11 Lucato, C.M. et al. (2017) Amyloidogenicity at a Distance: How Distal Protein Regions Modulate Aggregation in Disease. *J Mol Biol* 429, 1289-1304

12 Winblad, B. et al. (2016) Defeating Alzheimer's disease and other dementias: a priority for European science and society. *Lancet Neurol* 15, 455-532

13 Baumgart, M. et al. (2015) Summary of the evidence on modifiable risk factors for cognitive decline and dementia: A population-based perspective. *Alzheimers Dement* 11 (6), 718-726

14 Dahm, R. (2006) Alzheimer's discovery. *Curr Biol* 6, R906-910

15 Nixon, R.A. (2007) Autophagy, amyloidogenesis and Alzheimer disease. *J Cell Sci* 120, 4081-4091

16 Leon, R. et al. (2013) Recent advances in the multitarget-directed ligands approach for the treatment of Alzheimer's disease. *Med Res Rev* 33 (1), 139-189

17 Huang, Y. and Mucke, L. (2012) Alzheimer mechanisms and therapeutic strategies. *Cell* 148 (6), 1204-1222

18 Tomita, T. et al. (1997) The presenilin 2 mutation (N141I) linked to familial Alzheimer disease (Volga German families) increases the secretion of amyloid beta protein ending at the 42nd (or 43rd) residue. *Proc Natl Acad Sci U S A* 94 (5), 2025-2030

19 Querfurth, H.W. and LaFerla, F.M. (2010) Alzheimer's disease. *N Engl J Med* 362 (4), 329-344

20 Hardy, J. et al. (2014) Pathways to Alzheimer's disease. *J Intern Med* 275 (3), 296-303
21 Soreq, H. and Seidman, S. (2001) Acetylcholinesterase--new roles for an old actor. *Nat Rev Neurosci* 2, 294-302
22 Mattson, M.P. (2010) ER Calcium and Alzheimer's Disease: In a State of Flux. *Sci Signal* 3 (114), pe10
23 Sheng, B. et al. (2012) Impaired mitochondrial biogenesis contributes to mitochondrial dysfunction in Alzheimer's disease. *J Neurochem* 120 (3), 419-429
24 Calsolaro, V. and Edison, P. (2016) Neuroinflammation in Alzheimer's disease: Current evidence and future directions. *Alzheimers Dement* 12, 719-732
25 Da Mesquita, S. et al. (2016) Insights on the pathophysiology of Alzheimer's disease: The crosstalk between amyloid pathology, neuroinflammation and the peripheral immune system. *Neurosci Biobehav Rev* 68, 547-562
26 Hayden, E.Y. and Teplow, D.B. (2013) Amyloid beta-protein oligomers and Alzheimer's disease. *Alzheimers Res Ther* 5 (6), 60
27 Haass, C. and Selkoe, D.J. (2007) Soluble protein oligomers in neurodegeneration: lessons from the Alzheimer's amyloid beta-peptide. *Nat Rev Mol Cell Biol* 8 (2), 101-112
28 Hardy, J.A. and Higgins, G.A. (1992) Alzheimer's disease: the amyloid cascade hypothesis. *Science* 256 (5054), 184-185
29 Walsh, D.M. and Selkoe, D.J. (2007) A beta oligomers - a decade of discovery. *J Neurochem* 101 (5), 1172-1184
30 Benilova, I. et al. (2012) The toxic Abeta oligomer and Alzheimer's disease: an emperor in need of clothes. *Nat Neurosci* 15 (3), 349-357
31 Mc Donald, J.M. et al. (2010) The presence of sodium dodecyl sulphate-stable Abeta dimers is strongly associated with Alzheimer-type dementia. *Brain* 133 (Pt 5), 1328-1341
32 Shankar, G.M. et al. (2008) Amyloid-beta protein dimers isolated directly from Alzheimer's brains impair synaptic plasticity and memory. *Nat Med* 14 (8), 837-842
33 Hamley, I.W. (2012) The amyloid beta peptide: a chemist's perspective. Role in Alzheimer's and fibrillization. *Chem Rev* 112 (10), 5147-5192
34 Hong, S. et al. (2014) Soluble Aβ oligomers are rapidly sequestered from brain ISF in vivo and bind GM1 ganglioside on cellular membranes. *Neuron* 82 (2), 308-319
35 Gupta, V. et al. (2016) One protein, multiple pathologies: multifaceted involvement of amyloid beta in neurodegenerative disorders of the brain and retina. *Cell Mol Life Sci* 73, 4279-4297
36 Roychaudhuri, R. et al. (2009) Amyloid beta-protein assembly and Alzheimer disease. *J Biol Chem* 284 (8), 4749-4753
37 Kim, J. et al. (2014) Beta-amyloid oligomers activate apoptotic BAK pore for cytochrome c release. *Biophys J* 107 (7), 1601-1608
38 Cheng, B. et al. (2013) Inhibiting toxic aggregation of amyloidogenic proteins: a therapeutic strategy for protein misfolding diseases. *Biochim Biophys Acta* 1830 (10), 4860-4871

39 Lee, S.J. et al. (2017) Towards an understanding of amyloid-beta oligomers: characterization, toxicity mechanisms, and inhibitors. *Chem Soc Rev* 46 (2), 310-323
40 Mangialasche, F. et al. (2010) Alzheimer's disease: clinical trials and drug development. *Lancet Neurol* 9, 702-716, 2010
41 Schneider, L.S. et al. (2014) Clinical trials and late-stage drug development for Alzheimer's disease: an appraisal from 1984 to 2014. *J Intern Med* 275 (3), 251-283
42 McDade, E. and Bateman, R.J. (2017) Stop Alzheimer's before it starts. *Nature* 547, 153-155
43 Karran, E. and Hardy, J. (2014) A critique of the drug discovery and phase 3 clinical programs targeting the amyloid hypothesis for Alzheimer disease. *Ann Neurol* 76 (2), 185-205
44 Sevigny, J. et al. (2016) The antibody aducanumab reduces Abeta plaques in Alzheimer's disease. *Nature* 537, 50-56
45 Di Martino, R.M. et al. (2016) Versatility of the Curcumin Scaffold: Discovery of Potent and Balanced Dual BACE-1 and GSK-3beta Inhibitors. *J Med Chem* 59 (2), 531-544
46 Simoni, E. et al. (2016) Nature-Inspired Multifunctional Ligands: Focusing on Amyloid-Based Molecular Mechanisms of Alzheimer's Disease. *ChemMedChem* 11 (12), 1309-1317

Chapter I

Aß42 in vitro aggregation

1 Introduction

Identification of Aß oligomers

Amyloid plaques are one of the two hallmarks of Alzheimer's disease and their detection contributes to the post-mortem diagnosis of the disease. The primary component of plaques are fibrillar forms of Aß peptides, however these insoluble species of Aß are not correlated with the severity of dementia [1].

Starting from the late 90s, extensive evidence highlights a strong correlation between soluble pre-fibrillar aggregates of Aß peptides and the severity of cognitive impairment. This means that soluble Aß oligomers are the main neurotoxic mediators in AD [2], furthermore, also the ongoing polymerization process may be responsible for Aß toxicity and neurodegeneration in AD [3].

Since classified as amyloidogenic, Aß are natively disordered peptides. Conformational fluctuations of Aß result in partially folded or unfolded monomers which are characterized by an high aggregation propensity [4]. The aggregation of Aß monomers into oligomers abides by the nucleation-elongation process and it can be affected by several factors such as pH, peptide concentration and interaction with other biomolecules.

In the early stage of oligomerization, small oligomers form nuclei that rapidly lead to larger aggregates [5,6].

In general, a great diversity characterizes soluble oligomers, as well as fibrils [7,8] (**Figure 1**). There are several explanations for this variability: e.g. the non covalent and metastable nature of assemblies (which can interconvert into one another) and the presence of off-pathway oligomers generally regarded as unstructured and non toxic species. These latter assemblies arise from a deviation of the principal aggregation process by on-pathway oligomers [6,9].
Fibrils in amyloid plaques contribute to the heterogeneity of oligomeric populations and to the complexity of the amyloid process. Indeed, through secondary nucleation and fragmentation processes, also insoluble deposits represent a source of toxic oligomers [10,11].

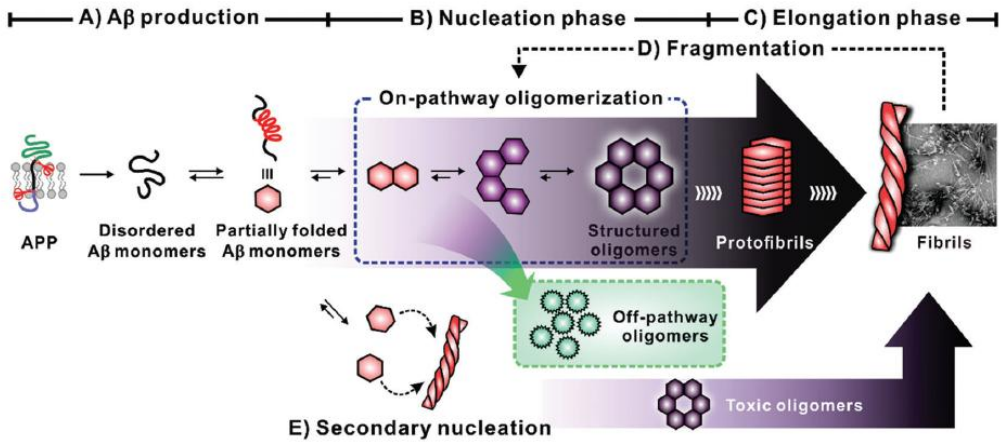

Figure 1. Aß production and aggregation [6].

Despite significant efforts, the structure of Aß oligomers, the molecular-level understanding of the aggregation process, as well as the exact mechanism of oligomer-induced toxicity, remain elusive.

Intrinsic limitations in investigating Aß oligomers are related to their peculiar nature. As described above, Aß oligomers consist of heterogeneous populations of polymorphic, non-covalent and transiently populated aggregates which are generated by multiple pathways [6,11]. Moreover, different Aß peptides can undergo distinctive aggregation processes and lead to diverse oligomers, as it is well known for Aß40 and Aß42 [12]. Therefore, it is challenging to characterize the structure and properties of these assemblies, by correlating their aggregation, structure and toxicity.

In this context, important progresses have been made through both *ex vivo* and *in vitro* studies performed with AD brain-derived oligomers and synthetic Aß peptides. Because of the target organ of amyloid aggregates, the availability of brain-derived species is clearly restricted and *ex vivo* studies are more difficult to approach.

However, both strategies present advantages and disadvantages.
In fact, the multiplicity of Aß species derives not only from the complex dynamic equilibrium existing among Aß oligomers, but also from the different approaches used to generate and to study the assemblies *in vitro*, or to isolate them from brain tissues. As a result, isolated and generated species might not completely overlap those found in the human brain [2,6,13].

The literature relative to this issue is widespread and controversial: both small and large aggregates seem to exert neurotoxicity. In **Figure 2** a schematic representation of synthetic and natural Aß oligomers described in the literature is reported [2].

In a seminal work on *Tg2576* mice (which expresses an APP variant linked to AD in humans), Lesnè and co-workers identified trimers as fundamental Aß assembly unit *in vivo*, as well as nonamers and the so called "Aß*56" (56-kDa soluble Aß-assemblies, namely dodecamers) as viable candidates that cause memory loss [14-16]. Notably, also smaller species have demonstrated to be toxic, including monomers, dimers and trimers [15,17-19], as well as tetramers and dodecamers [16]. In particular, dimers are defined as the smallest synaptotoxic species [20].

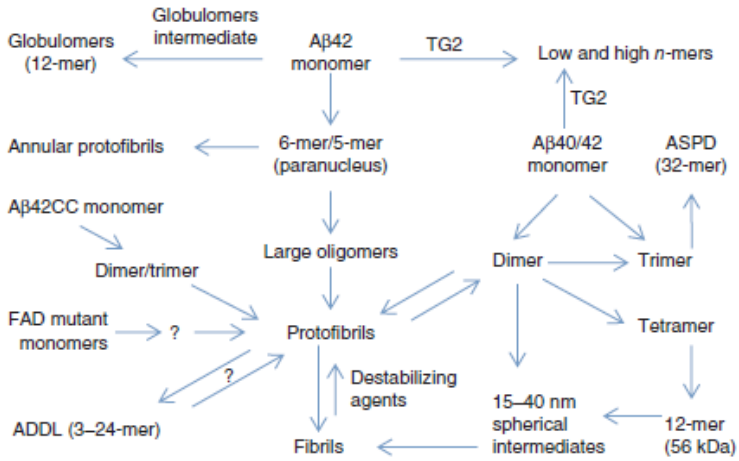

Figure 2. Overview of Aß assemblies described in the literature [2].

Studies on Aß aggregation

Ex vivo and *in vitro* studies on Aß aggregation necessarily need multiple techniques to provide complementary information and to address oligomers' structural and kinetic details, the mechanism of oligomers' formation and the related toxicity. Each technique has specific advantages and limitations, also depending on the aim of each specific study reported in the existing literature. Some examples, that are not intended to be exhaustive, are reported below.

Isolation and size estimation of oligomeric species have been achieved by sodium-dodecyl sulphate-polyacrylamide gel electrophoresis (SDS-PAGE) [12,18,21] size exclusion chromatography (SEC) [15,22] dynamic and multiangle light scattering (DLS and MALS) [22-25]. Knowledge on *in vitro* oligomer distribution and of the qualitative structure of the aggregates has been gained by ion mobility mass spectrometry (IM-MS) [16] and molecular dynamics (MD) modelling. Morphological data can be visualized by AFM, SEM and EM. Atomic details have been reported by NMR spectroscopy and X-ray crystallography [26].

Spectroscopic techniques such as dynamic and multiangle light scattering (DLS and MALS) yield the weight-averaged molar mass for all molecules in solution [6,27]. However, they are not separative techniques and thus they are not suitable for determining the size of small peptide oligomers or monomers especially when they co-exist with larger aggregates [6,13,27].
Fluorescence correlation spectroscopy (FCS) has been also proposed to monitor the size distribution of Aß species over time and nevertheless the need for non-native labelled peptide may alter the oligomerization kinetics [28].

The main drawbacks relative to MS approaches are the ionization and the detection of molecules with the same mass to charge ratios [29]. Notably, IM-MS is suitable to study amyloid assemblies since this technique allows the separation of species with overlapping mass to charge ratios [16,29].
The use of MS has also been reported with both matrix assisted MALDI or ESI as ionization sources. This is a critical step since it could induce oligomer dissociation, expecially in the strong conditions of MALDI and ESI. To overcome this problem, a native ESI can be used which could maintain the assembly structure [30]. Moreover, with MALDI the monitoring of high molecular weight (HMW) oligomers is restricted: these species have low ionization ability due to the fact that big aggregates are not desorbed from the matrix as readily as small oligomers [31].

Both non denaturing SEC and denaturing SDS-PAGE are limited in their ability to determine the exact size and precise distribution of oligomers [2,6,12,13,32]. Weak interactions, which constitute Aß assemblies, can be disrupted during the chromatographic run because of the adsorption on the stationary phase or because of secondary equilibria. In general, these techniques do not provide enough resolution to discriminate all the different species.
SDS-PAGE works under denaturing conditions and thus no information regarding oligomeric structure can be obtained. As recently established, the presence of SDS induces oligomeric dissociation which in turn produces mostly monomers and dimers [18,27,33]. In addition, SDS-PAGE is not easy and fast enough to allow kinetic studies.

Photo-induced cross-linking of unmodified proteins (PICUP) consists of the production of oligomers stabilized with covalent bonds [6,12,21]. This procedure allows the "freezing" of oligomers and overcomes the dissociation induced by techniques such as SDS-PAGE or SEC. However, by PICUP not all Aß42 oligomers were found to be covalently cross-linked [21]. Further, by the chemical cross-linking reaction, molecules are modified, therefore they do not exactly mirror native oligomers in solution.

In the last four decades, capillary electrophoresis (CE) has become a considerable analytical technique in protein separation analysis [34].

Furthermore, CE is characterized by high separation efficiency, fast analysis time, ease of operation and low sample and electrolyte consumption.

In this particular case, CE has proven to afford a real time snapshot of different soluble Aß populations during their formation [35]. Since it works in free solution, without a stationary phase or chaotropic agents, it can preserve the oligomeric structure. When equipped with a UV detector, no labels are required contrary to the detection based on fluorescence. CE-UV is able to detect and separate soluble oligomeric species of Aß peptides ranging from monomers [32,36-39] to aggregates larger than dodecamers [32,35,39-42]. Notably, insoluble material cannot be injected in a CE capillary, therefore the presence of fibrils does not affect the analytical separation of soluble oligomers.

Despite exact physiological conditions cannot be replicated *in vitro*, the advantage of *in vitro* generated Aß oligomers lies in the more precisely controlled starting materials and experimental conditions.
On the other hand, the standardization of the aggregation process is a difficult goal to reach when using synthetic peptides [8,43].
This is true especially for Aß42, because of its highly self-aggregating tendency. In fact, *in vitro* simulation of aggregation aiming at producing different oligomeric populations is strictly dependent on experimental parameters such as peptide concentration, type of solvent, incubation time and temperature. Nevertheless, also supplier-to-supplier and batch-to-batch reproducibility of synthetic peptides are relevant issues that are seldom addressed. This means that each specific solubilization protocol leads to different oligomeric species, thus contributing to the increase of data on Aß oligomers [2,13].

In the present work, CE is employed to monitor over time the aggregation process of Aß42 under quasi physiological conditions, until the precipitation into fibrils.

Experimental conditions of the Aß42 preparation are finely tuned to obtain as many oligomeric populations as possible and to extend the time window in which Aß42 oligomers are soluble. To this end, two novel solubilization protocols and a third protocol taken from literature [31,44] are used to solubilize synthetic Aß42. The resulting oligomers are analytically separated by CE and identified.

Ultrafiltration (UF) represents a simple strategy for the assignment of a range of molecular weight (MW) to the separated oligomers. To corroborate data obtained by UF followed by CE analyses, Aß aggregates are also analyzed by SDS-PAGE/Western Blot, since it is the most widespread technique for the characterization of Aß assemblies.

Oligomers isolated by UF can be also considered as independent populations for further investigations. First, the secondary structure of small and large aggregates is evaluated by attenuated total reflectance-Fourier transform infrared spectroscopy (ATR-FTIR). Finally, the cell neurotoxicity of the separated oligomers is assigned.

2 Materials and Methods

2.1 Reagents

Synthetic Aß42 was purchased as lyophilized powder from Anaspec (Fremont, CA, USA), (purity ≥95%; lots #1556608, #1556609, #1457203) and Bachem (Bubendorf, Switzerland) (purity ≥95%; lots #10533163, #1065556, #1056654) and stored at -20°C.
1,1,1,3,3,3-Hexafluoropropan-2-ol (HFIP), dimethylsulfoxide (DMSO), acetonitrile (ACN), and sodium carbonate (Na_2CO_3) were from Sigma-Aldrich (St. Louis, MO, USA). Sodium hydroxide (NaOH) and sodium dodecyl sulphate (SDS) were provided by Merck (Darmstadt, Germany). Na_2HPO_4 and NaH_2PO_4, supplied by Sigma-Aldrich, were used for the preparation of the background electrolyte (BGE) in the CE analyses. BGE solutions were prepared daily using Millipore Direct-Q ™ deionized water (Bedford, MA, USA) and filtered with 0.45 µm Sartorius membrane filters (Göttingen, Germany).
Two types of ultrafiltration devices were used: 10, 30 and 100 kDa cutoff membranes were purchased from Pall Corporation (New York, NY, USA), whereas 50 kDa cutoff membranes were from Millipore (Billerica, MA, USA).
Polyvinylidene difluoride (PVDF) membranes from Millipore, the primary antibody 6E10 from Covance (Princeton, NJ, USA) and the secondary antibody anti-mouse (Thermo Scientific, Waltham, MA, USA) were used in SDS-PAGE analyses.

2.2 Solubilization protocols

Aß42 oligomers were prepared by following three different solubilization protocols, as reported in **Figure 3**.
In protocol #1 and protocol #2, Aß42 was solubilized in HFIP (1 mg/mL, 221.5 µM). This stock solution was gently mixed and then kept for 30 minutes at 4°C, aliquoted in microfuge tubes and lyophilized via Speed-Vac.
In protocol #1 each Aß42 aliquot was redissolved in 20 mM Na_2HPO_4/NaH_2PO_4, pH=7.4.
In protocol #2 the aliquots were redissolved in DMSO/20mM phosphate buffer pH 7.4 solutions at increasing concentrations of DMSO.
In protocol #3, Aß42 was prepared as described by Bartolini et al [44]. Briefly, the peptide was dissolved in HFIP (149 µM) and kept at room temperature (25°C) overnight. This stock solution was aliquoted in microfuge tubes and kept at 25°C for one day, then HFIP was left to evaporate at 25°C overnight. The resulting peptide film was redissolved to obtain 500 µM Aß42: the redissolution mixture consisted of ACN/300µM Na_2CO_3/250mM NaOH (48.3:48.3:3.4, v/v/v). The final peptide solution (100 µM) was obtained by the dilution of 500 µM Aß42 with 20 mM Na_2HPO_4/NaH_2PO_4 (pH=7.4).

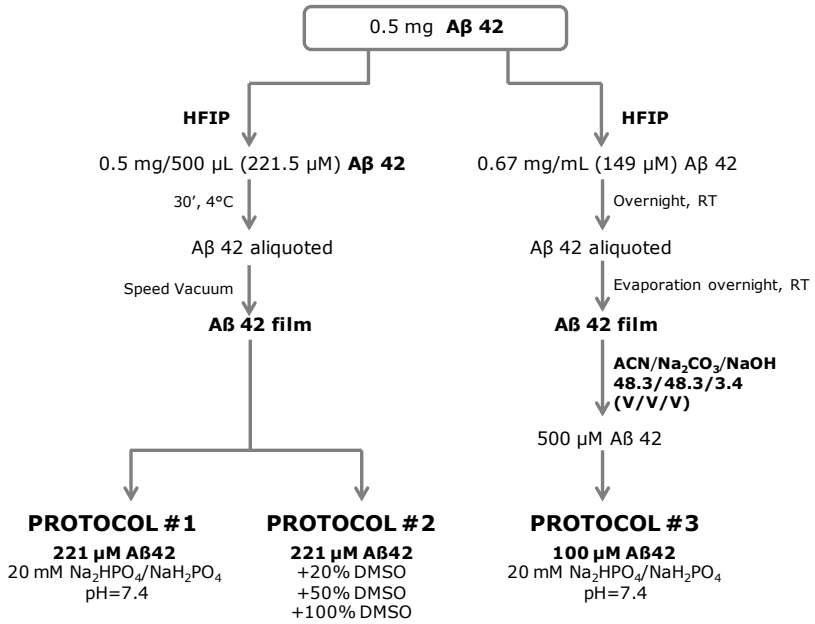

Figure 3. Outline of Aß42 solubilization protocols. For protocol #3 see [44].

2.3 Capillary electrophoresis

CE analyses were performed on an Agilent Technologies 3D CE system (Waldbronn, Germany) equipped with a diode-array detector set at the operative wavelength λ=200 nm. Data were collected using Chemstation A.10.02 software.

In the present work, two CE methods (A and B) were applied.

Uncoated fused-silica capillaries provided by Polymicro Technologies (Phoenix, AZ, USA) were prepared by flushing 1 M NaOH, deionized water and BGE (80 mM sodium phosphate buffer, pH=7.4) for 60 min, 60 min and 90 min (method A), or for 30 min, 30 min and 60 min (method B), respectively. Phosphate buffer was prepared by mixing 80 mM solutions of Na_2HPO_4 and 80 mM of NaH_2PO_4 in order to obtain the desired pH.

In method A [42] the analytical separation was carried out at 16 kV (current: 75-80 µA) on a capillary of 53 cm of total length (L=53 cm, l=44.5 cm). Samples were hydrodynamically injected by applying 50 mbar for 8 s.

In method B, a capillary of L=33 cm, l= 24.5 cm was used; the applied voltage was 12 kV (current 75-80 µA) and hydrodynamic injection parameters were set at 30 mbar for 3 s.

For both methods the between-run rinsing cycle consisted of 50 mM SDS (1.5 min), deionized water (1.5 min), and BGE (2 min). Capillary temperature was set up at 25°C.

2.4 Transmission electron microscopy (TEM)

Precipitated samples were fixed on carbon-coated Formvar nickel grids (200 mesh) (Electron Microscopy Sciences, Washington, PA, USA). Aß42 suspensions were diluted at 10 µM with 20 mM Na_2HPO_4/NaH_2PO_4. 10 µL of suspension were left to sediment on grids; after 15 minutes the excess of sample was drained off by means of a filter paper. The negative staining was performed with 10 µL of 2% w/v uranyl acetate solution (Electron Microscopy Sciences). Sample investigations were performed by using a Joel TEM 1400 plus electron microscope, operating at 80 kV.

2.5 Ultrafiltration experiments

At different elapsed times from solubilization time (defined as t0), Aß42 peptide solutions were ultrafiltrated on filters with different cutoff values by applying the best experimental conditions for each type of membrane, as suggested by suppliers: 14000 g for 10 minutes with 10, 30, and 100 kDa cutoff membranes and 60 minutes with 50 kDa cutoff membranes. In order to obtain enough volume for injection and to approximately restore the original concentration, a volume of 20 mM phosphate buffer (pH=7.4) equal to that of the ultrafiltrated sample was added to the retained portion, recovered by reverse spinning (14000 g, 5 minutes, for 50 kDa membrane).
Since the reverse spinning is not intrinsically possible on the filters by Pall Corporation (cutoff 10, 30 and 100 kDa) because of their geometry, in this case the recovery of the retained solution was carried out using a micropipette (i.e. as above but omitting the reverse spinning step).
Appropriate quantification of the retained sample amount is clearly not possible. However, the comparison of the electropherograms obtained before and after filtration was used to verify that the concentrations of the injected species were qualitatively comparable.
Filtrated and retained solutions were approximately diluted at 10 µM for cytotoxicity studies.

2.6 SDS-PAGE and Immunoblotting

By following protocol #1, Aß42 (maintained at room temperature) was sampled at different elapsed times (from t0 up to 5 days) and analyzed by SDS-PAGE/Western Blot. Each sample was diluted in SDS-sample buffer 2X (125 mM TRIS HCl pH 6.8, 4% SDS, 20% glycerol, blue bromophenol and 6% ß-mercaptoethanol).
5 µL sample was loaded and electrophoretically separated at 200 V on a 10-20% SDS-PAGE gradient gel. Thereafter, the sample was transferred to a polyvinylidene difluoride (PVDF) membrane by applying a current of 250 mA for 1 hour. PVDF membranes were blocked for 1 hour in 5% w/v milk in Tris-buffered saline containing 0.1% Tween 20 (TBS-T). Membranes were

immunoblotted with the primary antibody 6E10, an anti-amyloid antibody which binds to amino acid residues 1-16 of Aß peptides. The antibody 6E10 was diluted 1:1000 in 5% w/v BSA in TBS-T. The detection was carried out by incubation with horseradish peroxidase-conjugated goat anti-mouse IgG antibody (1:10000 dilution in 5% w/v BSA in TBS-T) for 1 h at room temperature. Membranes were then washed and Aß42 oligomers were visualized with chemiluminescence, according to manufacturer's protocol ECL Western Blotting Detection (Thermo Scientific).

2.7 Fourier Transform Infrared (FTIR) spectroscopy

Structural conformations of Aß42 solubilized by protocol #1 and those of filtrated and retained solutions as obtained after ultrafiltration on 50 kDa cutoff membrane were analyzed by FTIR measurements in attenuated total reflection (ATR). For analyses, 2 µl of each sample were deposed on the single reflection diamond crystal of the ATR device (Quest ATR, Specac, Fort Washington, PA, USA). To obtain a peptide hydrated film, samples were dried at room temperature. FTIR spectra of the hydrated films were collected by a Varian 670-IR spectrometer (Varian Australia Pty Ltd, Mulgrave VIC, Australia). Conditions applied were: 2 cm^{-1} resolution, scan speed of 25 kHz, 1000 scan coadditions, triangular apodization, and a nitrogen-cooled Mercury Cadmium Telluride detector. The second derivative analysis were performed using the Resolutions-Pro software (Varian Australia Pty Ltd) [45,46].

2.8 SH-SY5Y cell viability assay

SH-SY5Y human neuroblastoma cell cultures from European Collection of Cell Cultures (ECACC No. 94030304) were grown at 37°C in 5% CO_2/95% air in a medium composed of Eagle's minimum essential medium and Nutrient Mixture Ham's F-12, with the addition of 10% FBS, 2 mM glutamine, penicillin/streptomycin, non essential amino acids. All culture media and supplements were purchased from Euroclone (Life Science Division, Milan, Italy).

The mitochondrial dehydrogenase activity that reduces 3-(4,5-dimethylthiazol-2-yl)-2,5-diphenyl-tetrazolium bromide (MTT, Sigma, St Louis, MO, USA) was used to determine cellular redox activity, an initial indicator of cell death, in a quantitative colorimetric assay. At day 0, SH-SY5Y cells were plated at a density of $5x10^4$ viable cells *per* well in 96-well plates. The next day, cells were incubated for 24 h at 37°C in the presence of entire Aß42 peptide or of filtrated and retained solutions obtained after UF experiments and then exposed to a MTT solution in PBS (1 mg/mL). After 4 h incubation with MTT cells were lysed with lysis buffer (20% SDS in water/dimethylformamide 1:1) and incubated overnight at 37°C. The cell viability reduction was quantified by using a BIO-RAD microplate reader (Model 550; Hercules, CA, USA).

2.9 Statistical analysis

Data were analyzed by analysis of variance (ANOVA) followed, if significant, by an appropriate post hoc comparison test. The reported data is expressed as mean±SD or as mean±SEM of at three independent experiments. Values of $p<0.05$ were considered statistically significant.

3 Results and discussion

3.1 Monitoring of the aggregation process: capillary electrophoresis analyses

The use of CE for monitoring *in vitro* Aß40 and in particular Aß42 oligomer formation along the fibrillogenic pathway was pioneered by our group [35]. Other authors have also reported CE methods for the same application [32,36-38,47].

Aß42 has a very high tendency to aggregation and this makes these experiments intrinsically difficult. Thus, a crucial step before any CE analysis is the sample preparation, for a two-fold reason: first, to keep the standard peptide in solution for a suitable time window, so to obtain reproducible semi-quantitative data and to avoid in-capillary precipitation; second, to tune the formation of different soluble oligomeric populations.
To this end, in 2004 Sabella et al. set up a sample solubilization protocol aimed at increasing the solubility of acidic Aß42, in order to slow down the aggregation process. A basic solution (ACN/300 µM Na_2CO_3, 50:50 V/V) was employed and before the injection in CE, 100 µM Aß42 (in 20 mM phosphate buffer) was sonicated and centrifuged to break down preformed aggregates. A group of unresolved peaks corresponding to monomers up to undecamers was baseline separated from a broad band corresponding to higher molecular weight oligomers (larger than dodecamers) [35,40].
In our more recent works [41,42] a 1% NH_4OH solution was used as basic medium and two main peaks (a single sharp peak and a broad band) were separated by CE. Despite the different CE pattern as compared to [35], there was no improvement in the detection or separation of different oligomers, as these two peaks corresponded to species with a molecular weight below and above 50 kDa, with the earlier migrating peak corresponding to dimers and/or trimers but certainly not monomers.
Moreover, it has to be pointed out that in all the experiments mentioned above [35,40-42], the smaller oligomers rapidly converted into larger aggregates and that sample precipitation into amyloid fibrils was always observed within 4 days from solubilization. This resulted in a restricted time window which constitutes a main limit, in view of the intended application.
Other authors claimed to obtain monomeric Aβ42 by solubilization in TFA/HFIP/buffer mixtures: nevertheless from their CE profiles it was evident that peptide precipitation occured inside the capillary [37,38]. In general, in the attempt of monitoring aggregation inside a CE capillary, sharp peaks (very probably to be ascribed to electric spikes) have been mistaken for fibrils [47] and no further characterization has been reported.

Recently in another CE-UV method, particular attention has been paid to small species [32]. Here, by using a simplified sample preparation, the authors manage to maintain monomeric Aβ42 in solution and to characterize it by Taylor dispersion analysis. Further, a number of short-lived (20 hours) minor species were separated. These could be reasonably hypothesized to be small oligomers, although proper electropherograms and precision data showing their equilibrium with larger aggregates over time were not reported.

In order to obtain different oligomeric populations and in particular to promote the formation of low MW-species, to improve the efficiency of separation and to widen the time window for the evaluation of Aß42 self-assembly, we have developed two novel procedures (protocol #1 and protocol #2) for the solubilization of Aß42. Furthermore, we have investigated a protocol already reported in literature (protocol #3 [44]).
HFIP was chosen as the first solubilization solvent. Based on literature, for controlled aggregation studies it is crucial to remove any pre-existing aggregate structures in the lyophilized peptide. Fluorinated alcohols, alike HFIP, are able to promote α-helix conformation and disrupt ß-sheet structures, as demonstrated by circular dichroism (CD) and atomic force microscopy (AFM) data [44,48]. As reported in literature, 30 minutes of incubation time of Aß42 with HFIP should be sufficient to eliminate the "structural history" of Aß42 [43]. Then, depending on the degree of aggregation required, 20 mM phosphate buffer (protocol #1), different concentrations of DMSO in phosphate buffer (protocol #2) and a basic mixture (composed of acetonitrile, NaOH and sodium carbonate) with a consecutive dilution in phosphate buffer (protocol #3, [44]) have been investigated as redissolution solvents.

3.1.1 Protocol #1

As already mentioned, the reliability of peptide sample preparation and sample quality are crucial steps to guarantee the reproducibility of Aß42 self-assembly process. As we did in previous work [41,42], also for the new sample preparation protocol #1 Aß42 was purchased from Anaspec. After the treatment with HFIP, the following redissolution of Aß42 film with phosphate buffer (as described in **Figure 3** of Section 2.2) triggers conformational changes that lead to aggregates.

Immediately after solubilization (time zero, t0), 221 µM Aß42 is injected in CE at different elapsed times from t0 to monitor over time the aggregation process. Centrifugation of samples was omitted, so to avoid mechanical stress.
As shown in **Figure 4a)**, two main populations are detected by CE method A (see Section 2.3): the faster migrating population corresponds to Peak A, a very efficient electrophoretic peak, whereas Peaks B and C are slower migrating species. According to previous work [35,40-42] and following the hypothesis that mass prevails over charge in the migration observed, it is

plausible to conclude that Peak A represents low molecular weight oligomers, whereas Peaks B and C (slower migrating) should be high molecular weight species.

Reproducibility is an important issue in Aß42 *in vitro* studies because of the extreme variability of Aß42 peptide including supplier-to-supplier and batch-to-batch variability. Therefore reproducible data are mandatory before any further investigations.
As reported in **Table 1**, peak identification is made on the basis of precise effective electrophoretic mobilities (μ_{eff}) calculated for each species taken at each monitoring time point. In an electrophoretic system, the mobility of each species is defined as apparent mobility (μ_{app}) and has to be corrected by the mobility of the electroosmotic flow (EOF, μ_{EOF}), since EOF contributes to the migration velocity of ions.

	Peak A	**Peak B**	**Peak C**
μ_{eff} ($cm^2V^{-1}s^{-1}$)	-9.93×10^{-5}	-2.01×10^{-4}	$-2.17 * 10^{-4}$
SD	$\pm 5.73 \times 10^{-7}$	$\pm 1.75 \times 10^{-6}$	$\pm 2.17 \times 10^{-6}$
RSD	0.57%	0.87%	0.99%

Table 1. Protocol #1. Effective electrophoretic mobilities (μ_{eff}) of Aß42 oligomeric populations obtained with protocol #1 by CE method A. μ_{eff} ($\mu_{eff}= \mu_{app}-\mu_{EOF}$) are calculated by subtracting from the apparent mobility (μ_{app}) the contribute of the EOF (μ_{EOF}). μeff, standard deviation (SD) and relative standard deviation (RSD) values are calculated for 10 monitoring points of 5 independent experiments (n=5) using two different peptide batches.

As from **Table 1**, excellent precision is obtained, notably using two different peptide batches (n=3 with lot #1556608 and n=2 with lot #1556609 for a total of 5 independent experiments).

As evident in **Figure 4** and according to the literature, the pre-treatment with HFIP provides a longer time window than that previously reported [32,35-42]: oligomers are kept in solution at dynamic equilibrium for about two weeks. In CE, when precipitation occurs no more peaks are detected because the insoluble material deposited over time at the bottom of the vial is not injected.

a)

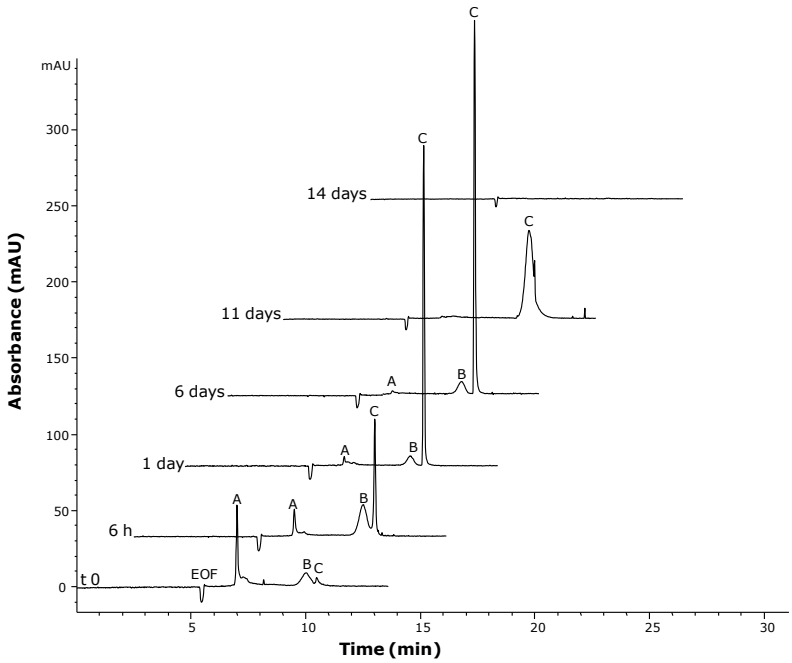

b)

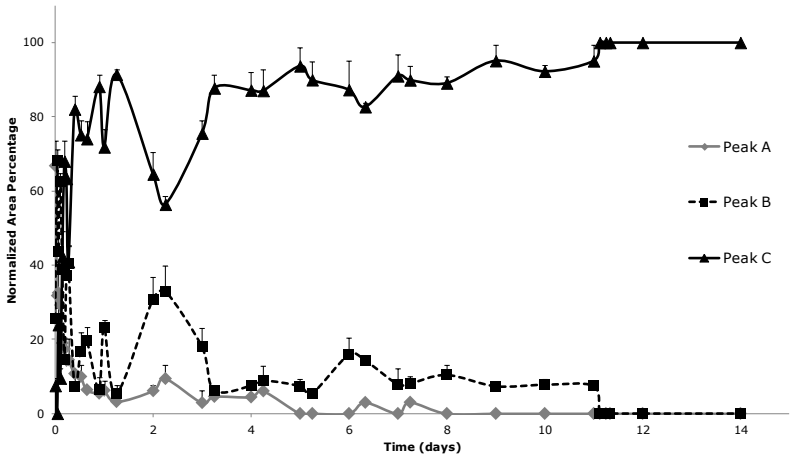

Figure 4. Protocol #1. **a)** Aggregation process of Aß42: monitoring over time by CE method A. Electrophoretic profiles of Aß42 at different elapsed times from t0 until precipitation. The negative peak labelled as EOF is due to the perturbation of the aqueous solution where peptide is solubilised, namely 20 mM Na_2HPO_4/NaH_2PO_4. **b)** Plot of the normalized peak area percentage {(peak area/electrophoretic migration time)x100/total area} of Peak A (grey line, diamonds), Peak B (dotted black line, squares) and Peak C (black line, triangles) at different elapsed times from t0 until precipitation (days); each monitoring point is in triplicate, error bars are standard deviations.

As emerges from **Figure 4**, these oligomeric populations are at dynamic equilibrium: the area of Peak A rapidly decreases over time and in turn that of Peaks B and C increase. This suggests that, with the progression of the self-assembly process, the putative small oligomers slowly disappear and contribute to the formation of larger aggregates. At late stage of aggregation, only Peak C is detected.
Since standards are not available, a quantitative evaluation of the oligomer peak area is intrinsically unaccessible. Therefore a semiquantitative analysis based on peak areas normalised on the peak migration times [49] is carried out (**Figure 4b)**).

In addition to the longer time window for the study of aggregation (14 days *vs*. less than a week [35,40-42]), also the goal of an improved separation efficiency has been reached with protocol #1. In fact all three peaks are more efficient than those previously reported [35,40-42]. In particular, the observation of a sharp and efficient peak (Peak C) after a broad band such as Peak B, may suggest the presence of a spike, an electric phenomenon that randomly occurs when microprecipitation events take place in the capillary [32,38,47]. Nevertheless, the high reproducibility of Peak C effective mobility rules out this hypothesis.
Moreover, Peak B and Peak C are at mutual equilibrium over the first 72 hours: the area of Peak B increases at the expenses of that of Peak C and vice versa. This mutual equilibrium is clearly appreciable in **Figure 4b)** and in particular in **Figure 5**.
In theory, the higher longitudinal diffusion of the latest migrating species cannot explain the efficiency of peak C. However, three pieces of evidence support the identification of peak C as protein material: i) the dynamic equilibrium between Peak B and Peak C; ii) the high reproducibility of Peak C mobility; iii) the UV spectrum taken by DAD detector.

a)

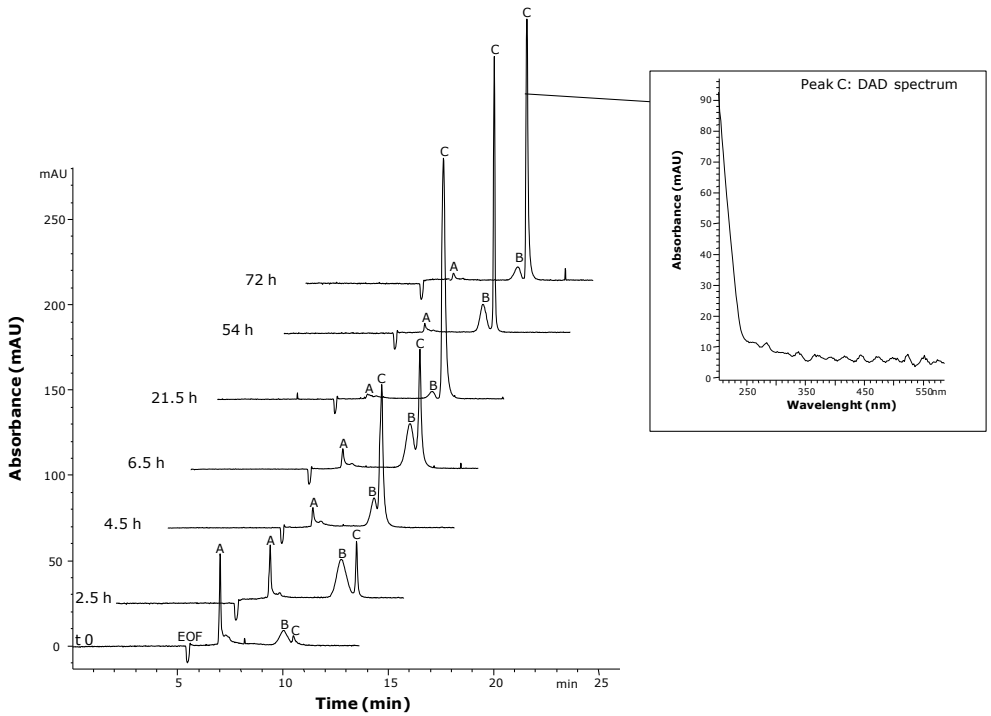

b)

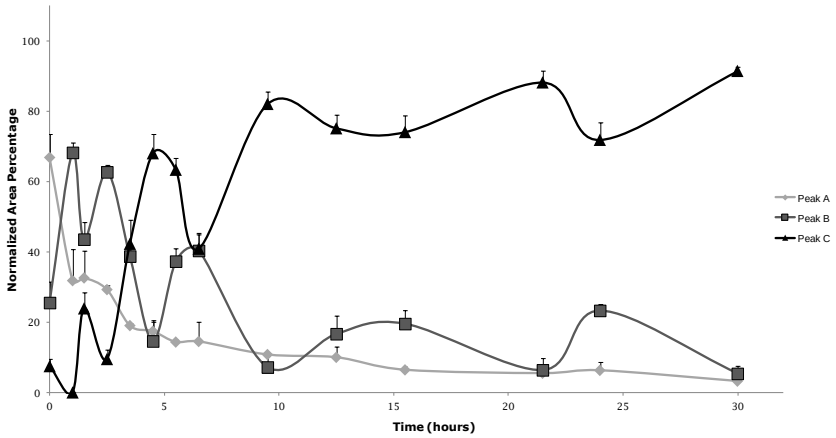

Figure 5. Protocol #1, CE method A. **a)** Detail of the aggregation process of Aß42 within 72 hours: electrophoretic profiles of Aß42 at different elapsed times from t0 up to 72 hours, when equilibrium between Peak B and C is evident. **b)** Plot of the normalized area percentage of Peaks A, B and C focused on the first 72 hours; each experimental point is in triplicate, error bars are standard deviations.

In order to investigate the supplier-to-supplier variability of Aß42 commercial peptide, protocol # 1 was applied using Aß42 provided by Bachem.
Figure 6 shows how the resulting electrophoretic profiles are considerably different from those in **Figure 4a)** and **Figure 5a)**: Peak A is significantly less abundant and at the migration times of Peaks B and C, a group of unresolved peaks is detected probably together with spikes. At 30 minutes from solubilization precipitation occurs. The electrophoretic pattern suggests that the peptide purchased from Bachem is never completely solubilized by using protocol #1.

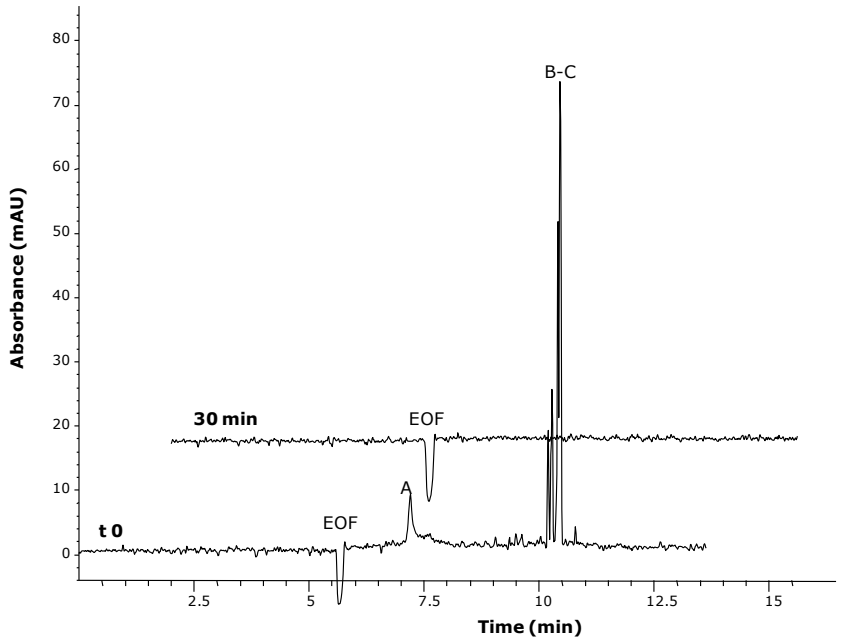

Figure 6. Protocol #1, CE method A. Electrophoretic profiles of Aß42 peptide supplied by Bachem immediately after solubilization (t0) and at 30 minutes when precipitation occurs.

The supplier-to-supplier and even the batch-to batch variability of standard Aß42 solubilization properties is an issue that should have been taken as a priority by all scientists using this peptide in experimental work. Solubility of standard solutions has an obvious impact on the quantity available for any experiment carried out with the prepared solutions and in our context also on the kinetics of oligomer formation. Conversely, to our knowledge a systematic study on different peptide suppliers, albeit limited to the effect on fibril polymorfism, was reported once only [50].

In this respect, as CE works in solution and under quasi physiological conditions, after injection it gives immediate access to semi-quantitative data on the proteinaceous material present in the sample, on the monitoring of the

dynamic formation of oligomeric assemblies over time after solubilization and on the reproducibility of the process.

3.1.2 Protocol #2

DMSO is a highly polar, water-miscible organic solvent which is also commonly used to solubilize Aß peptides. In a vast majority of toxicity studies on cells, highly concentrated Aß (e.g. 5 mM) is dissolved in 100% DMSO and then diluted with PBS [51] or in cell culture medium [52].
Its effect on aggregation is very controversial. Some studies have demonstrated that Aß40 and Aß42 in pure DMSO remain stable in a monomeric α-helical structure and give rise to the so called "unaggregated Aß peptides preparations", or "unaggregated fibril-free preparations" [43], since it prevents the organization of Aß in ß-sheet structures by hindering the formation of hydrogen bonds. Other experiments clarified that 100% DMSO is not sufficient to maintain a concentrated unaggregated peptide solution [48]. Finally, other papers reported that when pure DMSO is diluted with buffer or water, it can immediately induce the formation of oligomeric aggregates and protofibrils [43].
Based on this information, as described in **Figure 3** of Section 2.2, protocol #2 includes a pre-treatment of Aß42 (Anaspec) with HFIP and then a redissolution phase using increasing percentages of DMSO in phosphate buffer. Protocol #2 is intended to obtain smaller oligomeric populations, as compared to protocol #1 or even a single homogeneous monomeric population.

Since the addition of 20% DMSO does not affect the electrophoretic profile of Aß42 as compared with the CE profile obtained using protocol #1 (data shown in Supplementary material at the end of this Chapter, **Figure S1**), the aggregation process in the presence of 50% and 100% of DMSO in the peptide sample is investigated. As in both cases results are comparable, only those obtained by redissolving the liophylized samples in pure DMSO are reported below.
Peaks A, B and C are still present, together with other minor species. The same peak assignment of the first protocol is possible, given that the electrophoretic mobilities are statistically equal to those of peaks detected in samples solubilised with protocol #1. Therefore it is plausible that the size distribution is similar.
Some dissimilarities are found when comparing protocol #2 and protocol #1: here Aß42 is soluble for a longer time and in particular the faster migrating group of peaks is observed even at the 28^{th} day from t0 (**Figure 7a)**). However, as evident in **Figure 7b)**, a dynamic equilibrium between oligomers is not appreciable, as the normalized areas of all peaks detected decrease over time.

a)

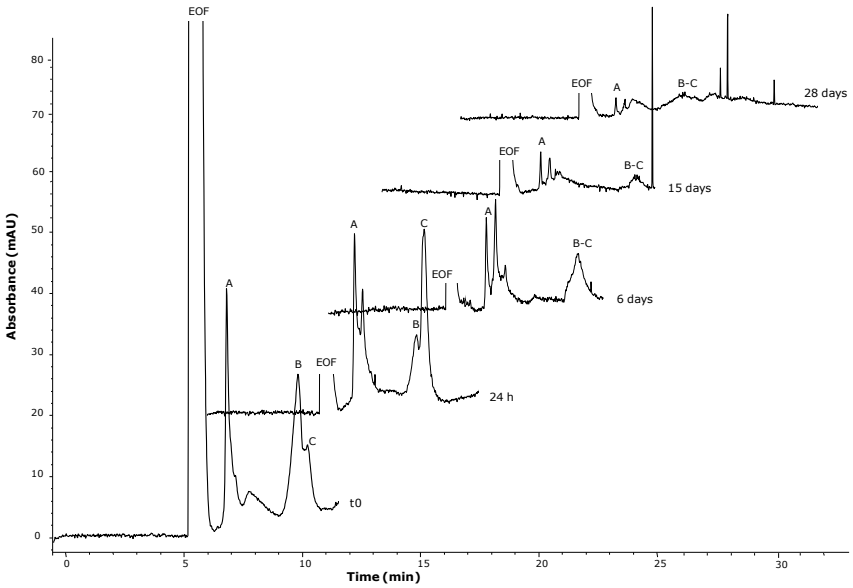

b)

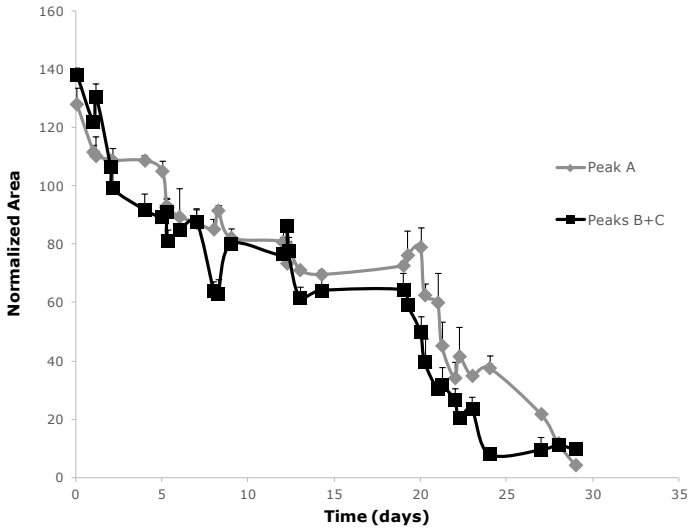

Figure 7. Protocol #2, (CE method A) redissolution in 100% DMSO. **a)** Monitoring of the Aß42 aggregation process from t0 up to 28 days. EOF peak is due to the absorption of DMSO; its signal is simplified for clarity. **b)** Plot of normalized areas of the first population (grey line, diamonds) and second population (Peak B + Peak C: black line, squares). Each experimental point is in triplicate, error bars are standard deviations.

From the CE traces it is demonstrated that in pure DMSO the self-assembly of Aß42 oligomers is slowed down and that the aggregates formed are kept soluble for about one month. Further, the CE traces at t0 show that more than

one population is already separated, therefore 100% DMSO does not produce a single and stable monomeric population.

3.1.3 Protocol #3

Compared to solubilization procedures developed in the past by us [35,40-42] and others [32,36-39,47] by preparing the sample according to protocol #1 the time window for the study of the aggregation process is considerably widened. By CE multiple equilibria are observed (**Figure 4** and **Figure 5**), i.e. that between faster (Peak A) and slower (Peaks B and C) migrating species and that between the putative bigger assemblies (peak B and peak C). However, the putative small oligomers rapidly contribute to the formation of large aggregates by progressively decreasing the area of Peak A, so that little information about smaller species is obtained.

In order to shift the aggregation process towards low molecular weight (LMW) oligomers, Aß42 was solubilized following a protocol set up by Andrisano and co-workers in 2007 [44]. When using this sample preparation (here defined as protocol #3), Aß42 purchased from Bachem was employed, to accurately replicate what reported by Bartolini *et al*. They showed that this procedure provides a solution containing the monomeric form of Aß42 [31] along with oligomers. By a multimethodological approach including MALDI-TOF; AFM, ESI-IT MS, CD and ThT fluorescence, they demonstrated the formation of assemblies ranging from monomers up to decamers immediately after solubilization, and of higher molecular weight (HMW) oligomers within 12 hours. The combination of different techniques becomes necessary to support MS data. MALDI-TOF MS and ESI-IT MS have limitations in the detection of HMW oligomers, because of the low ionization capability and the possible disaggregation in the ESI source, respectively [29]. Therefore the self-assembly of Aß42 into large aggregates can be inferred from monomer disappearance rather than from the evidence of HMW assemblies building up over time [31].

Protocol #3 is less aggregating than the first two protocols (see Section 2.2 and **Figure 3**). This could be explained by the longer contact time of lyophilized Aß peptide with HFIP: 24 hours for protocol #3 *vs* 30 minutes for protocol #1 and protocol #2. Moreover, the treatment of Aß42 in the redissolution step with ACN and with the basic mixture (NaOH and Na_2CO_3) keeps Aß peptide in a non amyloidogenic conformation, as Bartolini *et al.* demonstrated by CD analyses [44]. The basic mixture is essential for the solubility of Aß peptide purchased from Bachem: in particular ACN stabilizes disorganized and α-helix structures and NaOH increases the solubility of the acidic Aß peptide. This is not the case for the peptide from Anaspec, as

demonstrated by the complete solubilization using protocol #1 where basification is omitted. If this step is skipped in protocol #3, i.e. if the protocol becomes more similar to protocol #1, despite the longer contact with HFIP, Aß42 from Bachem still is not solubilized and precipitation occurs within 24 hours from t0 (see **Figure S2** in Supplementary material).

It has to be pointed out that Aß42 supplied by Anaspec and solubilized according to protocol #3 shows the same electrophoretic profile of the Bachem peptide (data not shown).
In view of what reported above, once again the issue of supplier-to-supplier variability is raised: clearly a given protocol cannot be applied to any purchased peptide standard but it strongly depends on the supplier. In particular methods of synthesis and purification must be source of variability. Notably, batch-to-batch variations in the declared degree of purity may be found as well as different instructions for standard peptide solubilization within the same supplier and among different suppliers.

Immediately after solubilization following protocol # 3, Aß42 is injected in CE and its self-assembly is monitored over time by an optimized CE method (method B). Optimization included the evaluation of different capillary lengths, different injection parameters, different types of injections (e.g. short-end), different voltages. Final conditions are reported in Section 2.3. As compared to method A [42], because of the shorter capillary (L=33 cm), CE method B ensures faster analysis time (less than 7 minutes) while peak efficiency is kept.

Electrophoretic profiles and mobilities are statistically different from those obtained by samples prepared according to the first and second protocols, in particular for the narrow early bands. Therefore, Peaks 1, 2 and 3 are identified on the basis of precise effective electrophoretic mobilities reported in **Table 2** as average values of 5 independent experiments. This may indicate that, especially for the first population, oligomers of different size could be formed.

	Peak 1	**Peak 2**	**Peak 3**
μ_{eff} ($cm^2V^{-1}s^{-1}$)	-9.79×10^{-5}	-1.19×10^{-4}	-2.36×10^{-4}
SD	$\pm 5.78 \times 10^{-7}$	$\pm 1.13 \times 10^{-6}$	$\pm 2.18 \times 10^{-6}$
RSD	0.59%	0.95%	0.92%

Table 2. Protocol #3. Effective electrophoretic mobilities (μ_{eff}) of Aß42 oligomeric populations obtained with protocol #3 by CE method B. μ_{eff} ($\mu_{eff} = \mu_{app} - \mu_{EOF}$) are calculated by subtracting, from the apparent peak mobility (μ_{app}), the contribute of the EOF (μ_{EOF}). μ_{eff}, standard deviation (SD) and relative standard deviation (RSD) values are calculated for 10 monitoring points of 5 independent experiments (n=5).

From electrophoretic traces shown in **Figure 8** it emerges that the faster migrating population consists of two peaks (Peak 1 and Peak 2) at dynamic equilibrium: Peak 1 slowly contributes to the formation of Peak 2. A progressive reduction of both Peaks 1 and 2 area is observed and the slower

migrating and broad band, namely Peak 3, is built up. This dynamic equilibrium is made clearer in the normalized area graph illustrated in **Figure 8b)**. Therefore, considering the electrophoretic mobilities, the aggregation is slowed down to such an extent that an equilibrium among the putative small species is observed by CE. Furthermore, Aß42 oligomers are soluble for about one month until precipitation occurs and no more peaks are detected in CE.

a)

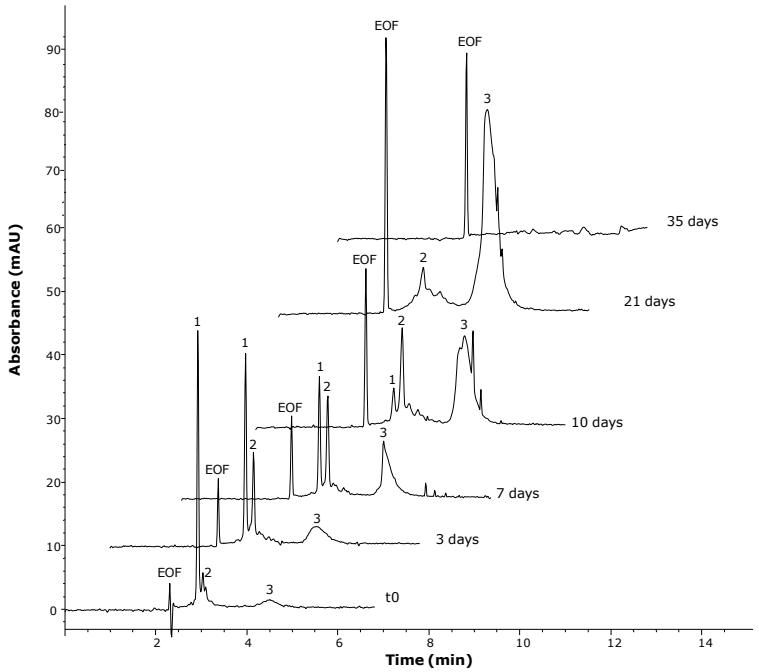

b)

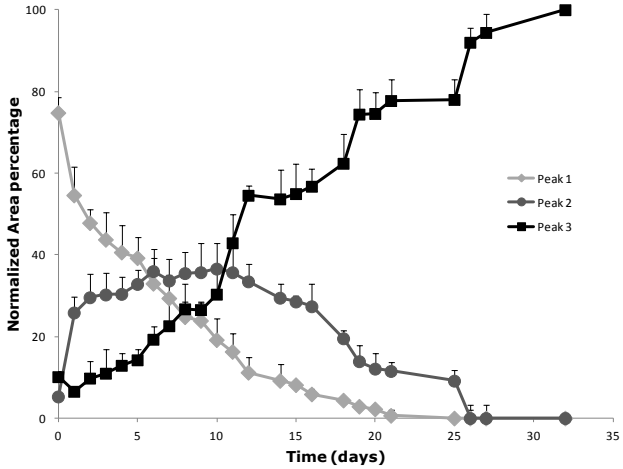

Figure 8. Protocol #3. **a)** Aggregation process of Aß42: monitoring over time by CE method B. Electrophoretic profiles of Aß42 at different elapsed times from t0 until precipitation. **b)** Plot of the normalized area percentage of Peak 1 (grey line, diamonds), Peak 2 (dark grey line, dots) and Peak 3 (black line, squares) at different elapsed times from t0 until precipitation (days); each monitoring point is in triplicate, error bars are standard deviations.

As evident in **Figure 8a)** by using protocol #3, the EOF shows a positive absorbance which increases slowly over time as opposed to the negative peak seen in traces obtained with protocol #1 (**Figure 4a)** and **Figure 5a)**). This difference is due to the different solvent in which Aß42 is solubilized: 20 mM phosphate buffer in protocol #1 *vs* phosphate buffer ACN, NaOH and sodium carbonate in protocol #3. In particular, in this basic milieu, the hydrolysis of ACN in two steps is possible [53].

$$CH_3CN \xrightarrow[-OH]{+H_2O} CH_3CONH_2 \xrightarrow{+NaOH} CH_3COO^-Na^+ + NH_3$$

Figure 9. Hydrolysis of ACN in a basic milieu [53].

Although the reaction is promoted by high temperatures, the degradation of ACN is also possible at room temperature. Acetamide and sodium acetate are characterized by a wavelength of maximum absorption (λmax) of 208 nm and 204 nm, respectively. Therefore, since the λmax of products are close to the operating wavelength (λ=200 nm) their absorption is higher compared to that of reagents.

3.2 Fibril formation: TEM analyses

Amyloid fibrils are characterized by a specific morphology: they are typically unbranched, linear structures composed of filaments which are twisted with regular helicity, with a diameter in the range of 7-13 nm. Therefore, amyloid fibrils are distinguished from amorphous aggregates when observed by transmission electron microscopy (TEM) [4,5,54].

Since TEM is the most common technique employed in the study of fibril morphology, precipitated samples of Aß42 peptide prepared by following the three solubilization protocols are analyzed by TEM.

Immediately after solubilization and when precipitation occurs, namely no more peaks are detected in CE and samples are visibly cloudy, Aß42 samples are fixed as described in Section 2.4 and observed at TEM.

In **Figure 10** the transmission electron microscopy images are reported as representative of three independent experiments for each sample at t0 and at the end of the aggregation process (tend). It is evident that typical amyloid fibrils are formed when preparing samples according to both protocol #1 and protocol #3. Interestingly, insoluble fibrils are present even at t0, this means that these *in vitro* aggregation processes simulate that *in vivo*, since in the brain, oligomers and fibrils are at equilibrium.

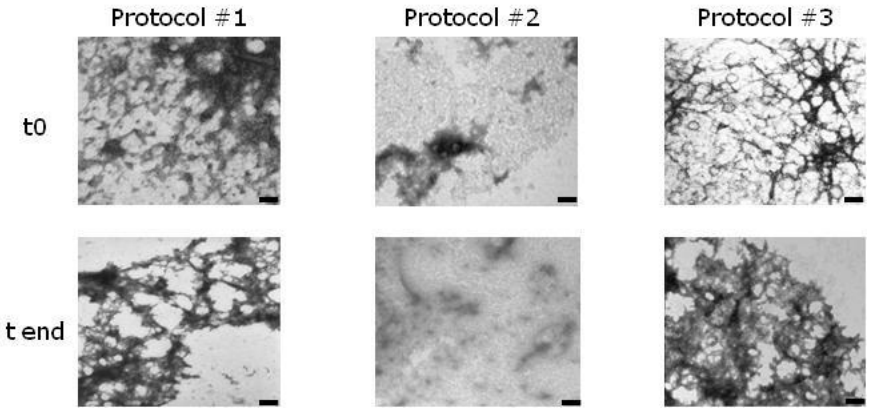

Figure 10. Transmission electron microscopy images of Aß42 prepared with protocols #1, #2 and #3 immediately after solubilization (t0) and at the sample precipitation (tend), (n=3). Scale bar: 100nm.

Conversely, for samples prepared according to protocol #2 (**Figure 10**), neither are fibrils present immediately after solubilization nor at the end of the process: Aß42 in the presence of DMSO precipitates as amorphous aggregates. This could explain also the observed absence of dynamic equilibrium between oligomers. A further limitation that hinders any further investigation is that the CE data obtained feature a DMSO concentration that is toxic for neuroblastoma cells and chemically incompatible with ultrafiltration devices.

3.3 Characterization of oligomers in solution

The structural characterization of Aß oligomers consists in elucidating the structure and size of the aggregates. Characterization represents a critical step in the aggregation studies, because of the transient nature of Aß42 assemblies which readily convert into other conformations.

3.3.1 Size distribution of Aß42 oligomers: UF experiments

In order to roughly assign a range of MW to the oligomers analytically separated by CE, ultrafiltration (UF) experiments are carried out at selected elapsed times from solubilization according to the relative abundance of peak areas observed by CE. The characterization of assemblies is made by considering membrane specifications provided by the manufacturer. By UF it is only possible to assign a range of MW.

Immediately after ultrafiltration, filtrated and retained solutions are injected in CE. The electropherograms obtained are compared to that of the entire peptide analyzed before UF experiments and taken as control.
The effective mobilities of species detected in the filtrated and retained solutions are statistically equal to those of the corresponding controls (unfiltrated samples), as reported in **Table 1** and **2**. Based on this data as well as on the comparison of electrophoretic patterns before and after ultrafiltration (**Figure 11**), it can be concluded that the aggregation process is not affected by the procedure and association/dissociation phenomena can be ruled out.

As an example of analyses carried out at least in triplicate, electrophoretic traces are reported in **Figure 11**. In order to evaluate the performance of the procedure, for all experiments the recovery percentage of filtrated and retained solutions is calculated on the basis of peak areas detected by CE. In **Table S1** (Supplementary Material), the recoveries are reported as mean ± SD. The RSD values associated are <15%.

Ultrafiltration presents several intrinsic limitations. However in general, it is reasonable to consider that, while the amount found in filtrated solutions has to be entirely ascribed to actual filtrated protein material, the amount found in the retained solution can partly be constituted by oligomers retained on the filter not necessarily retained by virtue of their size. Moreover because of the geometry of the membranes, the recovery of retained sample is critical and therefore the amount can be underestimated. For this reason the recoveries associated to the filtrated solutions are more reliable than those of the retained solutions.

All separated species obtained for samples solubilised by protocol # 1 and protocol #3 are smaller than 100 kDa, since the sample is quantitatively

recovered in the filtrated solution when using 100 kDa cutoff membrane (**Figure 11 a)**).

Figure 11b) shows the results on a 50 kDa cutoff membrane: bearing in mind that the MW of Aß42 monomer is 4514.1 Da, it can be derived that faster migrating species consist of oligomers which are equal or smaller than decamers. Since slower migrating bands are not detected in the filtrated solution, these species (Peaks B and C for protocol #1 and Peak 3 for protocol #3) are ranging from decamers up to 22-mers, because they are bigger than 50 kDa and smaller than 100 kDa. Incidentally, we can confirm the hypothesis that mass prevails over charge in governing migrations observed.

To better characterize small oligomers ($\leq$ decamers) cutoff membranes lower than 50 kDa are used.

As far as the sample prepared according to protocol #1, in **Figure 11c)**, the species migrating under Peak A would correspond to an heterogeneous population of oligomers of different size, since Peak A is partly filtrated and mostly retained by 30 kDa cutoff membrane; as in **Figure 11d)** it is clear that a 10 kDa cutoff membrane retains all species, it can be derived that oligomers migrating under Peak A include trimers up to decamers.

As far as the sample prepared according to protocol #3, assemblies migrating under Peaks 1 and 2 are quantitatively filtrated through a 30 kDa cutoff membrane. Interestingly, both peaks are partially filtrated and partially retained by a 10 kDa membrane.

It can be concluded that by sample preparation protocol #1, the solution obtained contains oligomers in the range of trimers up to decamers (separated and detected by CE-UV as Peak A) and of decamers up to 22-mers (Peak B and Peak C).

As expected, Protocol #3 results in smaller aggregates: monomers and dimers are the most abundant assemblies (Peaks 1 and 2), whereas the slower Peak 3 corresponds to decamers up to 22-mers.

a)

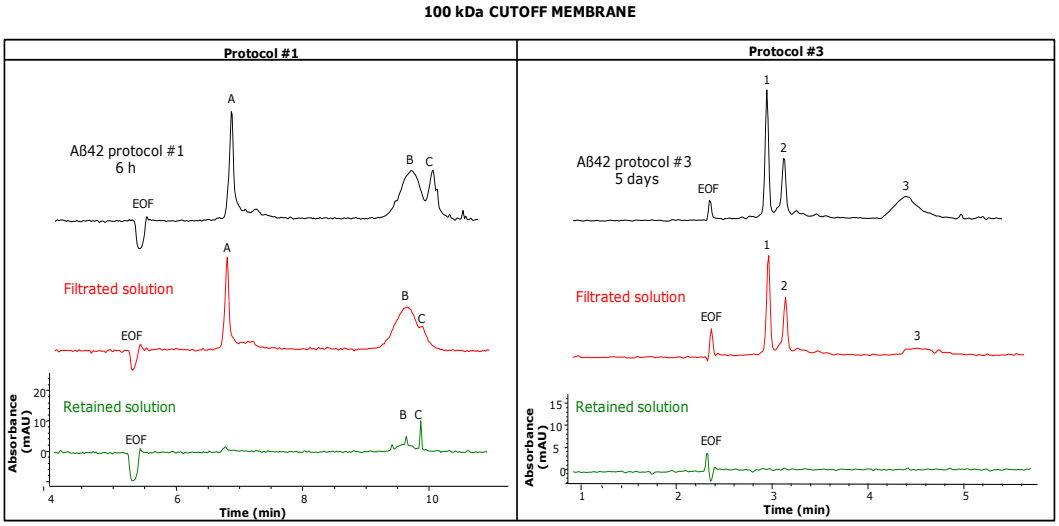
100 kDa CUTOFF MEMBRANE
Protocol #1
Protocol #3
Aß42 protocol #1
6 h
Aß42 protocol #3
5 days
Filtrated solution
Retained solution
EOF
A
B
C
1
2
3
Absorbance (mAU)
Time (min)

b)

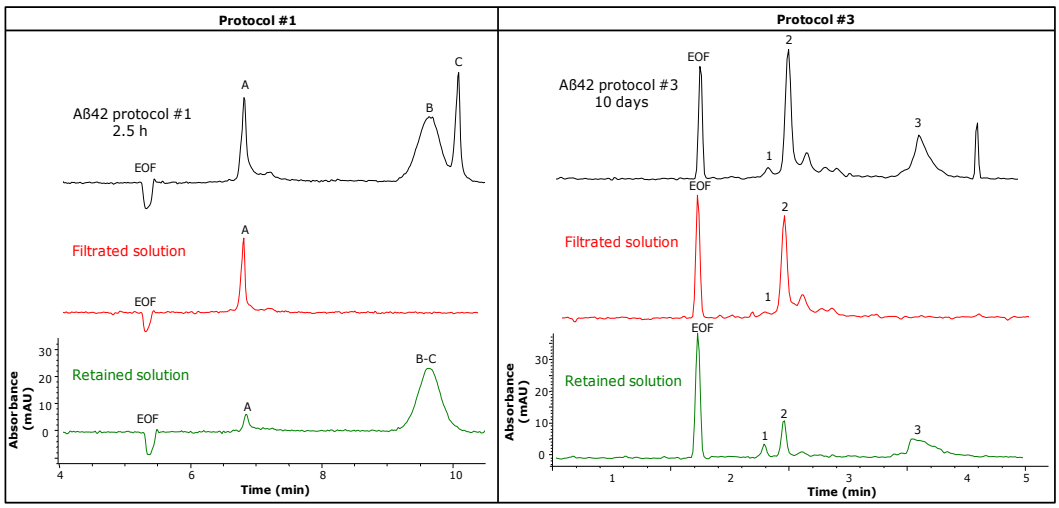
50 kDa CUTOFF MEMBRANE
Protocol #1
Protocol #3
Aß42 protocol #1
2.5 h
Aß42 protocol #3
10 days
Filtrated solution
Retained solution
EOF
A
B
C
B-C
1
2
3
Absorbance (mAU)
Time (min)

c)

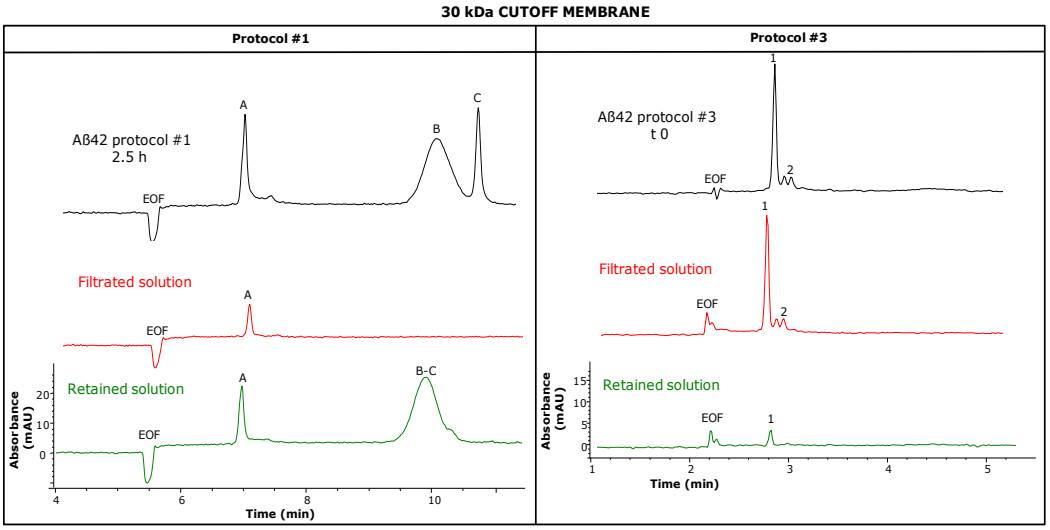

d)

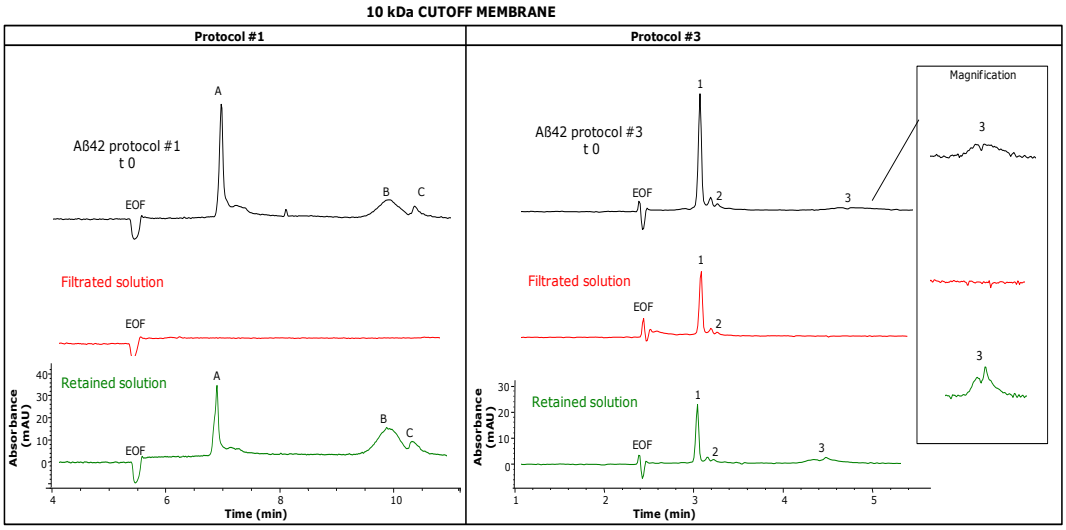

Figure 11. Ultrafiltration experiments and injection of Aß42 in toto (black trace), filtrated (red trace) and retained solutions (green trace) in CE. **a)** UF with 100 kDa cutoff membranes. **b)** UF with 50 kDa cutoff membranes. **c)** UF with 30 kDa cutoff membranes. **d)** UF with 10 kDa membranes. All experiments are in triplicate.

3.3.2 Size distribution of Aß42 oligomers: SDS-PAGE/Western Blot

As well established, the presence of surfactants may induce oligomer dissociation [18,33]. Nevertheless, SDS-PAGE/WB remains one of the most widespread techniques for Aß characterization [6]. For this reason, and also to corroborate the characterization data of Aß42 oligomers in solution obtained by UF experiments, the size distribution of Aß42 assemblies is carried out also by SDS-PAGE.

Aliquots of Aß42 solution prepared by protocol #1 are withdrawn at selected elapsed times from solubilization (t0, 2.5 h, 81 h and 126 h) and loaded on SDS-PAGE gel, as described in Section 2.6. Immediately before each SDS-PAGE analysis at the mentioned time intervals, a portion of the same sample is injected in CE, so to obtain the CE oligomeric profile in solution (**Figure 12a)**) of the sample analyzed by SDS-PAGE. Based on the Western Blot (WB) analyses shown in **Figure 12b)**, bands ranging from dimers up to 22-mers are detected. This is the same range of molecular weight assigned by UF experiments, however there are some discrepancies.
First, by CE large oligomers are detected starting from t0; inexplicably, bands at high molecular weight are revealed by antibody 6E10 only at late stages of the aggregation process. Second, bands corresponding to small species of Aß42 are detected in Western Blot even when (81 h, 126 h) the CE Peak A has already totally converted them into large aggregates. This could be reasonably due to the different sensitivity associated to the techniques.

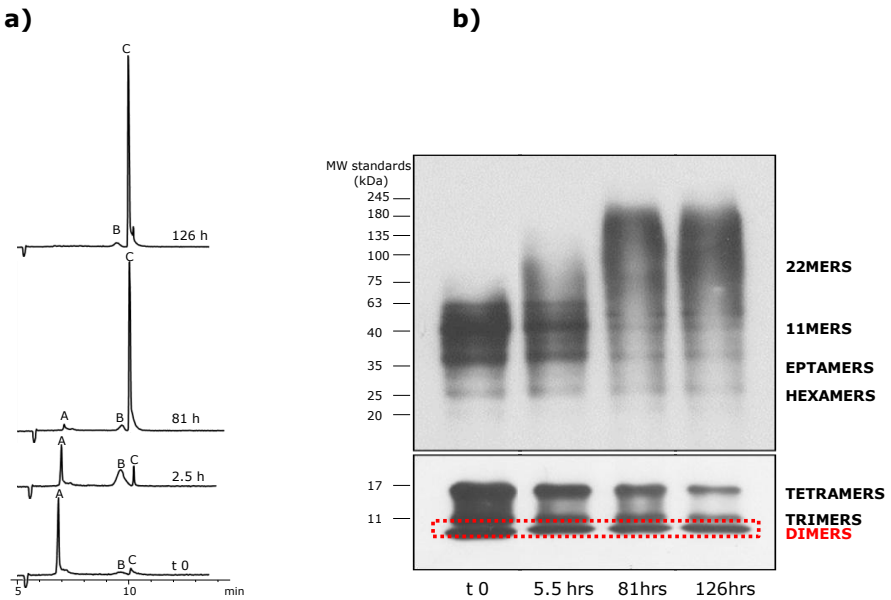

Figure 12. Aß42 oligomers size distributions by SDS-PAGE/Western Blot analyses. **a)** CE samples of Aß42 prepared by protocol #1 analyzed at selected elapsed times. **b)** WB analyses of Aß42 peptide sampled at selected elapsed times.

Notably, WB analyses show constant and abundant presence of dimers (MW around 9 kDa), not only at t0 but also at longer times, when from CE data any small oligomer population has clearly converted into higher MW species. According to the specifications provided by the manufacturer of the membranes, if dimers were present at early times, not only the filtrated solution in **Figure 11c)** should filtrate them, but also a quantitative amount should have been observed in **Figure 11b)**. Thus, it is concluded that UF data rule out the presence of dimers in free solution and that dimers observed by WB may well be an artefact due to oligomer disaggregation into dimers induced by SDS. That SDS-PAGE might not always reflect the exact content of the different Aß species present in a sample had been already reported [55].

3.3.3 Secondary structure of Aß42 oligomers: IR spectroscopy

Knowledge of the structural basis of peptide-peptide interactions that lead to Aß42 oligomers and in turn to fibrils may provide an insight to the underlying aggregation mechanism and therefore suggest a way to prevent protein aggregation.

One of the relatively few techniques that can be used to determine the conformation of aggregated proteins is Attenuated Total Reflectance-Fourier transform infrared spectroscopy (ATR-FTIR), where the sample is dried on a high-refractive index material as a thin film. As a result, ATR-FTIR is an extremely sensitive method to analyze protein secondary structure in aqueous samples.

By FTIR spectroscopy, secondary structures such as ß-sheets, α-helix conformations as well as random coil regions can be identified based on the analysis of the amide I (1700-1600 cm^{-1}) region. As far as the antiparallel ß-sheet structures, the amide I region displays two typical components: the major component has an average wavenumber located at ~1630 cm^{-1}, whereas the minor component is about 5-fold weaker than the major one and it is characterized by an wavenumber located at ~1695 cm^{-1}. As reported in literature [46], while for parallel ß-sheets the amide I region is characterized only by the major component, the 1695/1630 intensity ratio has been described to be proportional to the percentage of antiparallel arrangement of the ß-strands in a ß-sheet [56]. The absorbance of α-helical and random coil structures is observed at 1657 cm^{-1} [57,58].

As from literature, FTIR spectra of Aß42 fibrils confirm that they are rich in ß structure [59]. To our knowledge there are no studies on the characterization by ATR-FTIR of different oligomeric populations isolated from a solution where they are at dynamic equilibrium along the fibril formation pathway. Indeed two studies reported the characterization of Aß42 oligomers by ATR-FTIR [46,60]. By using dedicated sample preparation protocols, Stroud *et al*., prepared Aß42

oligomers of 60 kDa, as determined by SEC, and reported that their ß-sheet structure is antiparallel; Cerf *et al*. prepared instead an heterogeneous population of "large oligomers" (in the range 40-170 kDa, as assessed by Western Blot analysis) that resulted to have a higher percentage of ß-sheet and a lower percentage of random coil. In both studies the oligomeric structures were compared to those of preformed fibrils.

As reported above, the solubilization of Aß42 by following protocol #1 (**Figure 11)**, leads to two electrophoretic populations: oligomers ranging from trimers up to decamers (Peak A) and oligomers bigger than decamers but smaller than or equal to 22-mers (MW lower than 100 kDa, Peak B and C). By ultrafiltrating the peptide solution through 50 kDa cutoff membrane, it is possible to isolate small oligomers (trimers-decamers) from larger Aß42 assemblies (undecamers-22-mers): this gives access to three different solutions (whole peptide, filtrated and retained portions) that can be independently evaluated by ATR-FTIR.

Figure 13 shows the results obtained, where the traces are representative of one out of three replicates. These are intended as preliminary data, as proper quantitative analysis has not yet been carried out. Nevertheless important qualitative information can be derived.

In **Figure 13a)** secondary structure analyses of samples are reported as deconvoluted spectra obtained by applying Fourier spectra deconvolution (FSD), whereas in **Figure 13b)** second derivatives are shown.

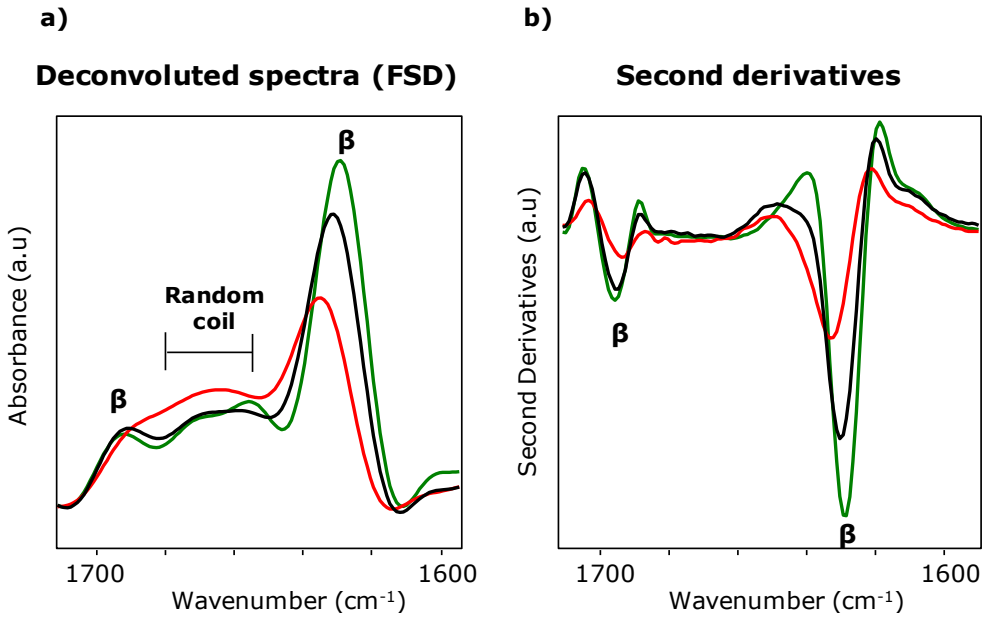

Figure 13. ATR-FTIR spectroscopy analyses. **a)** Deconvoluted spectra obtained by Fourier spectra deconvolution (FSD) and **b)** second derivatives spectra are collected for Aß42 peptide *in toto* (black trace), 50 kDa-filtrated solution (red trace) and 50 kDa-retained solution (green trace).

In all three samples analyzed, all the components mentioned above are present. The filtrated solution is characterized by the lowest amount of ß-sheets, as compared to that of the entire peptide and to that of the retained solution, in increasing order. Further, there is an increase of random coil in small aggregates in respect to the other samples. In the filtrated solution a shift of the band at ~1630 cm^{-1} towards higher wavenumbers is evident. This may indicate that the ß-sheets are more relaxed and hydrogen bonds are weaker in small oligomers than in large aggregates. In large aggregates the band at ~1695 cm^{-1} is substantially lower than in small oligomers or in the entire peptide.
These findings are consistent with what expected from the size of the species and from their dynamic equilibrium over time which is described as the progressive conversion of smaller species into larger ones to finally form fibrillar deposits.

3.4 Assessment of Aß42-induced neurotoxicity

By taking advantage of the possibility to isolate oligomeric populations formed in a solution, cell toxicity experiments are carried out on human neuroblastoma cells (see Section 2.8), a cellular model sensitive to Aß-induced cell death.
As already demonstrated, differences in oligomeric size mirror a diverse secondary structure and a different electrophoretic profile. Based on this consideration, it is plausible that different oligomeric populations spanning a wide MW range could explicate different toxicity and therefore could have different biological roles.
Therefore, SH-SY5Y neuroblastoma cells are exposed to the entire Aß peptide solution after 10 days from solubilization and to oligomers obtained after ultrafiltration of this solution on 50 kDa membrane (protocol #3, **Figure 11b)**).

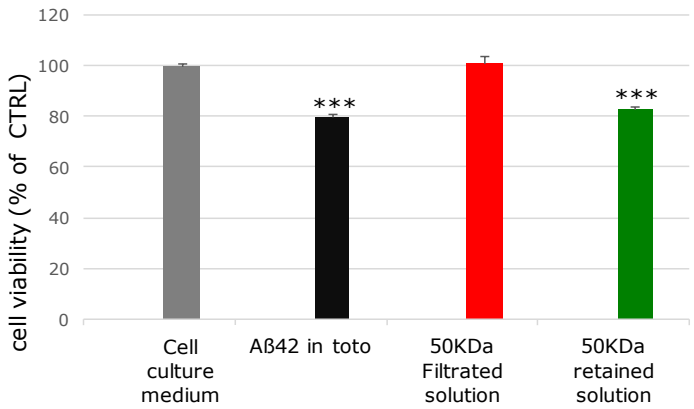

Figure 14. Toxicity test of Aß42 peptide: Data are expressed as cell viability percentage of control (CTRL, cell culture medium); error bars represent SEM. Analyses are performed on two independent experiments, n=4 replicates. ***$p<0.0001$ *vs* no treated cells, ANOVA + post-hoc Dunnett's test.

In **Figure 14** it is clear that Aß42 *in toto*, where both populations are abundant, induces a significant loss of cell viability. It is also clear that the cell toxicity of the entire peptide is to be ascribed to the large band migrating at later times in CE. Therefore, we can conclude that the oligomers bearing a MW between 50 and 100 kDa are toxic species on neuroblastoma cells, whereas small aggregates do not exert toxic effect.

4 Conclusions and remarks

Although incomplete, the current knowledge suggests that in the human brain different aggregation states of Aß (monomers and oligomers of different size) are at dynamic equilibrium with each other and with the amyloid fibrils [2,4,6,54]. Thus, there is a great need to fully characterize the soluble prefibrillar Aß oligomers, to establish which forms are the most toxic for the neurons and to investigate their physiological and pathological role. The information gained forms the basis for the selection of small molecules that would inhibit the Aß fibril formation at the oligomerization steps.

Enormous efforts have been made to generate this knowledge by applying numerous advanced techniques, as discussed below. However, the accomplishment of the relationship between size, structure and toxicity of Aß42 oligomers remains unclear. This is due to the transient nature of Aß aggregates and to the fact that each technique is not devoid of limitations and drawbacks. Therefore, it would be advisable to study Aß assemblies by an array of techniques which can provide different information.

In this part of the work, it has been demonstrated that a separative micro-technique like CE can play an alternative and unique role in the aggregation studies of Aß oligomers performed *in vitro*. CE is characterized by simplicity, low consumption of Aß peptides, speed of analysis, and above all it allows a real snapshot of the oligomers forming during the amyloid process.

The most amyloidogenic peptide (Aß42) is less frequently used in *in vitro* studies because of its highly aggregation tendency and in turn because of difficulties in its handling.
With this analytical platform, we were able to monitor over time the aggregation process of Aß42 obtaining high reproducible data, without the use of chaotropic agents and without the formation of covalent links.
The effect of solvents used in Aß solubilization protocols on oligomers formed is evaluated by the electrophoretic pattern of Aß42. Amyloid assemblies migrate in the separation capillary as a variety of peaks with a different mobility. Therefore, we first showed how different solubilization protocols lead to oligomers with a different electrophoretic mobility.

By using UF membranes, a size distribution of aggregates was correlated to the electrophoretic peaks: large aggregates ranging from 50 to 100 kDa migrate under slower migrating species, on the other hand, the first oligomeric population seen in electrophoretic pattern corresponds to small assemblies. In particular, we found that with a less aggregating protocol (protocol #3), monomers and dimers are detected whereas, with a more aggregating protocol (protocol #1) trimers represent the smallest specie formed. This finding is in contrast with what obtained by SDS-PAGE, as it is highly possible that the

formation of dimeric forms of Aß42 is an artefact of SDS-induced disaggregation.
Based on the characterization of oligomers and on their electrophoretic behavior, CE is able to monitor the equilibrium between soluble oligomers since for both protocols #1 and #3 small aggregates convert into larger species over time. In particular, by using protocol #1, it is demonstrated that CE provides a real snapshot of the mutual equilibrium between large oligomers (obtained with protocol #1). Since CE works in free solution, the conversion of the non-covalent assemblies into one another is clearly revealed.

Nevertheless, these studies remain challenging because of the high variability of synthetic peptides: from our investigations the inter- and intra-batch variability as well as the supplier-to-supplier variability represented important issues. As mentioned, this reproducibility issue includes toxicity as well.
Consequently, it is essential to assess the toxicity of each Aß42 oligomers for any preparation used. By UF, we were able to evaluate the toxic effect of small and big aggregates, independently.

The possibility to physically separate by UF assemblies of different MW has important implications also in structural investigations. To our knowledge, for the first time ATR-FTIR investigations were performed on separated oligomers. The differences found in secondary structure are in agreement with the different oligomeric size distribution of small and large aggregates.

Interestingly, by standardizing solubilization procedures for Aß42, identified and separated oligomers can be considered as independent targets in coincubation studies, to evaluate the potential antioligomeric and/or antifibrillogenic effect of compounds. This is the subject of the next chapter.

Supplementary material

Figure S1 reports the electrophoretic traces of Aß peptide redissolved in 20% DMSO in phosphate buffer. It is evident than no appreciable qualitative differences are detected between this sample and Aß prepared by following protocol #1.

a)

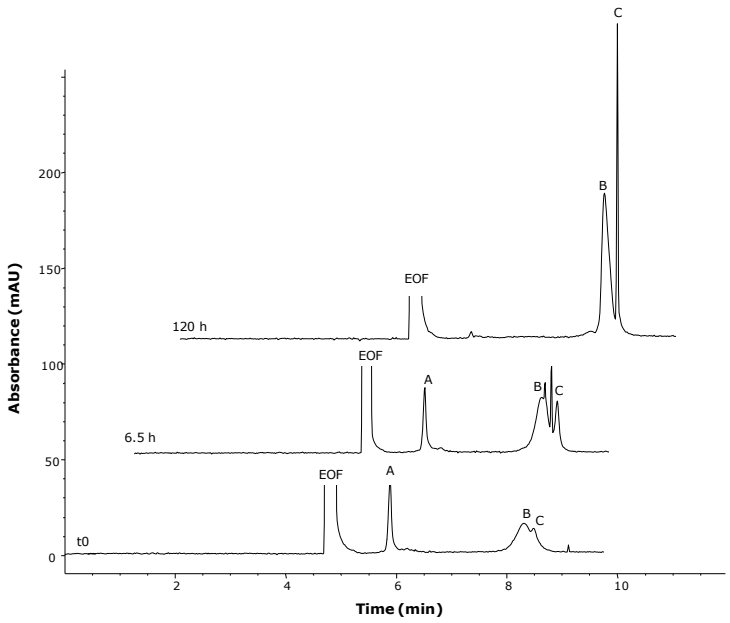

b)

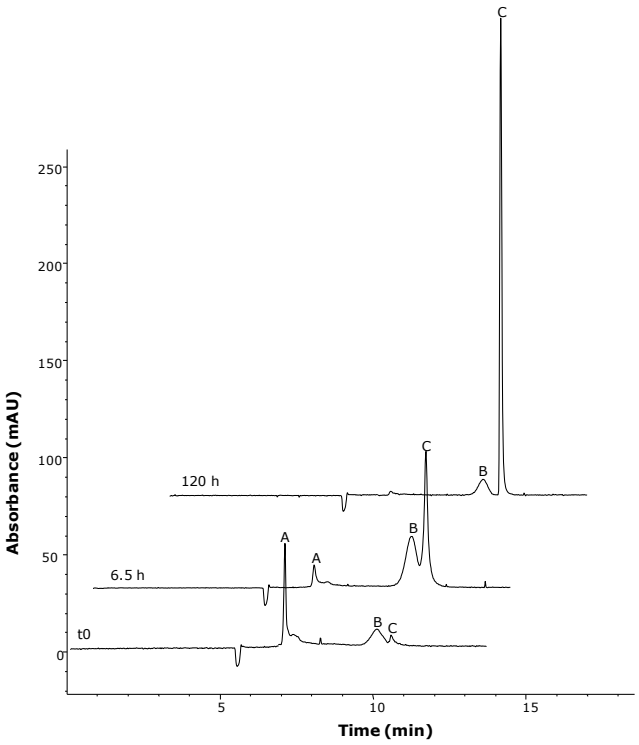

Figure S1. Protocol #2, CE method A. a) Electropherograms of Aß42 solubilised by following protocol #2 and diluted with 20% DMSO in phosphate buffer. Aß42 sample is injected in CE at different elapsed times. b) Electrophoretic traces of Aß42 solubilized with protocol #1 and analyzed at the same elapsed times.

Protocol #3

Modification of protocol #3. Despite the longer contact time with HFIP as compared to protocol #1, if Aß42 (Bachem) after the first step of solubilization is directly redissolved in 20 mM phosphate buffer, sample precipitation occurs after 24 hours.

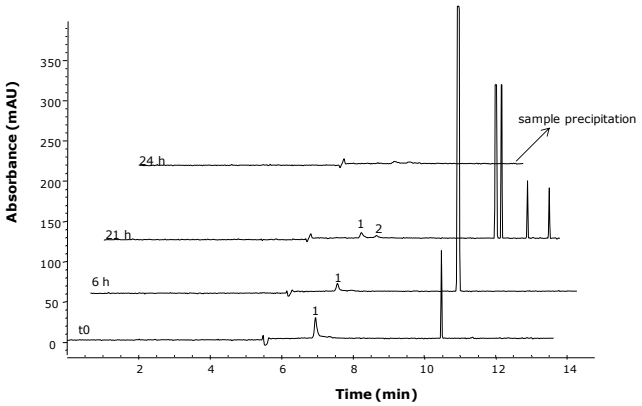

Figure S2. Electrophoretic profile of Aß42 (Bachem) analyzed by CE method A. Aß42 peptide is solubilized by omitting the dissolution phase with the basic miture (ACN/300 µM Na_2CO_3/250 mM NaOH).

Ultrafiltration

In **Table S1** filtrated and retained recoveries of UF experiments are reported. (see **Figure 11**). Recovery is calculated as Area counts (of each filtrated or retained peak)/Area counts (of each unfiltrated peaks).

Sample preparation protocol #1

100 KDa cutoff	Peak A	Peak B	Peak C
Filtrated recovery	**77.4%** ± 7.1	**83.6%** ± 5.2	**40.8%** ± 0.8
RSD	9.3%	6.3%	1.9%
Retained recovery	/	/	**24.8%** ± 3.7
RSD	0%	0%	14.8%

50 KDa cutoff	Peak A	Peak B +C
Filtrated recovery	**62.9%** ± 6.2	/
RSD	9.8%	0%
Retained recovery	**23.8%** ± 1.8	**72.5%** ± 1.3
RSD	7.6%	1.8%

30 KDa cutoff	Peak A	Peak B +C
Filtrated recovery	**16.8%** ± 0.6	/
RSD	3.7%	0%
Retained recovery	**58%** ± 2.3	**72.4%** ± 7.4
RSD	3.9%	10.2%

10 KDa cutoff	Peak A	Peak B	Peak C
Filtrated recovery	/	/	/
RSD	0%	0%	0%
Retained recovery	**74.9%** ± 10.2	**67.3%** ± 1	**84.7%** ± 3.7
RSD	13.6%	1.4%	4.3%

Sample preparation protocol #3

100 KDa cutoff	Peak 1	Peak 2	Peak 3
Filtrated recovery	**68.9%** ± 5.7	**86.7%** ± 9.3	**78.5%** ± 5.3
RSD	8.3%	10.7%	6.7%
Retained recovery	/	/	/
RSD	0%	0%	0%

50 KDa cutoff	Peak 1	Peak 2	Peak 3
Filtrated recovery	**63.8%** ± 2.7	**82.6%** ± 5.5	/
RSD	4.2%	6.6%	0%
Retained recovery	**36.8%** ± 1.2	**21.7%** ± 2.7	**68.1**% ± 5.1
RSD	3.2%	12.6%	7.4%

30 KDa cutoff	Peak 1	Peak 2	Peak 3
Filtrated recovery	**90.5%** ± 1.7	**79.3%** ± 3.1	/
RSD	1.9%	3.8%	0%
Retained recovery	/	/	/
RSD	0%	0%	0%

10 KDa cutoff	Peak 1	Peak 2	Peak 3
Filtrated recovery	**49.9%** ± 5.7	**53.5%** ± 6.3	/
RSD	11.5%	11.7%	0%
Retained recovery	**50.6%** ± 7.5	**61.8%** ± 9.2	**101.6%** ± 4.7
RSD	14.8%	14.9%	4.6%

Table S1. Filtrated and retained recoveries. Data are mean ± SD, also RSD is reported for n=3.

5 References

1 Winblad, B. et al. (2016) Defeating Alzheimer's disease and other dementias: a priority for European science and society. *Lancet Neurol* 15, 455-532

2 Benilova, I. et al. (2012) The toxic Abeta oligomer and Alzheimer's disease: an emperor in need of clothes. *Nat Neurosci* 15 (3), 349-357

3 Jan, A. et al. (2011) Abeta42 neurotoxicity is mediated by ongoing nucleated polymerization process rather than by discrete Abeta42 species. *J Biol Chem* 286 (10), 8585-8596

4 Chiti, F. and Dobson, C.M. (2017) Protein Misfolding, Amyloid Formation, and Human Disease: A Summary of Progress Over the Last Decade. *Annu Rev Biochem* 86, 35.1-35.42

5 Gillam, J.E. and MacPhee, C.E. (2013) Modelling amyloid fibril formation kinetics: mechanisms of nucleation and growth. *J Phys Condens Matter* 25 (37), 373101

6 Lee, S.J. et al. (2017) Towards an understanding of amyloid-beta oligomers: characterization, toxicity mechanisms, and inhibitors. *Chem Soc Rev* 46 (2), 310-323

7 Qiang, W. et al. (2017) Structural variation in amyloid-beta fibrils from Alzheimer's disease clinical subtypes. *Nature* 541 (7636), 217-221

8 Jan, A. et al. (2010) Preparation and characterization of toxic Abeta aggregates for structural and functional studies in Alzheimer's disease research. *Nat Protoc* 5, 1186-1209

9 Miller, Y. et al. (2010) Polymorphism in Alzheimer Abeta amyloid organization reflects conformational selection in a rugged energy landscape. *Chem Rev* 110 (8), 4820-4838

10 Castello, F. et al. (2017) Two-Step Amyloid Aggregation: Sequential Lag Phase Intermediates. *Sci Rep* 7, 40065

11 Cohen, S.I. et al. (2013) Proliferation of amyloid-beta42 aggregates occurs through a secondary nucleation mechanism. *Proc Natl Acad Sci U S A* 110 (24), 9758-9763

12 Bitan, G. et al. (2003) Amyloid beta -protein (Abeta) assembly: Abeta 40 and Abeta 42 oligomerize through distinct pathways. *Proc Natl Acad Sci U S A* 100 (1), 330-335

13 Walsh, D.M. and Selkoe, D.J. (2007) A beta oligomers - a decade of discovery. *J Neurochem* 101 (5), 1172-1184

14 Lesne, S. et al. (2006) A specific amyloid-beta protein assembly in the brain impairs memory. *Nature* 440, 352-357

15 Lacor, P.N. et al. (2004) Synaptic targeting by Alzheimer's-related amyloid beta oligomers. *J Neurosci* 24, 10191-10200

16 Bernstein, S.L. et al. (2009) Amyloid-beta protein oligomerization and the importance of tetramers and dodecamers in the aetiology of Alzheimer's disease. *Nat Chem* 1 (4), 326-331

17 Walsh, D.M. et al. (2002) Naturally secreted oligomers of amyloid beta protein potently inhibit hippocampal long-term potentiation in vivo. *Nature* 416 (6880), 535-539

18 Mc Donald, J.M. et al. (2010) The presence of sodium dodecyl sulphate-stable Abeta dimers is strongly associated with Alzheimer-type dementia. *Brain* 133 (Pt 5), 1328-1341

19 Hung, L.W. et al. (2008) Amyloid-beta peptide (Abeta) neurotoxicity is modulated by the rate of peptide aggregation: Abeta dimers and trimers correlate with neurotoxicity. *J Neurosci* 28, 11950-11958

20 Shankar, G.M. et al. (2008) Amyloid-beta protein dimers isolated directly from Alzheimer's brains impair synaptic plasticity and memory. *Nat Med* 14 (8), 837-842

21 Hayden, E.Y. et al. (2017) Preparation of pure populations of covalently stabilized amyloid beta-protein oligomers of specific sizes. *Anal Biochem* 518, 78-85

22 Nichols, M.R. et al. (2015) Biophysical comparison of soluble amyloid-beta(1-42) protofibrils, oligomers, and protofilaments. *Biochemistry* 54 (13), 2193-2204

23 Lomakin, A. et al. (1997) Kinetic theory of fibrillogenesis of amyloid beta-protein. *Proc Natl Acad Sci U S A* 94 (15), 7942-7947

24 Lomakin, A. et al. (1996) On the nucleation and growth of amyloid beta-protein fibrils: detection of nuclei and quantitation of rate constants. *Proc Natl Acad Sci U S A* 93 (3), 1125-1129

25 Rambaldi, D.C. et al. (2009) In vitro amyloid Abeta(1-42) peptide aggregation monitoring by asymmetrical flow field-flow fractionation with multi-angle light scattering detection. *Anal Bioanal Chem* 394 (8), 2145-2149

26 Abelein, A. et al. (2013) Formation of dynamic soluble surfactant-induced amyloid beta peptide aggregation intermediates. *J Biol Chem* 288 (32), 23518-23528

27 Pryor, N.E. et al. (2012) Unraveling the early events of amyloid-beta protein (Abeta) aggregation: techniques for the determination of Abeta aggregate size. *Int J Mol Sci* 13 (3), 3038-3072

28 Matsumura, S. et al. (2011) Two distinct amyloid beta-protein (Abeta) assembly pathways leading to oligomers and fibrils identified by combined fluorescence correlation spectroscopy, morphology, and toxicity analyses. *J Biol Chem* 286 (13), 11555-11562

29 Grasso, G. (2011) The use of mass spectrometry to study amyloid-beta peptides. *Mass Spectrom Rev* 30 (3), 347-365

30 Muneeruddin, K. et al. (2014) Characterization of small protein aggregates and oligomers using size exclusion chromatography with online detection by native electrospray ionization mass spectrometry. *Anal Chem* 86 (21), 10692-10699

31 Bartolini, M. et al. (2011) Kinetic characterization of amyloid-beta 1-42 aggregation with a multimethodological approach. *Anal Biochem* 414 (2), 215-225

32 Brinet, D. et al. (2014) An improved capillary electrophoresis method for in vitro monitoring of the challenging early steps of Abeta1-42 peptide oligomerization: application to anti-Alzheimer's drug discovery. *Electrophoresis* 35 (23), 3302-3309

33 Watt, A.D. et al. (2013) Oligomers, fact or artefact? SDS-PAGE induces dimerization of beta-amyloid in human brain samples. *Acta Neuropathol* 125 (4), 549-564
34 Dawod, M. et al. (2017) Recent advances in protein analysis by capillary and microchip electrophoresis. *Analyst* 142 (11), 1847-1866
35 Sabella, S. et al. (2004) Capillary electrophoresis studies on the aggregation process of beta-amyloid 1-42 and 1-40 peptides. *Electrophoresis* 25 (18-19), 3186-3194
36 Picou, R. et al. (2010) Analysis of monomeric Abeta (1-40) peptide by capillary electrophoresis. *Analyst* 135 (7), 1631-1635
37 Picou, R.A. et al. (2012) Separation and detection of individual Abeta aggregates by capillary electrophoresis with laser-induced fluorescence detection. *Anal Biochem* 425 (2), 104-112
38 Picou, R.A. et al. (2011) Analysis of Abeta (1-40) and Abeta (1-42) monomer and fibrils by capillary electrophoresis. *J Chromatogr B Analyt Technol Biomed Life Sci* 879 (9-10), 627-632
39 Brinet, D. et al. (2017) In vitro monitoring of amyloid beta-peptide oligomerization by Electrospray differential mobility analysis: An alternative tool to evaluate Alzheimer's disease drug candidates. *Talanta* 165, 84-91
40 Colombo, R. et al. (2009) CE can identify small molecules that selectively target soluble oligomers of amyloid beta protein and display antifibrillogenic activity. *Electrophoresis* 30 (8), 1418-1429
41 Butini, S. et al. (2013) Multifunctional cholinesterase and amyloid Beta fibrillization modulators. Synthesis and biological investigation. *ACS Med Chem Lett* 4 (12), 1178-1182
42 Brogi, S. et al. (2014) Disease-modifying anti-Alzheimer's drugs: inhibitors of human cholinesterases interfering with beta-amyloid aggregation. *CNS Neurosci Ther* 20 (7), 624-632
43 Stine, W.B. et al. (2011) Preparing synthetic Abeta in different aggregation states. *Methods Mol Biol* 670, 13-32
44 Bartolini, M. et al. (2007) Insight into the kinetic of amyloid beta (1-42) peptide self-aggregation: elucidation of inhibitors' mechanism of action. *Chembiochem* 8 (17), 2152-2161
45 Natalello, A. et al. (2016) Co-fibrillogenesis of Wild-type and D76N beta2-Microglobulin: the crucial role of fibrillar seeds. *J Biol Chem* 291 (18), 9678-9689
46 Cerf, E. et al. (2009) Antiparallel beta-sheet: a signature structure of the oligomeric amyloid beta-peptide. *Biochem J* 421, 415-423
47 Kato, M. et al. (2007) Analytical method for beta-amyloid fibrils using CE-laser induced fluorescence and its application to screening for inhibitors of beta-amyloid protein aggregation. *Anal Chem* 79 (13), 4887-4891
48 Stine, W.B., Jr. et al. (2003) In vitro characterization of conditions for amyloid-beta peptide oligomerization and fibrillogenesis. *J Biol Chem*. 278, 11612-11622
49 Ackermans, M.T. et al. (1991) Quantitative analysis in capillary zone electrophoresis with conductivity and indirect UV detection. J Chrom A 549, 345-355

50 Suvorina, M.Y. et al. (2015) Studies of Polymorphism of Amyloid-beta42 Peptide from Different Suppliers. *J Alzheimers Dis* 47, 583-593
51 Yin, F. et al. (2011) Silibinin: a novel inhibitor of Abeta aggregation. *Neurochem Int* 58,399-403
52 Davis, R.C. et al. (2011) Amyloid beta dimers/trimers potently induce cofilin-actin rods that are inhibited by maintaining cofilin-phosphorylation. *Mol Neurodegener* 6, 10
53 Gilomen, K. et al. Detoxification of acetonitrile-water wastes from liquid chromatography.
54 Merlini, G. and Bellotti, V. (2003) Molecular mechanisms of amyloidosis. *N Engl J Med* 349 (6), 583-596
55 Bitan, G. et al. (2005) Neurotoxic protein oligomers--what you see is not always what you get. *Amyloid* 12 (2), 88-95
56 Chirgadze, Y.N. and Nevskaya, N.A. (1976) Infrared spectra and resonance interaction of amide-I vibration of the antiparallel-chain pleated sheet. *Biopolymers* 15 (4), 607-625
57 Zandomeneghi, G. et al. (2004) FTIR reveals structural differences between native beta-sheet proteins and amyloid fibrils. *Protein Sci* 13 (12), 3314-3321
58 Lomont, J.P. et al. (2017) Not All beta-Sheets Are the Same: Amyloid Infrared Spectra, Transition Dipole Strengths, and Couplings Investigated by 2D IR Spectroscopy. *J Phys Chem B* 121 (38), 8935-8945
59 Fezoui, Y. et al. (2000) An improved method of preparing the amyloid beta-protein for fibrillogenesis and neurotoxicity experiments. *Amyloid* 7 (3), 166-178
60 Stroud, J.C. et al. (2012) Toxic fibrillar oligomers of amyloid-beta have cross-beta structure. *Proc Natl Acad Sci U S A* 109 (20), 7717-7722

Chapter II

Evaluation of curcumin-based analogues as Aß oligomerization modulators: in vitro and in vivo animal model studies

1 Introduction

The aggregation of Aß peptides into amyloid fibrils is one of the most important hallmarks of Alzheimer's disease (AD), indeed amyloid plaques are used as a diagnostic marker.
Although the aetiology of AD is still incomplete, compelling evidences indicate that Aß aggregation plays a key role in the onset and progression of the disorder. Therefore, agents able to block or reverse the amyloid process could be an effective approach for treating AD [1].
A variety of anti-amyloid agents have been developed and according to the amyloid cascade hypothesis, they target the process at different levels. Possible therapeutic strategies are [2,3]:

- to stop the production of Aß peptides by inhibiting enzymes involved in the amyloidogenic proteolitic cleavage of APP;
- to enhance the catabolism of Aß peptides *via* an up-regulation of enzymes, such as neprylsin (NEP), which degrade Aß and decrease Aß levels in the brain;
- to modulate the aggregation of Aß.

In a simplistic view of the amyloid process, Aß monomers convert into insoluble fibrils which constitute amyloid plaques. However, the aggregation of Aß peptides is extremely more complex: monomers interact to form different soluble oligomers involved in many toxic effects; in turn oligomers evolve in bigger aggregates up to insoluble fibrils throughout different and parallel pathways.
Indeed, the modulation of the aggregation can focus on the inhibition of the oligomerization process, on the disaggregation of fibrils and of pre-formed aggregates. Another interesting approach is the design of agents which are able to redirect the on-pathway oligomerization that leads to toxic oligomers to the off-pathway process and thus to non toxic aggregates [4].

Considering the complexity of the aggregation process and the fact that soluble oligomers and insoluble fibrils represent distinct aggregation pathways, it is evident that a potential inhibitor to be effective should block both the oligomerization and the fibrillogenesis.

As described in Chapter I, the assays and techniques commonly employed in aggregation studies still show limitations in providing simultaneous and comparable information on both fibrils and oligomers [2,4]. This means that a potential inhibitor of the oligomerization may not be identified by using a specific assay for fibrils, such as ThT fluorescence and therefore more than one technique has to be used.

Even though the characterization of all Aß assemblies involved in the neurodegeneration is not exhaustive, it is crucial to understand on which particular oligomeric population an inhibitor acts.
The transient and non covalent nature of Aß oligomers, the dynamic equilibrium among different populations which keep on aggregating during the experiments represent further important issues in the search for modulators of Aß aggregation. For *in vitro* aggregation studies this results in the set up of reliable and standardized procedures for the preparation of Aß oligomers and for their characterization. This is mandatory for the evaluation of the effects of molecules on the amyloid process [4,5].

All the disadvantages and limitations of techniques employed for the characterization of Aß aggregates are found also in this context. For example, mass spectrometry approaches are limited because of the ionization source-induced disassembly and the low ionization ability of HMW oligomers; consequently the effect of the inhibitor can be monitored only on the amount of monomer. Spectroscopic techniques, such as CD and ThT fluorescence, provide average information about all species present in the sample [6]. Nevertheless in the context of a multimethodological approach, the inhibition activity of different small molecules on the amyloidogenic process has been reported. For example in 2011 Bartolini *et al*. successfully applied MALDI–TOF, ESI–IT MS and ESI–QTOF MS for measuring the progressive disappearance of Aß42 monomer during inhibition studies with the known Aß inhibitor myricetin [7].

Capillary electrophoresis can be considered as an attractive tool for the identification of entities able to modify the kinetics of formation of Aß oligomers, since it is possible to monitor over time the aggregation of several oligomeric populations. By this separative micro-technique, information about the effect of modulators on the oligomerization can be obtained. Furthermore CE supported by TEM, can complete the activity profile of potential modulators [8-11].
CE has been previously used to verify the activity of different agents on the amyloid process. Starting from 2009 De Lorenzi and co-workers have applied an analytical platform based on CE and TEM to identify inhibitors of Aß aggregation. In 2009 two anthraquinone compounds, mitoxantrone and pixantrone, were investigated as Aß oligomerization modulators. Based on the intercalation with topoisomerase II by which they exert their anti-cancer activity, a similar mechanism in blocking peptide-peptide interactions was hypothesized. Both were demonstrated to have anti-fibrillogenic activity as well as to reduce or abrogate Aß42 oligomerization in a concentration and time dependent manner. Despite their intrinsic toxicity, it was also proved how pixantrone significantly recovers neuroblastoma SH-SY5Y cell viability.

Taverna and co-workers employed CE to determine the effect on oligomer formation exerted by glycosilated compounds [5], by a new class of

glycopeptidomimetics [12,13] and by Aß42 related ß-hairpin peptidomimetics [14]. As assessed by ThT fluorescence and TEM, these compounds prevent the formation of amyloid fibrils and furthermore totally suppress the Aß42-induced toxicity.

The multifactorial nature of AD and the difficulties in obtaining disease-modifying anti-Alzheimer's drug encourage a therapeutic approach based on multitarget-directed ligands (MTDLs). In more recent work by our group [10,11] CE was used to verify the anti-aggregation activity of multifunctional compounds able to target cholinesterase enzymes (ChEs) and Aß oligomers. By combining a bistacrine scaffold with a hydrophobic peptidomimetic sequence, three compounds have been identified as prototypic of a new class of multifunctional ChEs and Aß42 self-aggregation inhibitors.

A multitude of inhibitors of the Aß fibril formation has been reported in literature. These inhibitors can be classified in three main categories: small molecules, both of natural and synthetic origin, short peptides and antibodies [3].

Among the small molecules, an increasing number of reports have described natural products (NPs) as possible modulators of the amyloid process, such as (-)-epigallocatechin gallate (EGCG), curcumin, myricetin, rosmarinic acid and many others. NPs represent an important source of novel compounds since by rational design and structural modifications they can be considered as a scaffold for new chemical entities [3].

Curcumin (**Figure 1a)**) is the primary bioactive compound found in the rhizome of *Curcuma longa* (60-70% of crude extract), together with two structurally related compounds namely demethoxycurcumin (4-hydroxycinnamoyl(feruloyl)methane) (**Figure 1b)**) and bis-demethoxycurcumin (bis(4-hydroxycinnamoyl)methane) which constitute 20-27% and 10-15% of the turmeric extract, respectively (**Figure 1c)**) [15]. Recent X-ray and NMR studies have found that curcumin exists in solution as the keto-enol tautomer rather than the ß-diketone tautomer (see structures in **Figure 1a)**) [16].

a)

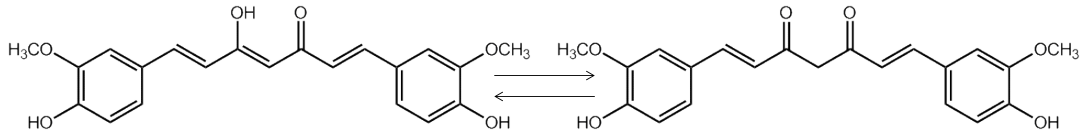

curcumin
ß-keto-enol tautomer

curcumin
ß-diketo tautomer

b)

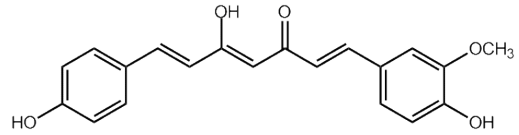

demethoxycurcumin

c)

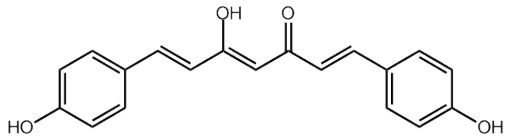

bis-demethoxycurcumin

Figure 1. Chemical structures of curcumin and its structurally related compounds. **a)** curcumin as keto-enol tautomer and ß-diketo tautomer; **b)** structure of demethoxycurcumin; **c)** structure of bis-demethoxycurcumin [15,17].

As reported in **Figure 2**, the trans-α,ß-unsatured carbonyl structural motif, being a Michael acceptor system, could act as a nucleophile scavenger by establishing covalent linkages with nucleophile functions of a number of target proteins. These protein-reactive properties confer a multitude of biological activities to curcumin [15].

Anti-oxidant, anti-inflammatory, anti-carcinogenic, epigenetic effects are some of the vast variety of activities ascribed to curcumin. Considering its potential activities established in *in vitro* and in *in vivo* animal studies, curcumin is often claimed as a promising compound for the treatment of several disorders including: cancer, inflammation, arthritis, acquired immunodeficiency syndrome, cardiovascular, gastric, pulmonary and renal diseases. Curcumin has been reported to exert an effect in neurodegenerative diseases, i.e. Alzheimer's and Parkinson's disease [15,18].

Curcumin is one of the most extensively studied NPs because of its pleiotropic properties. The close attention paid to curcumin is witnessed by the magnitude of scientific reports on this polyphenol. The Curcumin Resource Database (CRDB) is the first-ever comprehensive, up-to-date database that exclusively covers curcumin analogs, their molecular targets and patents. Based on the information of the CRDB, to date more than 10000 publications have been reported on curcumin and its analogues and a few less than one thousand of curcumin-based patents have been registered [19].

Despite this amount of information, literature regarding curcumin and its biological properties is controversial, as described by Nelson *et al*. in the miniperspective "The Essential Medicinal Chemistry of Curcumin" [19]. For example, data reported by Necula *et al*. suggest that curcumin seems to actually promote fibrillogenesis and does not inhibit Aß oligomerization. In addition, curcumin is not active at low micromolar concentrations [20]. These findings are consistent with the results observed by Thapa and co-workers in which curcumin does not inhibit Aß fibril formation, but rather is able to modulate the aggregation process by inducing the formation of non toxic aggregates [21].

As a consequence of its potential anti-oxidative, anti-inflammatory, and anti-excitotoxic effects, curcumin may be considered a promising therapeutic agent in the treatment of AD, since it passes through the blood-brain barrier (BBB). As recently demonstrated by animal model studies, not only curcumin does prevent the aggregation of Aß peptides *in vitro*, but it also enhances the clearance of pre-formed aggregates and fibrils and it is able to inhibit the metabolism of APP [15,18].

The importance of this turmeric compound is also demonstrated by the fact that it is a common template used for studying structure-activity relationships (SARs) of polyphenolic inhibitors against self-assembled amyloidogenic proteins [3]. Based on the vast literature, the properties of curcumin involved in its activity against the amyloid process are related to specific SAR.

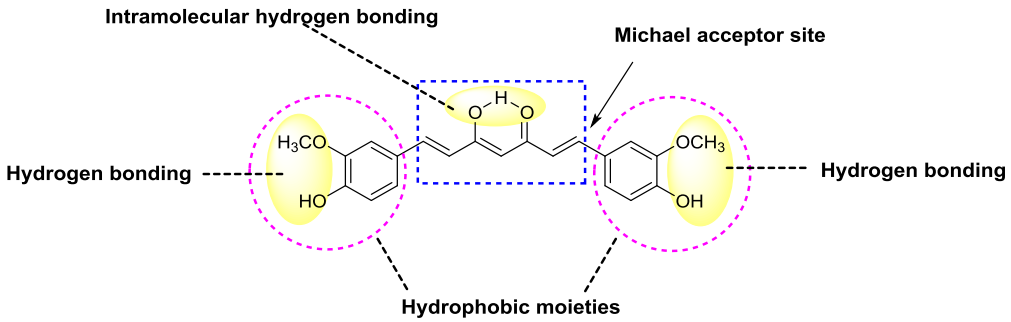

Figure 2. Representation of the principal pharmacophore elements of curcumin.

In fact, several SAR studies allowed the identification of some pharmacophore elements that make curcumin a favorable and versatile binding partner of different aggregation states of Aß peptides.
For example, the 4-hydroxyl and the 3-methoxy groups on the side aryl rings, as well as the ß-keto-enol function of the central framework, have been identified as the key structural elements involved in strong hydrogen-bonding interactions with Aß [22]. These functional groups are also relevant for the free-radical scavenger activity ascribed to curcumin [15]. The phenolic groups can inhibit the formation of Aß fibrils *via* binding to hydrophobic residues of Aß

peptides [3]. As demonstrated by Konno *et al*., the presence of *para*-halogenated groups on the aromatic rings reduces the inhibitory activity against BACE-1 [23]. Orlando and co-workers suggested that an unsaturated spacer is essential for the anti-aggregation activity, and at least one enone group should be present on the spacer to measure an inhibitory activity [24]. Linker length and flexibility are also crucial for activity: the optimal length is in the range of 8-16 Å, and 2-3 free rotatable carbons centers are not well tolerated. An inhibitor with a too long, too short or too flexible spacer, is not able to interact with the counter part residues of Aß peptide [24,25].
Aromatic C atoms adjacent to the –OH and to the $-OCH_3$ interact with the C atoms of Aß peptide [26]; π-π stacking interactions between curcumin aromatic rings and Aß aromatic rings would compete with Aß monomer-monomer interactions (involving the hydrophobic core residues Phe19 and Phe20) thus preventing aggregation [22]. In addition, from SAR investigations, the role of the co-planarity and of the rigidity of curcumin structure is emerged as an important feature for the establishment of π- π interactions and for the ability of curcumin to intercalate between ß-sheets.

Based on this evidence, curcumin demonstrated to be a ß-sheet breaker by twisting and bending the sheets [22]. However, its anti-oligomeric and anti-fibrillogenic activities are still controversial.

Despite the potential and promising biological activities, to date curcumin does not have success in clinical outcomes. The most important limitations of curcumin are related to its poor bioavailability, poor absorption, distribution, metabolism and excretion (ADME) properties, as well as potential toxicological effects [19]. For example, its intrisinc neuronal toxicity and the low bioavailability are mainly related to the 4-hydroxyl-3-methoxy groups of the two aryl rings [24].
Nevertheless, from a drug discovery standpoint curcumin still shows a great potential, since it is considered as a lead compound for the design of analogues with improved biological profile that might be exploited for further development as drug candidates for the treatment of several disorders, including AD.

In this work, we investigate two different sets of curcumin-based analogues (SET1 and SET2) as modulators of the amyloid process of Aß42 peptide. In order to assess the effects of these molecules on the aggregation of Aß42, the peptide is coincubated with decreasing concentrations of compounds: 50, 25, 10 and 1 μM.

Because of CE, the potential anti-oligomeric activity is evaluated by monitoring over time the aggregation of Aß42 in the presence of compounds. Therefore, standard Aß42 samples are prepared according to protocol #3 (described in detail in Chapter I), are analytically separated by CE (method B) and characterized by UF followed by CE analyses. Starting from this basis, it is

possible to define the effect of compounds on specific and characterized oligomeric populations. Moreover, results rely on the high reproducibility of the analytical data obtained (see Chapter I). Finally, the abrogation of the fibril formation is assessed by TEM.

In collaboration with two different groups of the University of Bologna, two sets of curcumin analogues have been selected and tested. For both sets, the chemical modifications applied would improve the biological profile of curcumin, and on the other hand would transfer to the scaffold additional activities, in the context of MTDLs.
SET1 includes 4 compounds selected from a small library of about 30 curcumin derivatives, as most promising in terms of lack of toxicity and of potential ability to cross the blood brain barrier based on the structural modifications. (Compounds 1-18 belonging to the small library have been already described [17], while the design strategy of the others are reported in the Supplementary material, **Figure S1**). The anti-amyloid activity as well as the toxicity on microglia and neuroblastoma cells have been investigated. In SET1 the structure of curcumin is roughly preserved and chemical modifications have been performed on functional groups found to be responsible for toxicity and/or anti-aggregation activity [24].
SET2 includes two compounds previously reported to have anti-aggregation activity (as assessed by ThT-based assay and ESI-MS) and/or anti-oxidant properties. In these compounds the cinnamoyl function of curcumin is combined with the allyl mercaptan moiety of diallyl disulfide (an active principle of garlic) [27]. Investigations on this set of molecules are in a preliminary phase.

The most promising compounds in terms of toxicity and anti-amyloid activity belonging to SET1 are also tested for their anti-fibrillogenic activity *in vivo* in genetically engineered *C. Elegans* expressing Aß42 peptide, an efficient animal model that has recently been reported for the screening of molecules as AD potential treatments [28]. The selected molecules have been evaluated for their ability to rescue the paralysis induced by the toxic amyloid deposited in the worm muscle cells. These studies are ongoing on those compounds that have demonstrated a good anti-oligomeric activity *in vitro*.

2 Materials and Methods

2.1 Reagents

Synthetic Aß42 was purchased from Bachem (Bubendorf, Switzerland) as lyophilized powder and stored at -20°C.
1,1,1,3,3,3-Hexafluoropropan-2-ol (HFIP), dimethylsulfoxide (DMSO), acetonitrile (ACN), and sodium carbonate (Na_2CO_3) were from Sigma-Aldrich (St. Louis, MO, USA). Ethanol 96° was supplied by Carlo Erba (Cornaredo, Italy). Sodium hydroxide (NaOH) and sodium dodecyl sulphate (SDS) were provided by Merck (Darmstadt, Germany). Na_2HPO_4 and NaH_2PO_4, supplied by Sigma-Aldrich, were used for the preparation of the background electrolyte (BGE) in the CE analyses. BGE solutions were prepared daily using Millipore Direct-Q™ deionized water (Bedford, MA, USA) and filtered on 0.45 µm Sartorius membrane filters (Göttingen, Germany). Uncoated fused-silica capillary was from Polymicro Technologies (Phoenix, AZ, USA).
All cell culture reagents, culture medium and chemicals were purchased from Sigma-Aldrich.
Curcumin was purchased from Sigma Aldrich (analytical standard, purity ≥98%), whereas curcumin-based analogues of SET1 and SET2 were kindly provided by Prof. Federica Belluti and Prof. Michela Rosini (University of Bologna) and used as received. For all compounds, purity ≥ 95% was confirmed by ^{1}H NMR, ^{13}C NMR and mass spectrometry [17, 27].

2.2 Curcumin-based analogues

2.2.1 SET1

Compounds belonging to SET1 were synthesized by Federica Belluti and co-workers from the University of Bologna. (1E,4Z,6E)-5-hydroxy-7-(4-hydroxy-3-methoxyphenyl)-1-(4-((3-methylbut-2-en-1-yl)oxy)phenyl)hepta-1,4,6-trien-3-one (Cur6); (1E,4Z,6E)-5-hydroxy-1,7-bis(4-((3-methylbut-2-en-1-yl)oxy)phenyl)hepta-1,4,6-trien-3-one (Cur5); (1E,4E)-1,5-bis(4-((3-methylbut-2-en-1-yl)oxy)phenyl)penta-1,4-dien-3-one (monocarbonyl Cur5) and (1E,4E)-1-(4-hydroxy-3-methoxyphenyl)-5-(4-((3-methylbut-2-en-1-yl)oxy)phenyl)penta-1,4-dien-3-one (monocarbonyl Cur6) were used in this work. In **Figure 3** compound structures are reported.

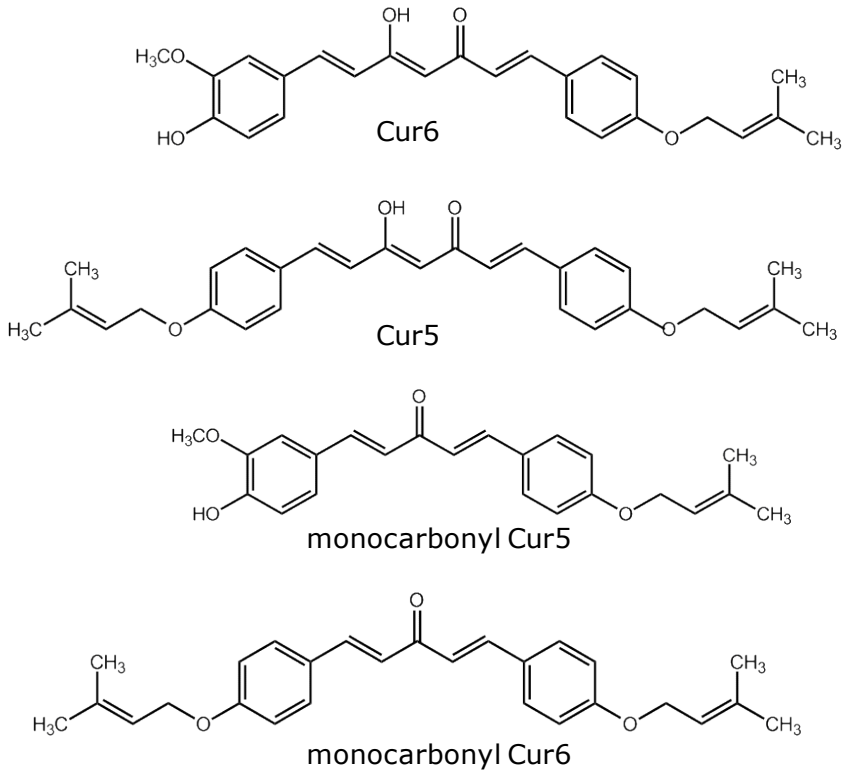

Figure 3. Chemical structure of compounds included in SET1: Cur6, Cur5, monocarbonyl Cur5, monocarbonyl Cur6.

2.2.1 SET2

SET2, synthesized by Michela Rosini and collaborators, consists of two compounds (S)-allyl (E)-3-(3-hydroxyphenyl)prop-2-enethioate (RC10) and (S)-allyl (E)-3-(3,4-dihydroxyphenyl)prop-2-enethioate (GS29) already reported in literature [27]. Their structures are shown in **Figure 4**.

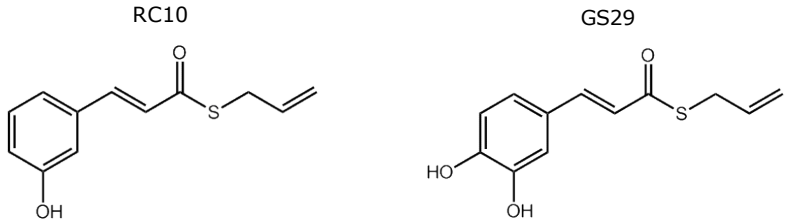

Figure 4. Chemical structure of compounds of SET2: RC10 and GS29.

2.3 Sample preparation

Aß42 peptide was solubilized by following the procedure of protocol #3 described in Chapter I (see Section 2.2) and developed by Bartolini *et al*. [6]. Briefly, lyophilized Aß42 was dissolved in HFIP. After an appropriate incubation time, the solvent was left to evaporate. Then, the Aß42 aliquots were redissolved in a basic mixture (ACN/300 µM Na_2CO_3/250 mM NaOH, 48.3:48.3:3.4, v/v/v) to obtain 500 µM Aß42. This solution was then diluted to the operative concentration (100 µM Aß42 control peptide) with 20 mM phosphate buffer pH=7.4, with or without small molecules.
Stock solutions of curcumin-based analogues (1.53 mM) were prepared in ethanol.
When co-incubation studies were carried out, 500 µM Aß42 peptide (in the basic mixture) was dissolved in an appropriately diluted compound solution, so as to keep the peptide concentration at 100 µM and obtain different peptide/compound ratios: 1:100, 1:10, 1:4, 1:2 for curcumin and Cur6; 1:10, 1:4, 1:2 for Cur5 and 1:2 for monocarbonyl Cur5, monocarbonyl Cur6, RC10 and GS29. In this way the final percentage of EtOH was lower than 3.26%.
For body bends assay, curcumin, Cur6 and Cur5 were solubilised in EtOH, so to obtain a concentration of 3 mM.

2.4 Capillary electrophoresis

All CE experiments were performed on an Agilent Technologies 3D CE system with built-in diode-array detector (Waldbronn, Germany). Data were collected and analyzed using a Chemstation A.10.02 software. CE method B was applied (see Chapter I, Section 2.3): the uncoated fused-silica capillary (50 µm i.d., 33 cm total length, 24.5 cm effective length) was prepared by flushing 1 M NaOH for 30 minutes, followed by water for 30 minutes and BGE (80 mM Na_2HPO_4/NaH_2PO_4) for 1 hour. The between-run rinsing cycle was carried out by pumping through the capillary 50 mM SDS and water for 1.5 min each, and BGE for 2 min. The injection of the samples was carried out by applying a pressure of 30 mbar for 3 s. The capillaries were thermostated with circulating air at 25°C and separations were carried out at 12 kV (operative current: 75–78 mA) with the anode at the sample injection end. The acquisition wavelength was 200 nm.

2.5 Transmission electron microscopy (TEM)

Amyloid fibril identification was carried out by using a Joel TEM 1400 plus electron microscope, operating at 80 kV. Precipitated samples were prepared as follows: Aß42 suspensions were diluted at 10 µM with 20 mM Na_2HPO_4/NaH_2PO_4 and then 10 µL of diluted suspensions were left to sediment on carbon-coated Formvar nickel grids (200 mesh) (Electron Microscopy Sciences, Washington, PA,USA). After 15 minutes the excess of sample was

drained off by means of a filter paper. The negative staining was performed with 10 µL of 2%w/v uranyl acetate solution (Electron Microscopy Sciences).

2.6 SH-SY5Y cell viability assay

SH-SY5Y human neuroblastoma cell cultures from European Collection of Cell Cultures (ECACC No. 94030304) were grown at 37°C in 5% CO_2/95% air in a medium composed of Eagle's minimum essential medium and Nutrient Mixture Ham's F-12, with the addition of 10% FBS, 2 mM glutamine, penicillin/streptomycin, non essential amino acids. All culture media and supplements were purchased from Euroclone (Life Science Division, Milan, Italy). The quantitative colorimetric assay based on the reduction of MTT performed by mitochondrial dehydrogenase was used to determine cellular redox activity, an initial indicator of cell death. At day 0 SH-SY5Y cells were plated at a density of $5x10^4$ viable cells per well in 96-well plates. The next day, cells were incubated for 24 hours at 37°C in the presence of decreasing concentrations of compounds: curcumin, Cur6, Cur5, monocarbonyl Cur5 and monocarbonyl Cur6 were tested at 50, 40, 25, 20, 10, 5 and 1 µM. After the treatment, cells were exposed to a MTT solution in PBS (1 mg/mL). After 4 hours of incubation with MTT, cells were lysed with lysis buffer (20% SDS in water/dimethylformamide 1:1) and incubated overnight at 37°C. The cell viability reduction was quantified by using a BIO-RAD microplate reader (Model 550; Hercules, CA, USA).

2.7-Caenorhabditis elegans: body bends assay

N2 wild-type strain *C. elegans* and CL2120 *C. elegans* expressing Aß3-42 peptide were purchased from Caenorhabditis Genetics Center (University of Minnesota, St. Paul, MN, USA).
Worms were maintained at 20°C on nematode growth medium (NGM) agar plates seeded with E. coli OP50 for food. Synchronization of worm cultures was achieved by hypochlorite treatment of gravid hermaphrodites [30].
For the body bend assay, plates containing curcumin, Cur6 and Cur5 were prepared as follows: 150 µL of concentrated stock solutions of each compound were added to molten NGM at 50°C and then 3 mL were poured into each plate. The plates were placed in a laminar flow hood at room temperature for 30 min and then 20 µL of a suspension of E. coli OP50 was spotted to form a circular lawn on the centre of each plate. Body bends assay was performed at room temperature using a stereomicroscope (M165 FC Leica) equipped with a digital camera (Leica DFC425C and SW Kit). After 48 h exposure to 100 µM curcumin, Cur6 and Cur5, adults synchronized worms were picked and transferred into a 96-well microtiter plate containing 100 µL of M9 buffer (45 mM KH_2PO_4, 42 mM Na_2HPO_4, 85 mM NaCl, 1 mM $MgSO_4$ in water). At this point, the number of left–right worms tail movements in 1 min was recorded.

Three independent assays were performed (N=30 animals for each group). A subset of worms of the N2 strain was used as a negative control strain.

2.8 Statistical analysis

The data were analyzed by analysis of variance (ANOVA) followed, if significant, by an appropriate post hoc comparison test. The reported data are expressed as mean±SD or as mean±SEM of at three independent experiments. Values of $p<0.05$ were considered statistically significant.

3 Premises: selection of curcumin-based analogues

3.1 SET1

Notwithstanding its great potentiality, curcumin presents some drawbacks, namely the reduced bioavailability and the intrinsic neuronal toxicity which are mainly related to the the 4-hydroxyl-3-methoxy groups of the two aryl rings [24].

In order to identify disease-modifying drug candidates useful for AD with multitarget features and with an improved biological profile as compared to curcumin, newly synthesized curcumin-based analogues were tested (SET1).
The design strategy, carried out by the University of Bologna (F. Belluti *et al*.), was focused on groups related to toxicity and poor bioavailability of curcumin, which are also identified as the key structural elements involved in interactions with Aß [22,24].
Among molecules of the small library (**Figure S1**), in the compounds selected for this work and belonging to SET1 one or both 4-hydroxyl-3-methoxy groups were replaced by a 3,3-dimethylallyloxy also known as prenyloxy group. The prenyl group, largely found in nature, was selected as it could offer promises to overcome the classical curcumin's drawbacks. Indeed in plants, the prenylation of aromatic metabolites results in a derivative with an improved or modified pharmacological profile if compared to not-prenylated compounds [31-33].
Therefore, the choice of the functional group was mainly addressed to reduce curcumin neuronal toxicity, as well as to favour the crossing of the BBB by modulating the hydrophilic/lipophilic balance of the compounds. Moreover, since to date natural prenylated compounds are extensively studied for their activity against cancer and inflammation, the prenylation of curcumin-based analogues may also enhance the anti-inflammatory properties of curcumin. **Figure 5** shows the design strategy applied to these compounds starting from the chemical structure of curcumin.
Cur6 and Cur5 (see **Figure 3** for the structure) are chemical entities belonging to SET1.

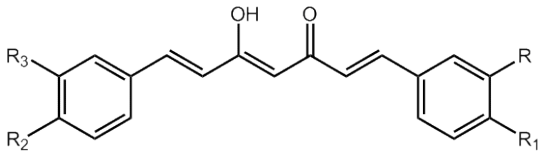

Curcumin: R,R_3= OCH_3; R_1, R_2 =OH

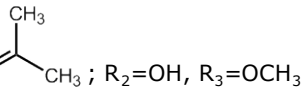

Cur6: R=H; R_1= O ; R_2=OH, R_3=OCH_3

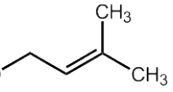

Cur5: R, R_3= H; R_1, R_2=O

Figure 5. Design strategy for Cur6 and Cur5.

To verify the effects of the substitution, the neurotoxicity and anti-inflammatory properties of these compounds were investigated by Morena Zusso and collaborators at the University of Padua. As far as toxicity, Cur6, Cur5 (and curcumin, Cur, taken as reference compound) were tested at decreasing concentrations on LPS-stimulated cortical primary microglia cells. The treatment with LPS induces the M1 activation state in microglia cells [29,34] which produces high levels of pro-inflammatory cytokines including IL-1ß and TNF-α. Therefore, LPS-stimulated microglia cells mirror the neuroinflammation which represents an important pathological condition in the onset of AD [34,35].

The cell viability of microglia cells exposed to compounds (at a concentration ranging from 1 to 40 μM) is reported in Supplementary material (**Figure S2**).
Cur5 shows the worst biological profile as it exerts high neurotoxicity at low concentrations (5 μM). Starting from 10 μM, Cur induces cell death and microglia viability decreases. Conversely, Cur6 results to be not toxic even at higher concentrations (20 and 40 μM).

Given this intrinsic toxicity, Cur and Cur6 were tested for their anti-inflammatory activity at non toxic concentrations. As described above, LPS promoted a marked release by microglia of proinflammatory cytokines such as IL-1ß and TNF-α. A molecule which prevents or down-regulates microglia inflammatory response should inhibit the release of proinflammatory cytokines. In LPS-stimulated microglia cells treated with Cur or Cur6, the amount of and TNF-α and IL-1ß is reduced if compared to that of the control (LPS-stimulated microglia cells not treated with compounds).
Both Cur and Cur6 inhibited the LPS-induced release of TNF-α and IL-1ß in a concentration dependent manner; in particular, the inhibitory effect of Cur6 is stronger than that of Cur. Results are reported in **Figure S3 a)** and **b)**.

This means that, as expected, the replacement of one 4-hydroxyl-3-methoxy group of Cur with a prenyloxy motif in Cur6 leads to a less toxic and more potent inhibitor of the release of proinflammatory cytokines compared to Cur [31-33].
Nevertheless, the presence of two preniloxy groups has detrimental effects on the biological profile of compounds, as indeed Cur5 is the most toxic compound tested.

Taken into account these preliminary pharmacological data, in this work Cur6 and Cur5 were selected among the small library and here investigated for their potential activity on Aß42 oligomer and fibril formation. Given that the two 4-hydroxyl-3-methoxy groups of aryl rings of Cur are also involved in its anti-aggregation activity [3,22,23] and that the effect of the prenyloxy substituent on Aß aggregation is unknown, Cur6 may have an anti-aggregation activity at least comparable to that of curcumin.

On the other hand, since in Cur5 both 4-hydroxyl-3-methoxy groups are replaced, it is possible that its inhibitor activity on the aggregation process is lower than that of curcumin and Cur6.

In view of what stated above, in the coincubation studies with Aß42 carried out by CE and TEM, curcumin is taken as reference compound (Cur) and Cur5 is considered as a negative control.

3.2 SET2

The two curcumin-based analogues belonging to SET2 and already reported in literature [27] have been designed by the University of Bologna (M. Rosini *et al*.) in the context of MTDLs and to get a deeper understanding of the connections between Aß aggregation, oxidative stress and the tumor suppressor p53.

The design strategy of these compounds is based on the combination of chemical functions derived from natural compounds. These chemical groups are related to the modulation of Aß aggregation and to the reduction of oxidative stress (**Figure 6**). In particular, in SET2 the hydroxycinnamoyl function, which is a recurring motif found in many polyphenols including curcumin, is preserved, since it is related to the ability of polyphenols to modulate several AD pathways such as Aß aggregation and oxidative stress [36,37]. The hydroxycinnamoyl function is combined with the allyl mercaptan moiety of diallyl disulfide, an active principle of garlic endowed with anti-oxidant activity [38]. The design strategy is illustrated in **Figure 6**.
Molecules derived from the combination of these two functions are expected to counteract oxidative stress and the aggregation of Aß.

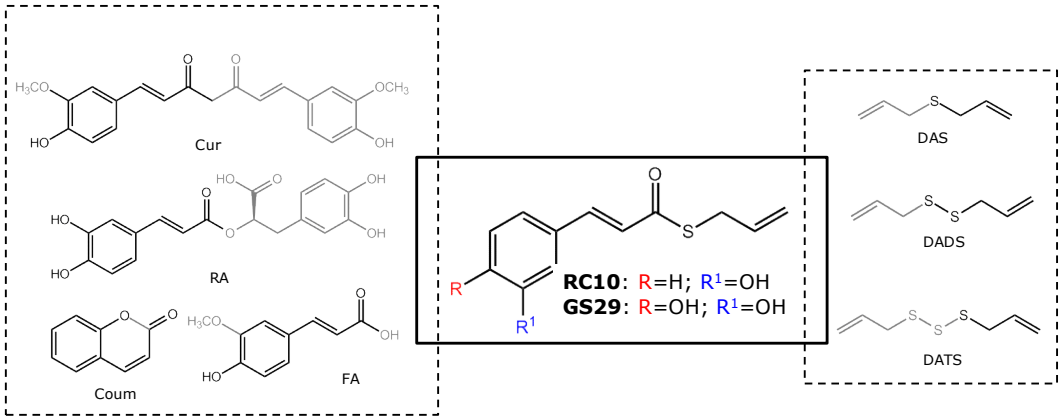

Figure 6. Design strategy for SET2. Cur: curcumin, Coum: coumarin, FA: ferulic acid, RA: rosmarinic acid, DAS: diallyl sulfide, DADS: diallyl disulfide, DATS: diallyl trisulfide. Modified from [27].

In a work published in 2016 [27], Rosini and co-authors tested RC10 and GS29 for their *in vitro* anti-aggregation activity and for their potential ability to protect neuroblastoma cells from Aß42-induced toxicity and oxidative stress. In all experiments curcumin was used as reference compound.

Results showed that the catechol moiety of GS29 was essential for the anti-aggregation activity; indeed RC10, which lacks the *para*-hydroxyl function, did not have effects on the aggregation process, as demonstrated by ThT-based assay. On the other hand, GS29 almost completely inhibited the assembly of Aß42 and demonstrated to be more potent than curcumin. Notably, literature reports that the ThT assay is potentially unsuitable as a probe for amyloid fibril formation in the presence of polyphenols like, among many, curcumin and curcumin derivatives. Indeed, strong π-π electronic transitions in polyphenols make them intrinsically fluorescent, thus an interference at the wavelengths of ThT fluorescence is likely to occur [39]. In this regard, the literature on curcumin is once again controversial [15,20,21].
However, to confirm the ThT data, the authors used ESI-IT MS and they finally postulated that GS29, more than curcumin, retards the Aß42 assembly process by stabilization of the monomeric form and inhibition of its inclusion into growing oligomers.
Curcumin, GS29 and RC10 significantly suppressed the production of H_2O_2-induced intracellular ROS. RC10 showed the highest anti-oxidant activity compared to that of the other two compounds [27].

Prompted by the potency of compound GS29, preliminary investigations on its anti-oligomerization activity are here carried out by CE, taking compound RC10 as negative control.

4 Results and discussion

4.1 Evaluation of the anti-oligomeric activity assessed by CE

The analytical platform based on CE described in Chapter I includes the standardization of Aß42 oligomeric preparations, the separation and characterization of oligomers obtained, as well as the identification of amyloid fibrils by TEM and the evaluation of Aß42-induced cell toxicity. As already mentioned, by this platform, oligomeric populations observed and amyloid fibrils can be considered as independent targets for molecules with anti-oligomeric and/or anti-fibrillogenic properties.

Our analytical tool has been applied to evaluate the effect of compounds belonging to SET1 and to SET2 on the aggregation process of the most amyloidogenic peptide (Aß42).

In order to investigate the potential perturbation of the oligomeric equilibrium induced by compounds, it is necessary to have available a standardized Aß42 aggregation process in the absence of compounds.
In Chapter I, the aggregation of oligomers obtained by following three solubilization protocols has been standardized: oligomeric populations have been identified by effective electrophoretic mobilities (μ_{eff}) and, if present, the equilibrium among oligomers has been assessed. It has been demonstrated that protocol # 3 (see Chapter I Section 2.2 and Section 3.1.3) [6] slows down the aggregation process and results to be the least aggregating procedure. Indeed oligomers are kept in solution for about one month until precipitation into fibrils and small oligomers slowly contribute to the formation of large aggregates. Based on the oligomeric characterization, small oligomers consist of monomers and dimers, whereas the electrophoretic population relative to large aggregates is constituted by assemblies bigger than decamers. This oligomeric population has demonstrated to be the responsible of the toxicity of entire peptide, as reported in Chapter I Section 3.4.

Taking into account that:

- using protocol #3 the time window for studying Aß42 aggregation has been considerably widened
- monomers and dimers are soluble for many days
- as curcumin has effects on small assemblies of Aß and in particular it seems to stabilize Aß dimers [22], also the curcumin-based analogues may act on small oligomers

Aß42 has been solubilized in accordance with procedures relative to protocol #3 for off-line coincubation studies (See Section 2.2) [6].

Since compounds included in both SET1 and SET2 are soluble in pure EtOH, the evaluation of the effect of EtOH at the operative concentrations on the Aß42

aggregation process has also been assessed. To address this issue, the peptide has been solubilized in 3.26% EtOH in phosphate buffer. This is the highest percentage of EtOH that is in contact with the peptide when 100 μM Aß42 samples are coincubated with compounds at the highest concentration tested (50 μM). As compared to the scheme presented in **Figure 3,** Section 2.2 (Chapter 1) for protocol #3, no differences are detected either in the electrophoretic pattern or in the equilibrium between oligomers, moreover at this concentration EtOH does not affect the formation and the morphology of amyloid fibrils as observed by TEM (see Supplementary material, **Figure S4**). For this reason results are presented on data obtained following protocol #3 as reported in Chapter I.

4.1.1 SET1

The oligomerization of Aß42 is monitored by CE in the presence of decreasing concentrations of compounds. In detail, the effect of Cur and Cur6 was investigated at 50 μM, 25 μM, 10 μM and 1 μM whereas for Cur5 at 50 μM, 25 μM and 10 μM. All coincubation studies are performed in triplicate.

Electrophoretic traces were recorded for all compounds, at all concentrations, at different elapsed times from sample solubilization. In **Figure 7**, only the electropherograms relative to the aggregation process of 100 μM Aß42 in the presence of 10 μM Cur, Cur6 and Cur5 are reported. The overall data are elaborated as graphs reporting normalized peak area percentages over time.

Immediately after solubilization, no differences are detected among samples. The presence of compounds does not affect the electrophoreic profile of Aß42 at t0: Peak 1 is the most abundant species and also larger oligomers (Peak 3) are present.
As detailed in Chapter I and also reported here (black traces), the aggregation of 100 μM Aß42 proceeds through the formation of HMW toxic aggregates: oligomers bigger than decamers (Peak 3) build up over time at the expenses of smaller assemblies (Peaks 1 and 2).
As clearly illustrated in **Figure 7**, Cur, Cur6 and Cur5 are able to modulate the aggregation pathway of Aß42.
From a first qualitative evaluation of the electrophoretic traces, Cur and curcumin-based analogues shift the equilibrium towards the non toxic small oligomers, as Peaks 1 and 2 are detected for a wider time window than in control peptide; consequently, the self-assembly of Aß42 in toxic species is strongly slowed down. In addition, Aß42 alone precipitates into amyloid fibrils within one month, whereas in the presence of compounds electrophoretic peaks and thus soluble oligomeric species are detected for about 50 days.

Overall, Cur, Cur6 and Cur5 demonstrate to perturb the aggregation of Aß42 peptide.
As expected on the basis of the structural modifications applied, the electrophoretic traces show that each compound exerts a different effect on the kinetics of formation of the oligomers. A detailed semi-quantitative analysis of these data and of those obtained at all concentrations tested is reported and discussed in the following paragraphs.

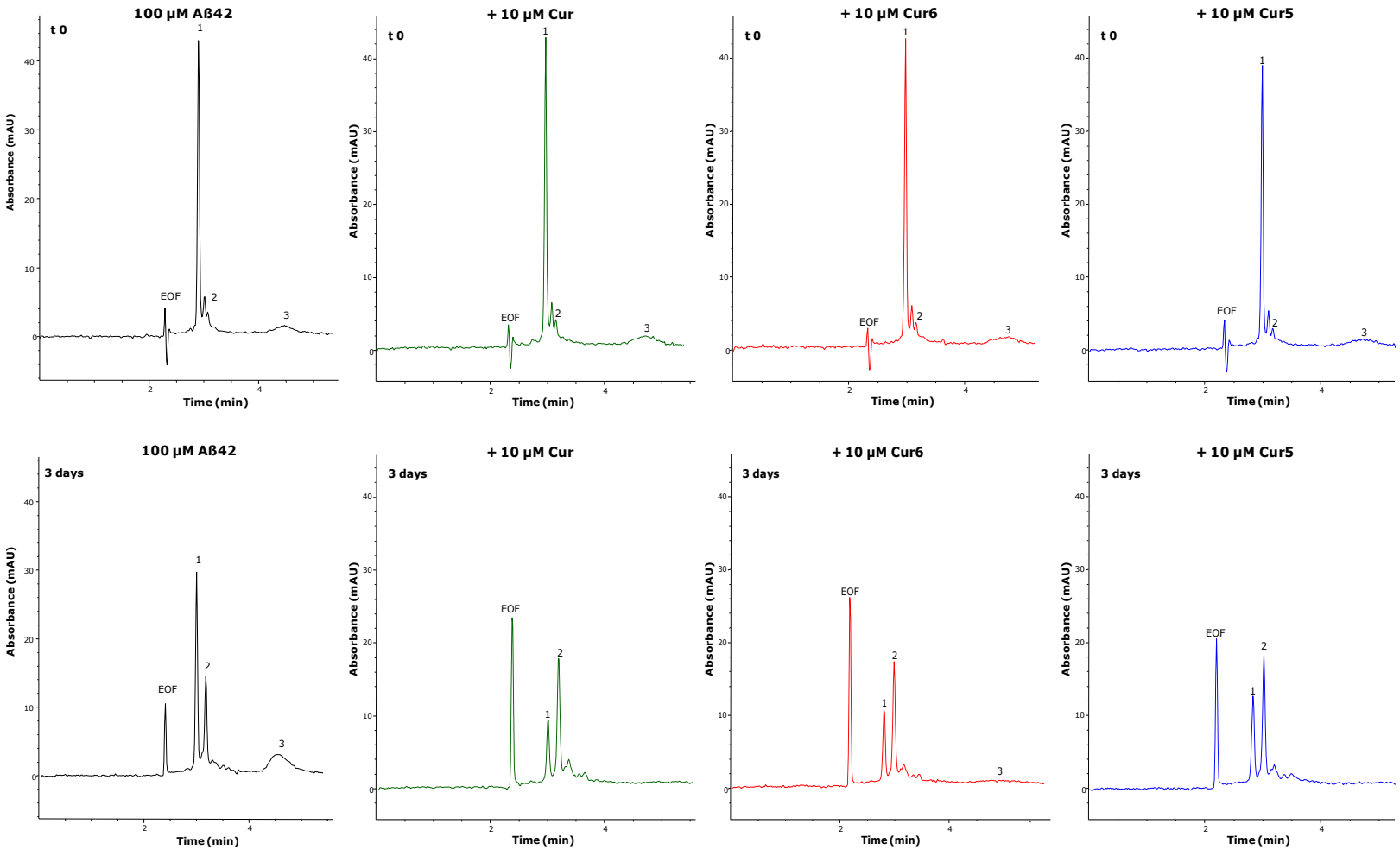
100 µM Aß42
t 0
+ 10 µM Cur
t 0
+ 10 µM Cur6
t 0
+ 10 µM Cur5
t 0
100 µM Aß42
3 days
+ 10 µM Cur
3 days
+ 10 µM Cur6
3 days
+ 10 µM Cur5
3 days
Absorbance (mAU)
Time (min)
EOF
1
2
3

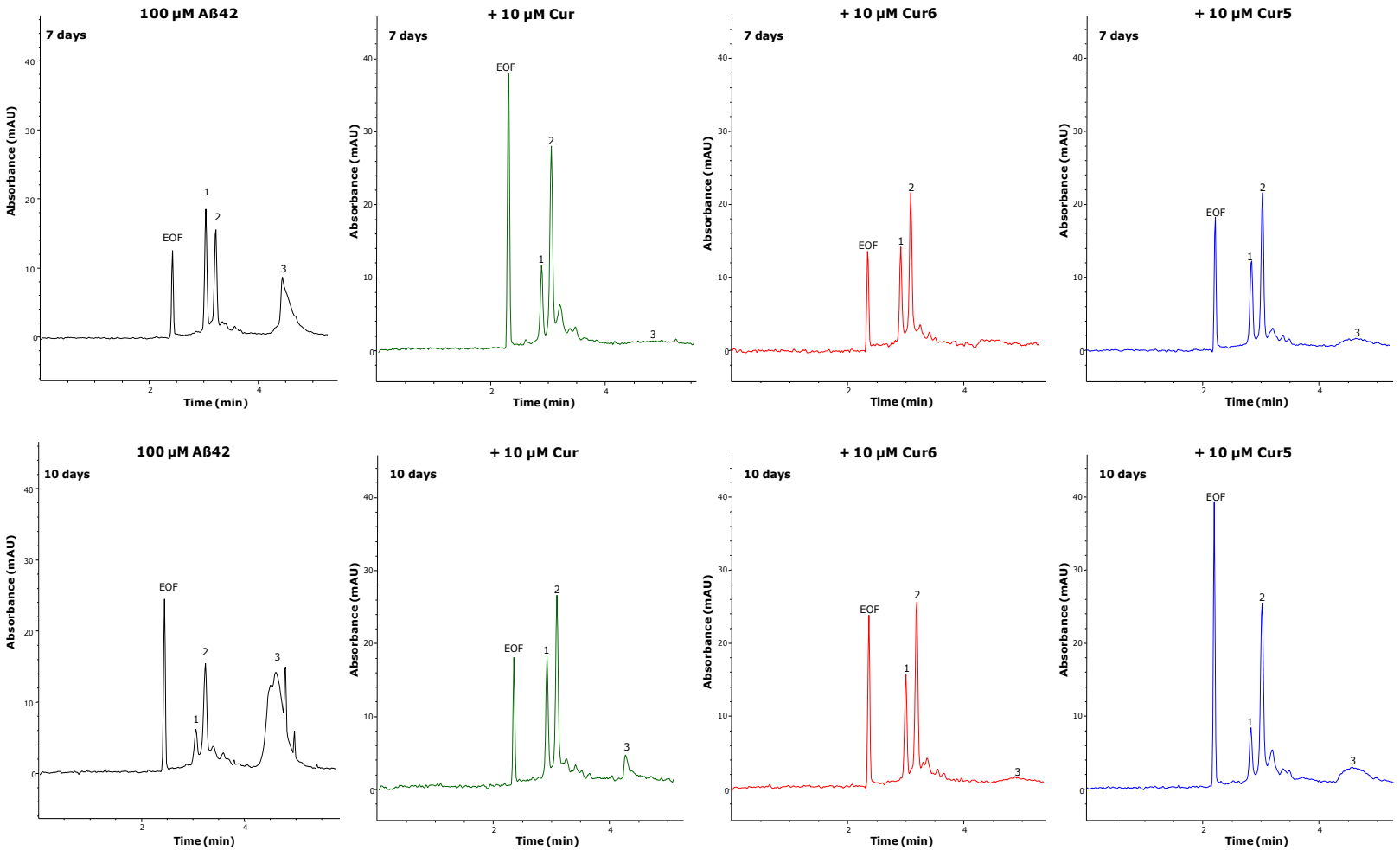
100 µM Aß42
7 days
+ 10 µM Cur
7 days
+ 10 µM Cur6
7 days
+ 10 µM Cur5
7 days
100 µM Aß42
10 days
+ 10 µM Cur
10 days
+ 10 µM Cur6
10 days
+ 10 µM Cur5
10 days
Absorbance (mAU)
Time (min)
EOF
1
2
3

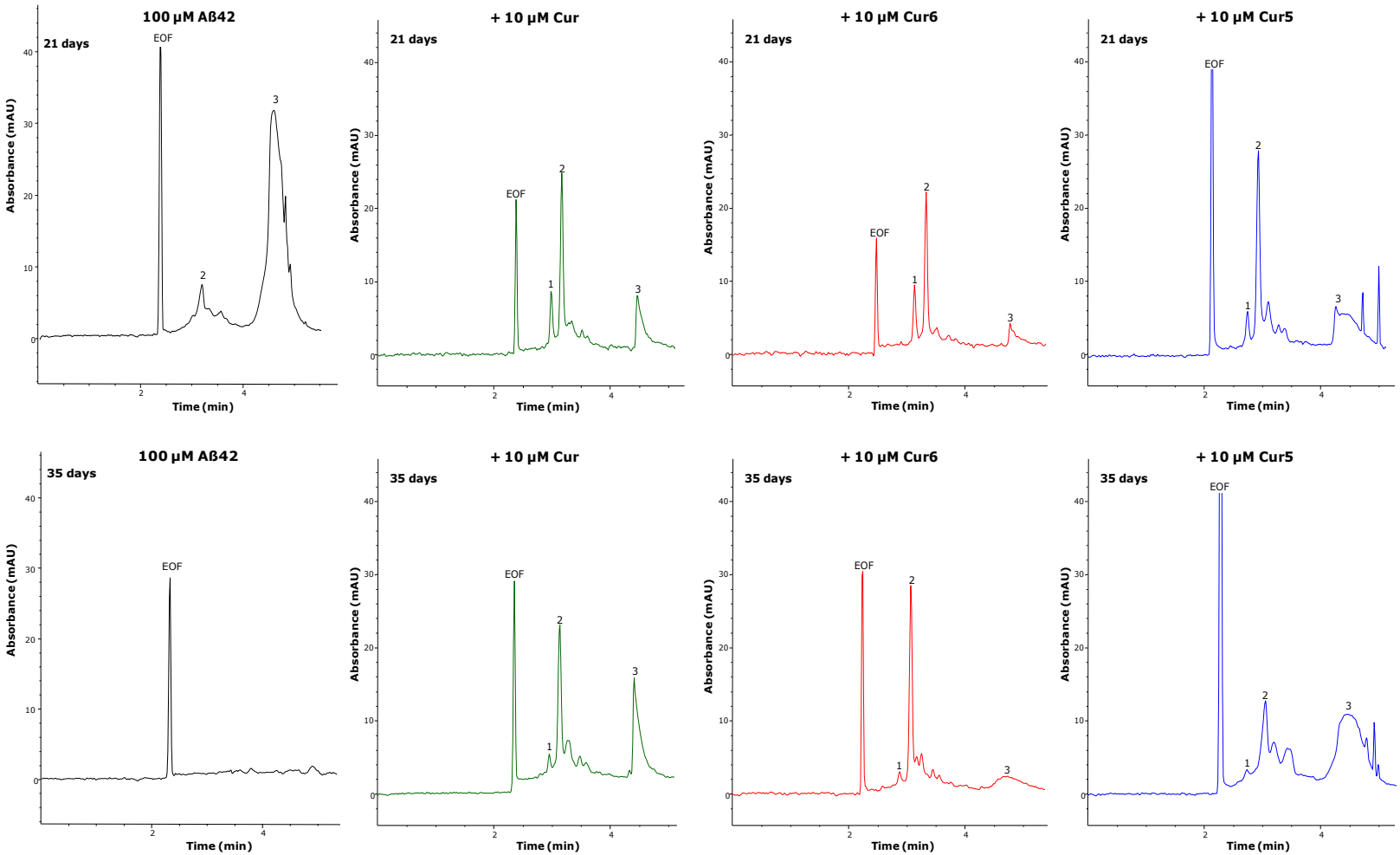
100 µM Aß42
21 days
EOF
2
3
Absorbance (mAU)
Time (min)
+ 10 µM Cur
21 days
EOF
1
2
3
Absorbance (mAU)
Time (min)
+ 10 µM Cur6
21 days
EOF
1
2
3
Absorbance (mAU)
Time (min)
+ 10 µM Cur5
21 days
EOF
1
2
3
Absorbance (mAU)
Time (min)
100 µM Aß42
35 days
EOF
Absorbance (mAU)
Time (min)
+ 10 µM Cur
35 days
EOF
1
2
3
Absorbance (mAU)
Time (min)
+ 10 µM Cur6
35 days
EOF
1
2
3
Absorbance (mAU)
Time (min)
+ 10 µM Cur5
35 days
EOF
1
2
3
Absorbance (mAU)
Time (min)

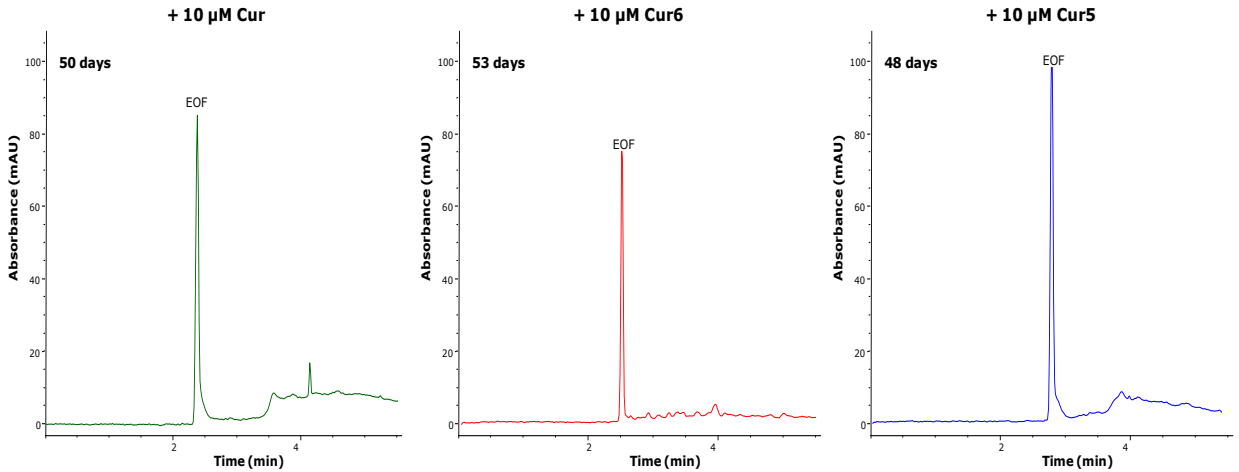

Figure 7. Comparison between electrophoretic profiles at different elapsed times from solubilization (t0, 3 days, 7 days, 10 days, 21 days, 35 days, and at about 50 days) of 100 µM Aß2 alone and in the presence of 10 µM Cur, 10 µM Cur6, 10 µM Cur5.

4.1.1.1 Anti-aggregation activity: effects on small oligomers

As shown previously (see Chapter I, Section 3.1.3 **Figure 8**) and also reported here for clarity (**Figure 7** and **Figure 8**), in a 100 μM Aß42 control solution the normalized area of Peak 1 decreases over time contributing to the formation of Peak 2 and Peak3. In turn, the area of Peak 2 increases during the early stage of oligomerization. Then, also oligomers migrating under this peak self-assemble to form larger aggregates. Indeed, at long times from solubilization, also Peak 2 is depleted.

As evident from the electrophoretic traces in **Figure 7**, the presence of compounds modifies the existing equilibrium among oligomeric populations.
The analysis of the normalized area of Peaks 1 and 2 suggests that, even at the lowest compound concentration here tested (10 μM), the equilibrium is shifted towards the small oligomers. In particular, the trend of Peak 1 is not different from that observed in the absence of small molecules: it is slowly depleted over time (**Figure 8a)**). On the other hand (**Figure 8b)**), even at long coincubation times oligomers migrating under Peak 2 remain highly soluble, as opposed to the behaviour of the control peptide. This result is consistent with the stabilization of Aß dimers induced by curcumin and reported in [22]. This is also supported by the fact that, within 48 hours and in presence of compounds, dimers (Peak 2), become the main species at the expenses of monomers. However, in 100 μM Aß42 control, this interconversion occurs at 5 days.
Notably, at later stages of aggregation and in the presence of 25 and also of 10 μM Cur5, Peak 2 area decreases and completely converts into larger aggregates (Peak 3), suggesting a weaker stabilization of dimers exerted by Cur5 at lower concentration.

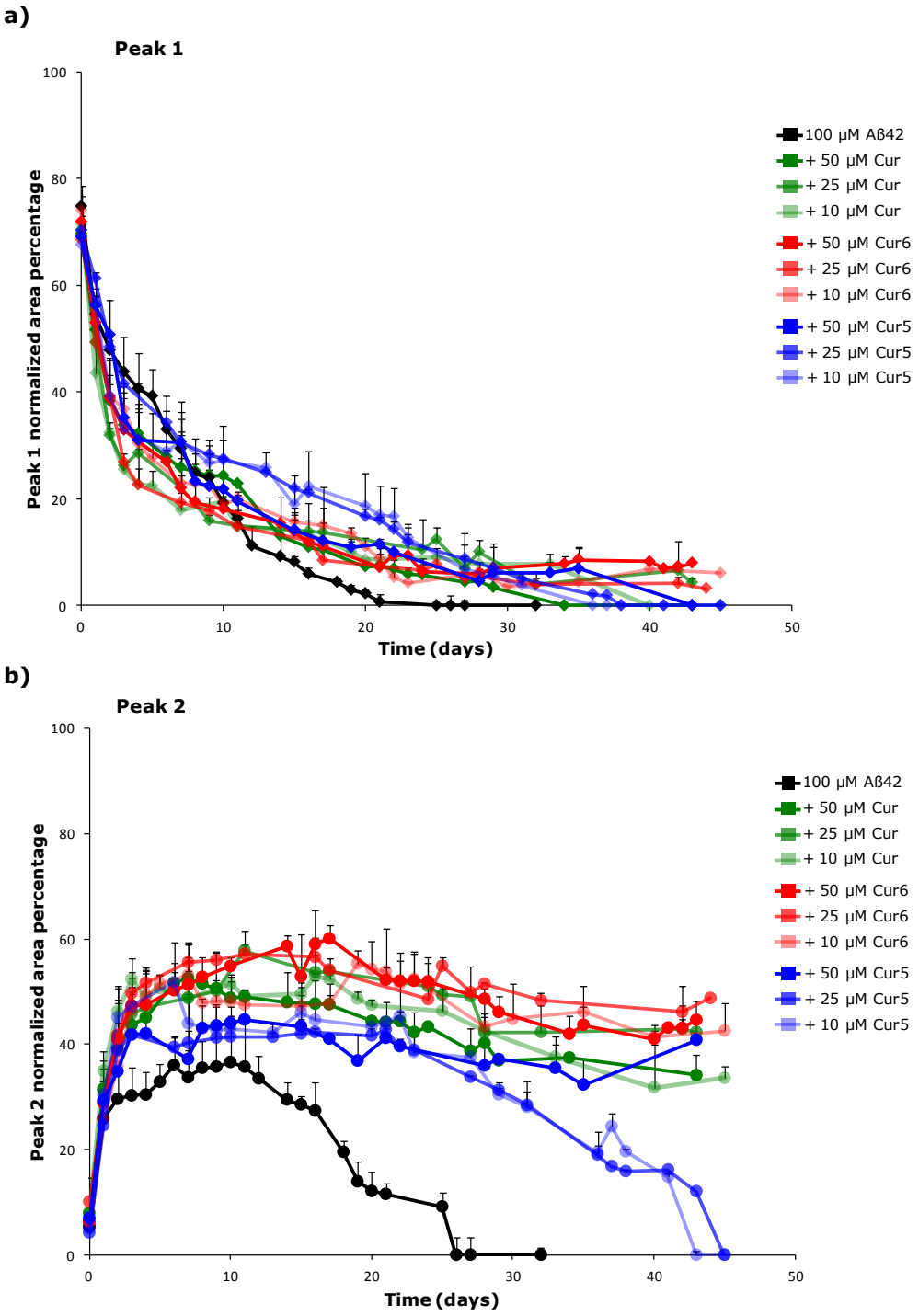

Figure 8. Effect of Cur, Cur6 and Cur5 (50, 25, 10 µM) on small oligomers: **a)** plot of Peak 1 and **b)** Peak 2 normalized area *versus* elapsed times from solubilization. Data are expressed as means ± SD for n=3 replicates.

4.1.1.2 Anti-aggregation activity: effects on large oligomers

Curcumin and newly synthesized curcumin-based analogues have demonstrated to stabilize small aggregates and consistently to hinder the formation of larger assemblies (**Figure 7**). From traces in **Figure 7** and from the normalized area plots of Peak 3 (i.e. oligomers bigger than decamers) reported in **Figure 9**, it is evident that the anti-aggregation activity of Cur (**Figure 9a)**) Cur6 (**Figure 9b)**) and Cur5 (**Figure 9c)**) is concentration dependent.

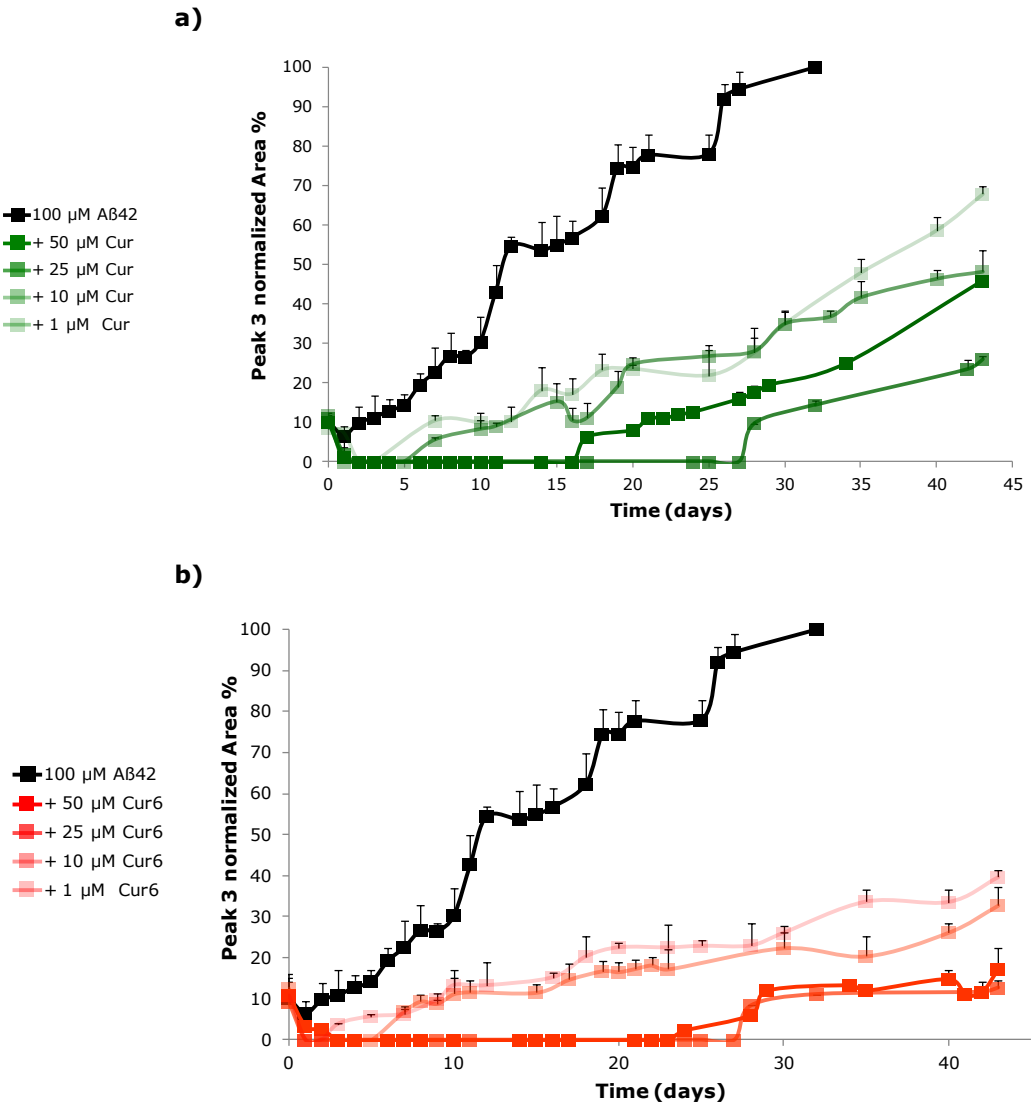

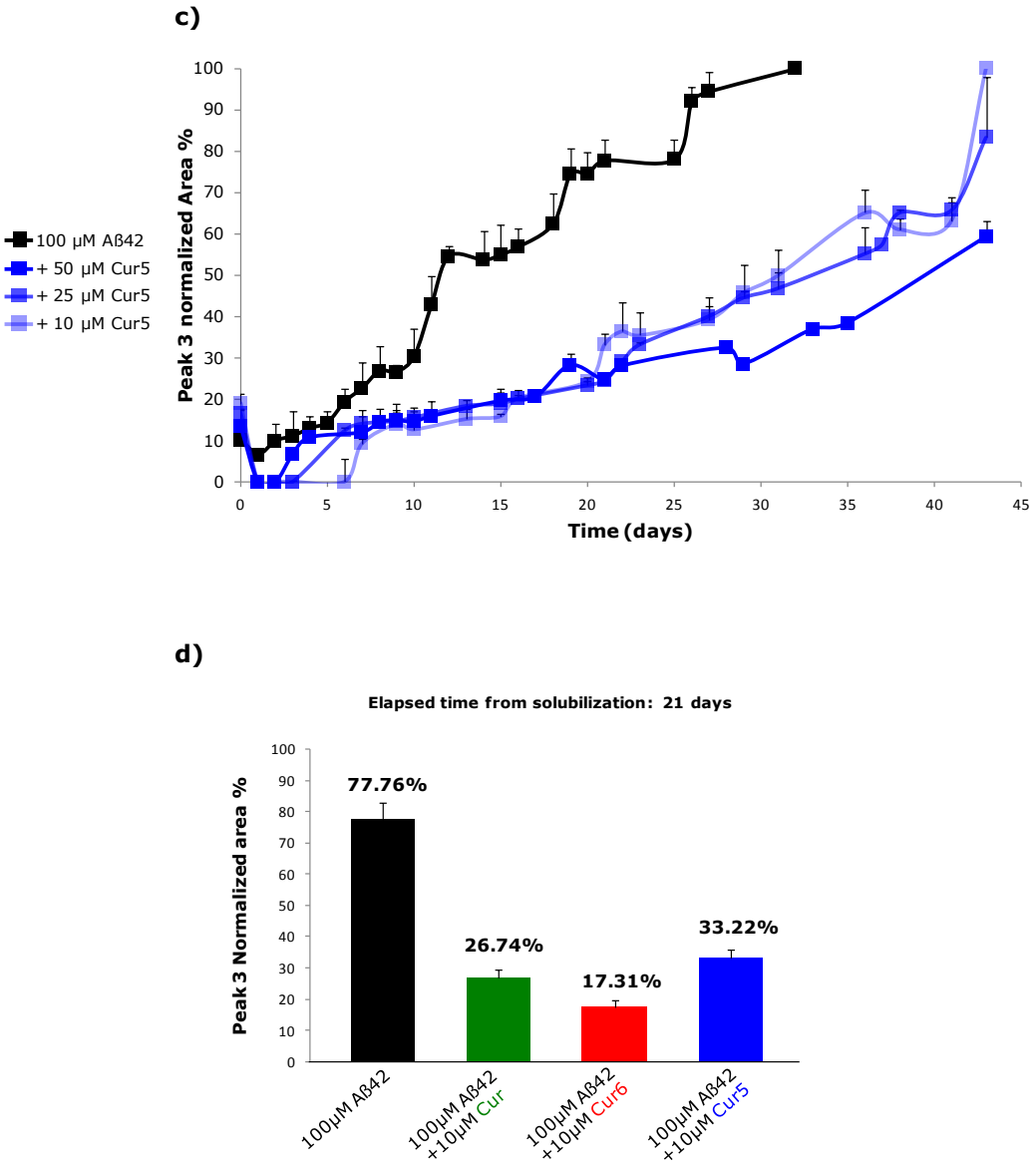

Figure 9. Anti-oligomeric effect of compounds on toxic large oligomers over time. Normalized area percentage plot of Peak 3 of 100 µM Aß42 alone and in presence of decreasing concentrations of: **a)** Cur, **b)** Cur6**, c)** Cur5. **d)** Normalized area percentage of Peak 3 at 21 days from the solubilization as observed in control peptide and in the presence of 10 µM Cur, Cur6 and Cur5. Data are expressed as mean±SD, for n=3.

In the presence of higher concentrations (50 and 25 µM) of Cur and Cur6, Peak 3 is not detected for long time, while over this same time Cur5 already promotes the formation of HMW assemblies, albeit to a lesser extent as compared to that of control peptide. Alike in control peptide, in the presence of Cur5 at 25 and 10 µM the normalized area of Peak 3 eventually reaches 100%, therefore at late stage of oligomerization it is the unique species detected.

Contrary to Aß42 alone, the total conversion of small oligomers into larger species is achieved at longer time as shown in **Figure 9c)**. Since the inhibitory activity of Cur5 is not strong enough to hinder the formation of toxic aggregates, for this compound the lowest concentration (1 μM) is not investigated.
On the other hand, in presence of both Cur and Cur6 the aggregation process of Aß42 is considerably slowed down in a concentration-dependent manner. As illustrated in the normalized area plots of **Figure 9a)** and **Figure 9b)**, Cur and Cur6 display a similar inhibitory effect on the self-assembly of Aß42 peptide, especially at higher concentration levels (50 and 25 μM). At lower concentrations (10 and 1 μM) Cur6 is more potent than Cur, in that the normalized area of Peak 3 is lower in the presence of Cur6 rather than in coincubation with Cur.

Figure 9d) highlights this difference. After 21 days from solubilization of Aß42 control peptide, Peak 3 is detected as the most abundant species (77.76% ± 5.08), while in the presence of 10 μM compounds the normalized area of Peak 3 is statistically decreased. Noteworthy, Cur6 exhibits the strongest anti-oligomeric activity by inducing a significant reduction of the normalized area relative to toxic oligomers (17.31% ± 2.15).

CE data seem to be consistent with the activity expected by virtue of structural modifications.
As reported above, the anti-amyloid activity of curcumin is related to its substituents on the aryl rings, namely the 4-hydroxyl-3-methoxy groups, and the ß-keto enol function [3,22,24]. Therefore, since both 4-hydroxy-3-methoxy groups have been replaced in Cur5 (see **Figure 3** and **Figure 5**), this compound shows the lowest anti-oligomeric activity among the small molecules tested. On the other hand, despite Cur6 only bears one 4-hydroxyl-3-methoxy group, it is found to be a more potent antioligomeric compound than curcumin, even at low concentrations. In this respect and at this stage of the studies, it can be only hypothesized that the prenyl functional group may play a favourable role in disrupting peptide-peptide interactions by intercalation. Molecular docking and molecular dynamic simulation studies will be carried out, as they should provide further information to elucidate the data observed [10].

4.1.1.3 A SAR approach

As reported in literature, along with methoxyl and hydroxyl functions in the *meta* and *para* positions on the aryl rings, also the ß-keto enol group [3,22,24] as well as the linker length [24,25] play a key role in the anti-aggregation activity of curcumin.

Since Cur5 is endowed with all these chemical features, it shows some anti-oligomeric activity, although much lower than that of Cur and Cur6.

In order to approach a structure-activity relationship study, also the role of ß-keto enol group is investigated. To this end, the chemical structures of Cur6 and Cur5 are modified to produce monocarbonyl derivatives.
In monocarbonyl Cur6 and in monocarbonyl Cur5 the ß-keto enol group is removed, so that the linker chain between the two aromatic rings consists of 5 carbon atoms, instead of 7. The chemical structures of compounds are reported in **Figure 3** (see Section 2.2.1).
As for the other curcumin-based analogues, the anti-oligomerization activity of monocarbonyl derivatives is evaluated by analytically monitoring over time the aggregation process of Aß42 in the presence of these small molecules. To date, coincubation studies with monocarbonyl Cur6 and monocarbonyl Cur5 have been performed at 50 µM.
Because of the removal and the modification of other two functional groups related to the anti-aggregation activity of curcumin and of curcumin-based analogues, the ability in hindering the formation of large oligomers should be more limited. Indeed, as evident from Peak 3 normalized area plot illustrated in **Figure 10**, monocarbonyl Cur6 and monocarbonyl Cur5 at 50 µM exhibit a lower anti-aggregation activity, compared to that of their reference compounds (Cur6 and Cur5).
As for what seen with Cur5, also its monocarbonyl derivative retains some antioligomeric activity: Peak 3 is formed and over time it represents an abundant species. The normalized area of Peak 3 is lower than that of Aß42 alone, but it is higher in respect to that observed in Aß42 samples coincubated with Cur5. Therefore, as expected, the monocarbonyl derivative is characterized by a lower potency compared to its reference compound.
In an analogous fashion, Cur6 is a more potent inhibitor of the Aß42 aggregation process compared to monocarbonyl Cur6. However, in contrast to the couple Cur5-monocarbonyl Cur5, the removal of the ß-keto enol group in Cur6 structure has a stronger effect on the potency of compound. In the presence of monocarbonyl Cur6 (50 µM) Peak 3 is detected since the early phase and during this phase its normalized area is higher than that obtained in coincubation with Cur5 and monocarbonyl Cur5. On the other hand, focusing on the late stage of aggregation, the activity expected is confirmed: monocarbonyl Cur6 demonstrates to be a weaker inhibitor of the formation of large aggregates than Cur6, and compared to Cur5 and monocarbonyl Cur5 its activity is higher.

Noteworthy, by CE it is possible to monitor the effect of new chemical entities on toxic oligomers and to verify their expected activity based on the structural modifications applied. In this case, the substitution of 4-hydroxyl-3-methoxy groups and the modification of the ß-keto enol functions of curcumin resulted in a gradual decrease in the ability of hindering the formation of toxic large Aß42 assemblies (monocarbonyl Cur5 < Cur5 < monocarbonyl Cur6 < Cur 6).

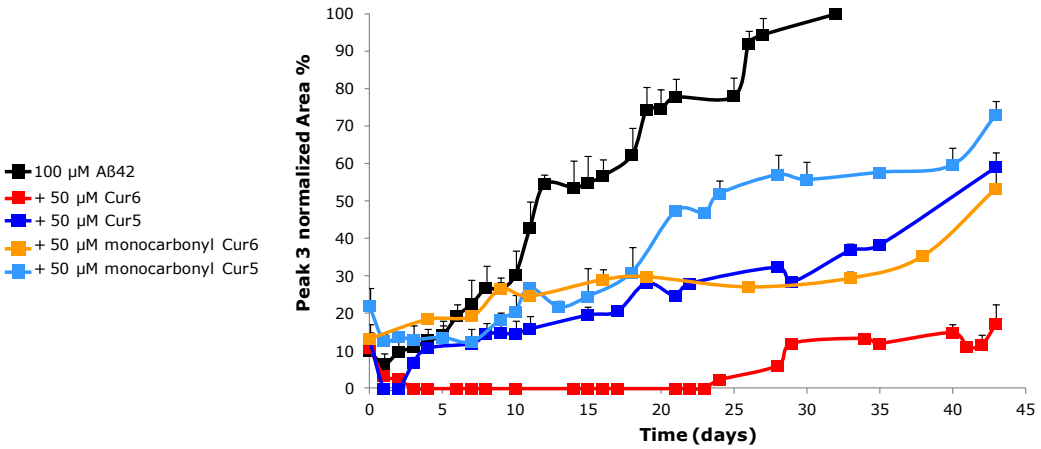

Figure 10. Anti-aggregation activity of monocarbonyl Cur6 and monocarbonyl Cur5 and comparison with the anti-oligomeric activity of Cur6 and Cur5. Peak 3 normalized area percentage of 100 µM Aß42 alone or in the presence of 50 µM monocarbonyl Cur6 and monocarbonyl Cur5. Each experimental poin is in triplicate, data are expressed as means±SD.

4.1.2 SET2

SET2 includes two compounds (here named GS29 and RC10) in which the cinnamoyl function of curcumin is combined with the allyl mercaptan moiety of diallyl disulfide to combine the anti-aggregation activity of curcumin with the anti-oxidant properties of garlic [27]. These authors demonstrated that the presence of an additional hydroxyl group in *ortho* position on the phenolic ring plays a crucial role in the enhancement of the antiaggregation properties. They reported that the antiamyloid activity of GS29 is more potent than that of curcumin. Hydroxyl substituents on the aromatic ring act as "on-off switch" to tune the anti-aggregating efficacy in this set of compounds [27]. Indeed, for RC10, in which only the phenolic moiety is present, the anti-aggregation activity is completely suppressed. On the other hand both compounds showed protective effects against H_2O_2-induced oxidative damage. The inhibitory activity of these compounds and of curcumin was assessed by ThT fluorescence assay and by ESI-IT MS.

Based on these results, the analytical platform developed by us is applied also for these compounds in order to get a deeper characterization of the anti-amyloid activity of GS29. An important issue in the aggregation studies is the availability of negative controls useful to verify the anti-aggregation properties of small molecules in a more precisely fashion in respect to the mere comparison with the peptide in absence of compounds.

Therefore in this study, RC10 is considered as the negative control, bearing in mind that abrogation of fibril formation does not necessarily imply anti-oligomeric activity [4,20].

In **Figure 11a)**, electropherograms acquired at 21 days from the solubilization of Aß42 in the presence or not of 50 µM GS29 and 50 µM RC10 are reported. In the trace relative to the coincubation with RC10, in addition to the EOF peak and to peaks referred to oligomeric populations (Peaks 1, 2 and 3) another peak is detected over time. It is hypothesized that the species, which migrates slower in respect to Aß42 oligomers (μ_{eff}= 2.48 x 10^{-4} $cm^2V^{-1}s^{-1}$± 7.38 x 10^{-6} $cm^2V^{-1}s^{-1}$) may be the RC10 itself, as supported by its UV-DAD spectrum **Figure 11a)** and **b)**.

GS29 confirms to be a very potent compound, in fact Peak 3 is not detected for long times, as evident from the normalized area plot illustrated in **Figure 11c)**. Interestingly, from CE analysis, also the negative control RC10, is able to shift the equilibrium towards non toxic small species: although peak 3 is formed over time, its area is significantly lower than that of control peptide**.**

That the graph in **Figure 11c)** shows a similar trend for GS29 and RC10, although with lower peak 3 area values in presence of GS29, is in strong contrast with the activity found by ThT and ESI-IT MS analyses at the same compound concentration (50 µM). However, in the work of Simoni *et al*., data were only produced on overall anti-fibrillogenic activity, as classically assessed by ThT fluorescence, while by ESI-IT MS only the effect on the Aß42 monomer's amount was monitored. Therefore no information about the activity on soluble oligomers was available.

a)

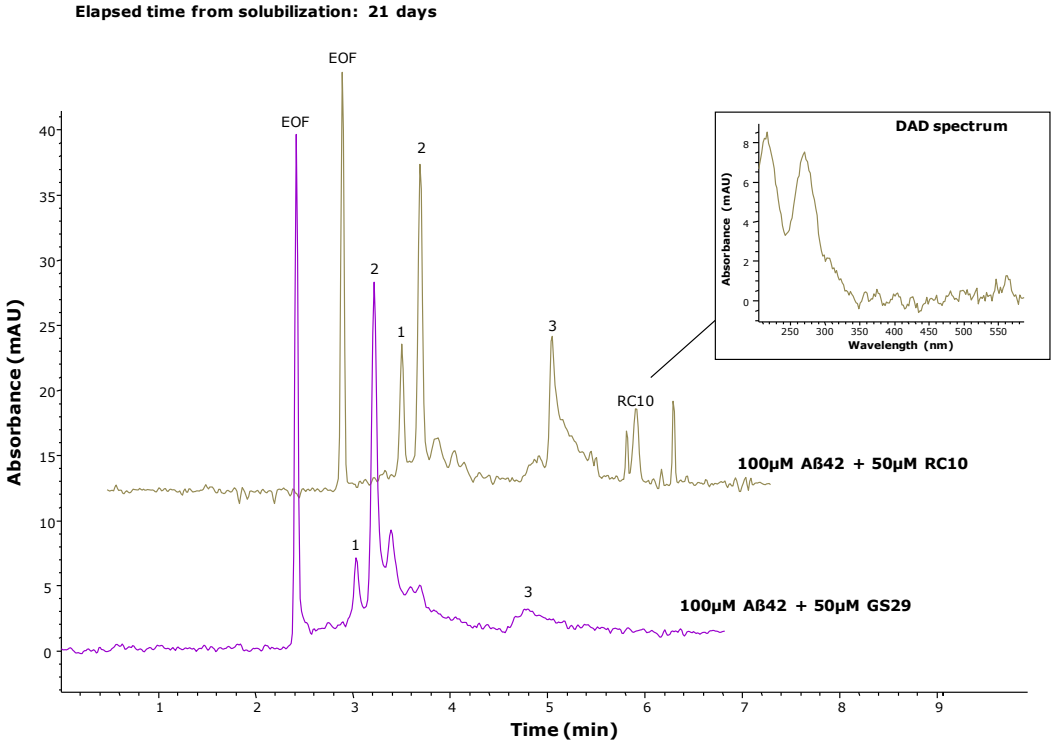
Elapsed time from solubilization: 21 days
EOF
EOF
2
2
1
3
RC10
100µM Aß42 + 50µM RC10
1
3
100µM Aß42 + 50µM GS29
DAD spectrum
Absorbance (mAU)
Wavelength (nm)
Absorbance (mAU)
Time (min)

b)

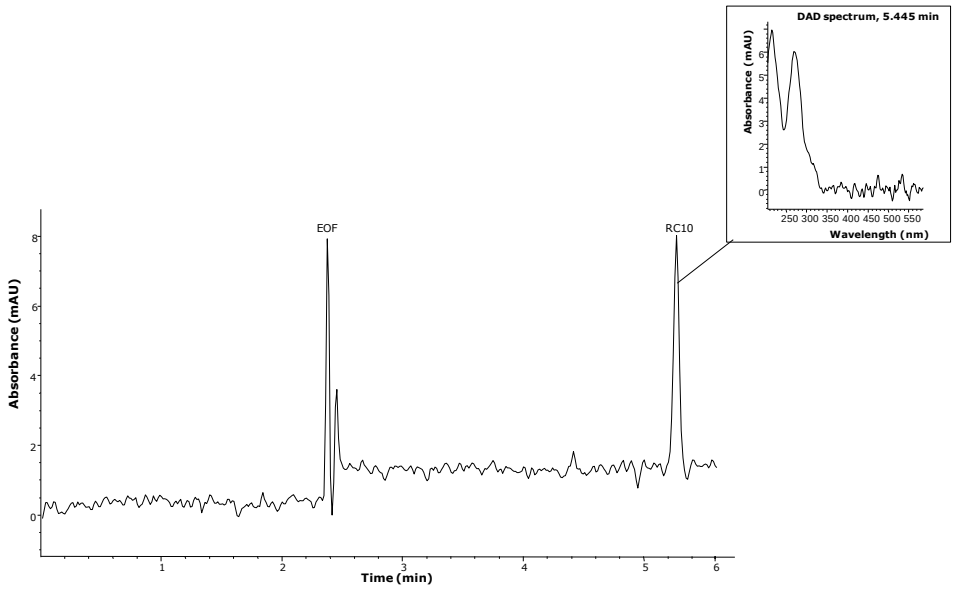
DAD spectrum, 5.445 min
Absorbance (mAU)
Wavelength (nm)
EOF
RC10
Absorbance (mAU)
Time (min)

c)

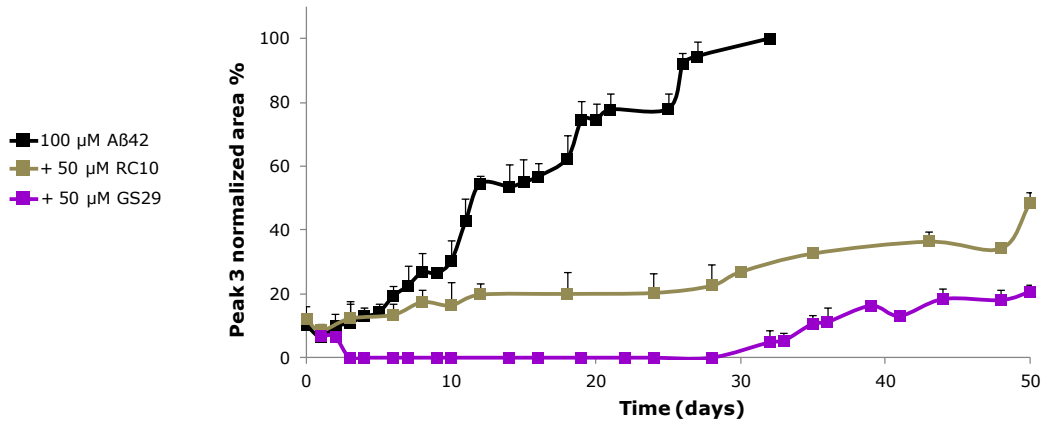

Figure 11. Evaluation of the anti-aggregation activity of compounds belonging to *SET2*: 50 µM GS29 and RC10. **a)** Electrophoretic profiles of 100 µM Aß42 alone or in the presence of 50 µM compounds after 21 days from the solubilization. Inset: UV-DAD spectra of peptide Peak 3 and of RC10. **b)** electropherogram of pure RC10 injected in CE and DAD spectrum of RC10 peak. **c)** Peak 3 normalized area percentage plot of Aß42 alone and in coincubation with 50 µM GS29 or RC10. Data are expressed as mean ± SD, each experimental point is in triplicate.

In **Figure 12**, the anti-aggregation activity of compounds of SET2 at 50 µM is compared to that of Cur, Cur6 and Cur5. As described above, GS29 strongly inhibits the formation of large oligomers, indeed its activity is comparable to that of Cur6, which in turn demonstrated to be the most active compound of SET1. Therefore also GS29 shows a higher activy in respect to Cur. In the presence of 50 µM RC10 large aggregates build up over time and after 30 days from solubilization the normalized area of Peak 3 is 32.74%. Based on these studies, the anti-oligomeric activity of RC10 and Cur5 is similar.
Futher studies at decreasing concentrations of compounds should be performed to deeper compare the two sets of curcumin-based analogues.

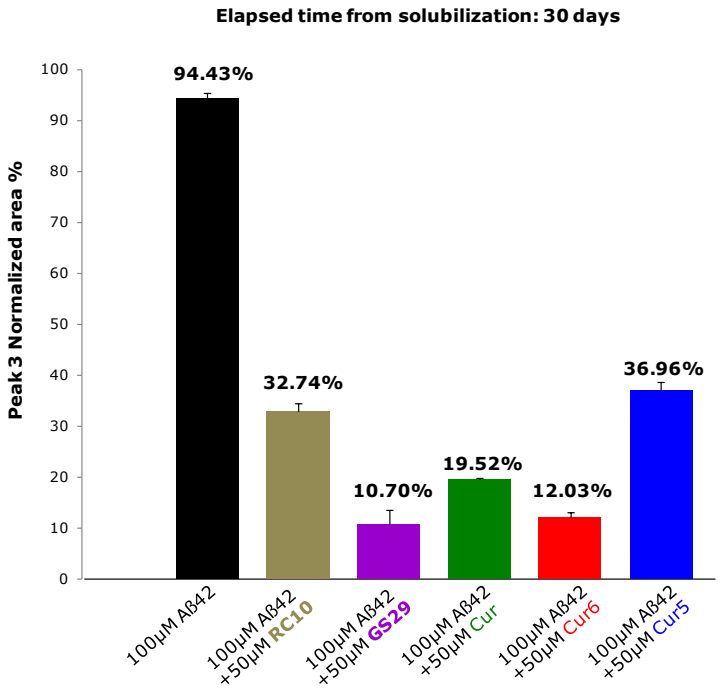

Figure 12. Comparision of the anti-aggregation activity of RC10, GS29, Cur, Cur6 and Cur5. Normalized area percentage of Peak 3 at 30 days from the solubilization as observed in control peptide and in the presence of 50 μM RC10, GS29 Cur, Cur6 and Cur5. Data are expressed as mean ± SD, for n=3.

4.2 SET1: evaluation of neurotoxicity

In view of evaluating if the Aß42 oligomers-induced toxicity is ameliorated in presence of compounds, the intrinsic toxicity of the compounds has to be assessed first. Cur, Cur6 and Cur5 were previously tested for their neurotoxicity on microglia cells (see **Figure S2**): Cur5 and Cur resulted toxic at concentrations equal or higher than 5 μM and 10 μM, respectively. Conversely, Cur6 showed to be not toxic up to high concentrations (40 μM).

The toxicity of SET1 (Cur, Cur6, Cur5, monocarbonyl Cur6 and monocarbonyl Cur5) is also examined on neuroblastoma cells.

Cells are exposed to compound concentrations ranging from 0 to 50 μM for 24 hours and cell viability is measured by MTT assay. As shown in **Figure 13**, high concentrations (20-50 μM) of all compounds induce a significant loss of cell viability if compared to cell exposure only to cell culture medium. Cur5 and monocarbonyl Cur5 show a comparable toxic profile: both are toxic at 5 μM. For Cur5, this data is consistent with the toxicity exerted on microglia cells. On the other hand on this cellular line, a similar trend is observed in Cur6- and

curcumin-induced toxicity: both compounds are toxic at concentration equal or higher than 20 µM and cell viability remains high and comparable with that of untreated cells when exposed to low concentrations (<20 µM).
Interestingly, monocarbonyl Cur6 presents an intermediate toxic profile, i.e. between that of more toxic compounds (Cur5 and monocarbonyl Cur5) and that of Cur and Cur6: at high concentrations (20-50 µM) it has an important toxic effect, conversely at concentrations ranging from 10-5 µM it is not toxic, alike Cur and Cur6.
Considering the chemical modifications applied to these compounds, it is not clear why monocarbonyl Cur6 shows this toxicity profile: this effect does not seem to be correlated to the presence of prenyloxy groups or to the reduction of the spacer length from 7-C to 5-C. Indeed Cur6, endowed with one prenyloxy substitution and monocarbonyl Cur5, with a shorter spacer, have a different profile. We hypothesize a synergic effect between these two modifications, however further investigations on a larger number of compounds should be performed to get a deeper understanding of the potential correlation between structure and toxicity profile.

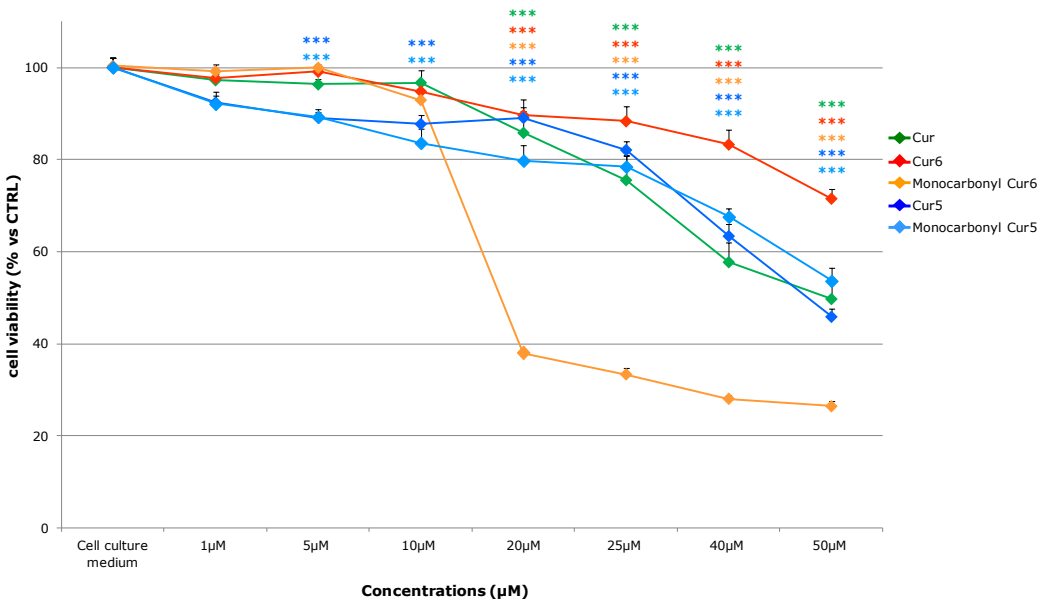

Figure 13. Neurotoxic effects of compounds belonging to SET1 on neuroblastoma cells (SH-SY5Y). Data are expressed as mean ± SD (n=3 replicates, three independent experiments). * p<0.05, **p<0.01, ***p<0.001 *vs* non treated cells, ANOVA + post-hoc Dunnett's test.

4.3 SET1: evaluation of the antifibrillogenic activity *in vitro* and *in vivo*

4.3.1 TEM analyses

Together with ThT fluorescence assay, transmission electron microscopy (TEM) is one of the most widespread techniques to probe or exclude the presence of fibrils, both in *in vitro* and in *ex vivo* studies [40]. These techniques have been successfully applied also by us and others to appreciate the effect on fibril formation, fibril morphology and fibril density in presence of small molecules [9,10,41].

In Chapter I it has been shown that when prepared by following the least aggregating protocol (protocol #3), Aß42 precipitates as a dense network of fibrils. Consequently, by appling this sample preparation protocol, it is possible to verify the potential anti-fibrillogenic activity of compounds.

To this end, the ability of SET1 (Cur6, Cur5, monocarbonyl Cur6 and monocarbonyl Cur5) of inhibiting fibril formation is investigated, taking curcumin as reference compound. In this work, because of the intrinsic fluorescence of curcumin and considering that all compounds tested preserve the chemical scaffold of curcumin, ThT fluorescence assay is precluded [39].

As argued above, numerous findings on the anti-aggregation activity of curcumin are inconsistent and contradictory [21]. The dominant view is that curcumin exerts an anti-amyloid activity, not only because it stabilizes small oligomers [22], but also because it hinders the formation of amyloid fibrils and destroys the pre-existing fibrillar deposits, both *in vitro* and *in vivo* [25]. However, contrary to this general view, curcumin has also demonstrated to inhibit oligomerization while promoting fibrillization [20]. Furthermore, in a recent work it was found that indeed curcumin does not prevent fibril formation, but rather it modifies the on-pathway Aß aggregation toward an alternative off-pathway, a mechanism that produces non toxic aggregates. Morphologically, these aggregates are not distinguishable from toxic fibrils [21].

As shown, Aß42 oligomers in the presence of compounds are kept in solution for longer time compared to Aß42 in the absence of small molecules. This wide time window allowed to better appreciate the effects on the formation of oligomeric populations by the selected compounds. At sample precipitation, i.e. when no more peaks are detected in CE, samples are fixed and observed at TEM.

In **Figure 14** TEM images of Aß42 alone or in the presence of compounds belonging to SET1 are reported. Images are taken at different elapsed times from the solubilization.
The final precipitation of Aß42 leads to the typical dense network of amyloid fibrils, although amyloid fibrils are present since 24 hours. Conversely to the

control peptide, already after 24 hours Aß42 samples coincubated with Cur or Cur6 contain amorphous aggregates. The presence of non fibrillar aggregates is kept at a later stage of oligomerization, as also after 21 days amorphous granular assemblies are observed. This is consistent with the anti-oligomeric activity demonstrated by both compounds (see **Figure 7** and **Figure 9**). However, at sample precipitation in the presence of Cur, a network of fibrils is evident, comparable to that observed for the control peptide. Based on these findings, our results support recent reports that suggest that curcumin only has an anti-oligomeric activity [20,21,25].

In the same fashion, both monocarbonyl derivatives of Cur6 and Cur5, which demonstrated to have a lower anti-oligomeric activity among compounds of SET1, lead to amyloid fibrils as end products of the amyloid process. This is in accordance with structural modifications.

Based on the CE analyses, Cur6 has shown to be the most active compound in inhibiting the formation of toxic large aggregates. In **Figure 14** only sporadic fibrils are detected in precipitated samples of Aß42 (t end) in the presence of Cur6, thus indicating also an anti-fibrillogenic activity of this curcumin-based analogue.

Interestingly and surprisingly, Cur5 is able to abrogate the formation of amyloid fibrils: only amorphous granular assemblies are observed at the end of the aggregation process.

Taken together, data obtained from CE analyses and those obtained by TEM show that: Cur is an inhibitor of the formation of large assemblies of Aß42 but it is not able to block the assembly into amyloid fibrils. Cur6, the most active inhibitor towards large oligomer formation shows a moderate anti-fibrillogenic property by leading to sporadic fibrils.

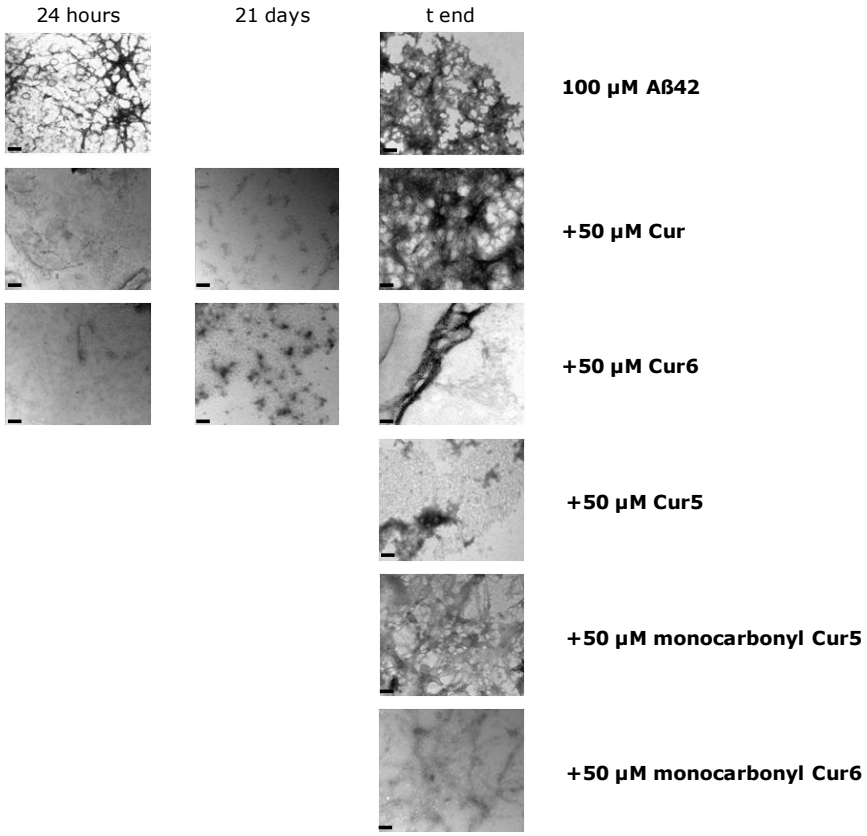

Figure 14. TEM images of Aß42 control peptide and Aß42 coincubated with compounds of SET1, analyzed at different times from solubilization. Scale bar=100nm. 60000x. n=3.

These findings are consistent with the most prevalent hypothesis to date, namely that multiple pathways may contribute to the formation of oligomers (on-pathway and off-pathway) [4]; in turn oligomers can be generated by several mechanisms [20,42]. In particular these results support that the oligomeric formation is independent from the fibril assembly.

Cur6, which retains a 4-hydroxyl-3-methoxy group, strongly hinders the formation of large oligomers, even at low concentrations and it blocks the deposition of oligomers into fibrils. Cur5 shows a low anti-oligomeric activity since it lacks of two important functional groups related to the anti-amyloid activity of curcumin, and nevertheless it leads to amorphous assemblies. As already mentioned, based on chemical structures of compounds it seems that the anti-fibrillogenic activity has an opposite trend in respect to the anti-oligomeric one. In particular this could be hypothesized to be due to the presence of the prenyloxy substituent that may serve as a ß-sheet breaker by intercalating in the amyloid fibrillar core. To confirm this hypothesis further investigations are necessary.

4.3.2 C. elegans body bends assay

Animal models can be useful for understanding the molecular mechanisms which lead to AD by way of specific mutations which reproduce an AD-related behaviour phenotype. For example, in rodent models, the accumulation of Aß peptides causes cognitive deficits similar to those observed in humans, namely memory loss and behavioural changes. The evaluation of deficits by specific tests as well as the maintenance of populations are extremely expensive and time consuming. For these reasons, despite the availability of a variety of transgenic mouse models of AD, drug evaluations with these animals are rarely performed [28,43].
Consequently, in the last decades increasing attention has been paid on the generation of *in vivo* animal models which allow cost reduction as compared to rodent models for a high-throughput screening (HTS) of potential therapeutics in the initial phase of drug discovery [44].

The nematode *Caenorhabditis elegans* responds to this urgent need.
C. elegans was first introduced as a model organism by Sydney [30]. It is a small (1 mm in length) and transparent worm; its life cycle is short (only 3 days from eggs to adult) and the lifespan is about 20 days. These features make manipulation easy and facilitate the study of its biology. Furthermore, since roughly 38% of *C. elegans* genes have a human ortholog, including *APP* and *tau* [45] the nematode represents an effective and less expensive animal model for the study of AD and other neurodegenerative diseases [28,43].
Different *C. elegans* strains mutated for AD have been generated [28] to replicate molecular mechanism of AD including several transgenic worms which express human Aß peptides [46]. In particular, the non endogenous intracellular production of Aß peptides offers the opportunity to address which specific mechanisms of intracellular toxicity are induced by Aß.
Although it may not be universally accepted that *C. elegans* has a direct relevance for AD pathology, it is well suited for *in vivo* validation of targets related to Aß toxicity and for compound screening.

The most common *C. elegans* strains mutated for AD overexpress Aß42 total length or a truncated form (Aß3-42), due to miscleavage of a synthetic signal peptide [47]. Also in worms, Aß peptides mirror the human conditions by leading to oligomers and eventually to amyloid fibrils. Based on the type of transgenic strain, the aggregation and deposition of amyloid peptides can occur in muscles or in neurons. When the muscle tissue is affected, *C. elegans* shows an age-dependent paralysis at 20°C, which makes it easy to score the induced pathological behavioural phenotypes. Indeed the most widespread assay used to evaluate the effect of compounds on the aggregation process is the paralysis behaviour assay, also named body bends assay.

Because of these advantages, *C. elegans* is increasingly employed for HTS screening of potential inhibitors of the amyloid process [48], either for synthetic small molecules [47], or for modified peptides able to prevent Aß oligomers formation [49] or for natural products [50,51] including curcumin [52,53].

In Section 4.3.1, the anti-fibrillogenic activity of the two newly synthesized curcumin-based analogues (Cur6 and Cur5) has been demonstrated *in vitro* by TEM analyses. Conversely, curcumin does not prevent fibril formation.

Prompted by these interesting results, a preliminary investigation of Cur, Cur6 and Cur5 on the *in vivo* inhibition of Aß fibrillogenesis is carried out.

As reported in detail in Section 2.7 and illustrated in **Figure 15**, *C. elegans* CL2120 expressing Aß3-42 are treated with Cur, Cur6 and Cur5 at concentration of 100 µM and 50 µM. These concentrations are commonly found in literature for this type of experiments. To evaluate the effect of these compounds, the body bends assay is carried out *in vivo* on untreated worms and on worms exposed to compounds. N2 strain represents the negative control, since it does not express Aß3-42, whereas mutated CL2120 is the positive control because it does not receive treatment.

In **Figure 15** the results of body bends analyses are reported. As expected, worms belonging to N2 group maintain normal movements, as more than 200 body bends/min are counted. On the contrary, in the mutated strain CL2120 the deposition of amyloid fibrils leads to a progressive paralysis and a reduction in the number of body bends per minute is observed. Despite Cur did not demonstrate to be an anti-fibrillogenic compound *in vitro* (see Section 4.3.1), *in vivo* at both concentrations it determines a recovery in worm mobility (compared to non treated *C. elegans* CL2120) equal to 14% and 20% in the presence of 50 µM and 100 µM Cur, respectively.

On the other hand, from TEM data, Cur6 and Cur5 have shown a moderate and a strong activity in inhibiting the fibril formation, respectively (see **Figure 14**). The higher activity of Cur6 and Cur5 in respect to that of Cur is mirrored also in the *in vivo* study. The recovery in worm mobility in treated nematodes is higher than that induced by Cur. As for Cur, also the anti-fibrillogenic activity of Cur6 and Cur5 seems to be concentration-dependent.

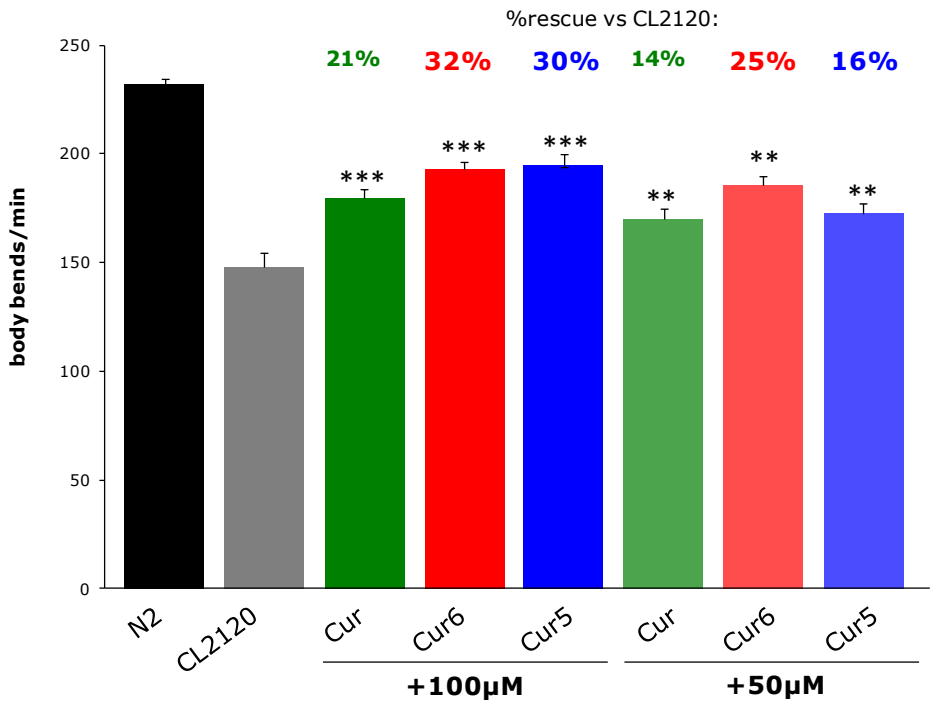

Figure 15. Effect of Cur, Cur6 and Cur5 (100 µM and 50 µM) on behavioral phenotype of *C. elegans*. Body bends assay was performed in triplicate on adult worms after 48 h exposure to small molecules. Data are mean ±SD (N=30 animals for each group); ***$p<0.0001$ versus not-treated CL2120 according to one-way ANOVA. N2 is the non mutated strain, CL2120 is the AD strain.

5 Conclusions

To date no disease-modifying drugs are available for Alzheimer's disease. One of the main reasons for the lack of effective treatments is the incomplete knowledge of its aetiology [54,55]. Considering the difficulties in obtaining clear information about the onset and progression of the disease, AD is reasonably caused by several interconnected phenomena which enhance themselves by leading to diffuse toxicity on cellular pathways [34,35,54,56].

According to the most accepted standpoint, the main neurotoxic mediators involved in AD are toxic aggregates of Aß peptides [1,55]. As discussed in General Remarks, these aggregates generated from the amyloid process of Aß peptides can exert toxic effects at different intracellular and extracellular levels [35,57]. Even though the soluble intermediates of the aggregation process are addressed as the most toxic species, also fibrils may contribute to toxicity mainly because insoluble deposits are in equilibrium with oligomers and may be produced through secondary nucleation processes [1,4].

In the last decades, since the numerous failures in clinical trials of potential therapeutics, it emerged the need to hit the disease from different, multiple and simultaneous fronts. This strategy is known as the multitarget-directed ligands (MTDLs) approach [54,55].

Therefore an effective tool for the treatment of AD should plausibly:

- modulate the amyloid process by halting or reversing the formation of oligomers and fibrils, and
- degrade pre-existing soluble aggregates and fibrils;
- reduce neuroinflammation and oxidative stress;
- block the aggregation of tau proteins;
- rescue mitochondria and neurovascular dysfunctions

or at least it should be active against more than one pathological pathway [54].

With this goal, we applied our analytical platform to investigate potential modulators of the aggregation process of the most amyloidogenic and toxic Aß peptide (Aß42).

The key asset of the platform described in Chapter I is that toxic oligomers have been first analytically separated under quasi physiological conditions to preserve their non covalent structure and then characterized in terms of size and of the toxicity induced. Under the optimized experimental conditions, oligomers larger than decamers (MW>45000 kDa) are found to be responsible for the Aß42-induced toxicity on neuroblastoma cells. This means that, along with the amyloid fibrils produced at the end of the aggregation process, they are important targets for compounds.

Because of its pleiotropic behaviour, curcumin was the starting point in coincubation studies in this work. As reported in literature, curcumin exerts numerous protective effects including anti-oligomeric, anti-fibrillogenic, anti-inflammatory and anti-oxidant activity [3,15,18,20,21]. Nevertheless, reports often are inconsistent and controversial, in addition curcumin exhibits an intrinsinc toxicity and very poor bioavailability, which limits its use as therapeutic agent [15,19]. The high attention paid on curcumin allowed the identification of its pharmacophore elements related to its activities [20,22,25].

Consequently, a reasonable strategy is to modify curcumin structure, to enhance properties of interest and to reduce or abrogate those associated to its limitations [23,24,27,58].

In collaboration with two groups of the University of Bologna two sets of small molecules have been selected and tested. The compounds are classified in this work as SET1 and SET2.
In both sets chemical modifications would improve the biological profile of curcumin in the context of the MTDLs strategy [54]. In SET1 the addition of a prenyloxy function on one (Cur6 and monocarbonyl Cur6) or on both aryl rings (Cur5 and monocarbonyl Cur5) may confer to these molecules also anti-inflammatory properties [31-33]. Cur6, which demonstrated to be the less toxic compound among those tested, also strongly inhibits the release of pro-inflammatory cytokines. In SET2 a portion of the curcumin structure was linked with allyl mercaptan disulfide and, as reported in a published work [27], these compounds exert anti-oxidant activity.
Four curcumin-based analogues belong to SET1: Cur6, Cur5, monocarbonyl Cur6 and monocarbonyl Cur5. In these small molecules, functional groups of curcumin mainly related to its drawbacks and to its antiamyloid properties were rationally modified.
Based on CE analyses of Aß42 samples coincubated with compounds, we found that the anti-oligomeric activity of these small molecules is consistent with the structural modifications applied. Overall, all compounds exhibit an anti-oligomeric activity by either largely or mildly slowing down and reducing the formation of large toxic oligomers. Monocarbonyl derivatives are characterized by the lowest anti-aggregation activity even at the highest concentration tested (50 µM) because all portions related to this activity in the curcumin structure were modified (the 4-hydroxy 3-methoxy groups, the ß-keto enol group and the linker length) [3,22,24-26].
Therefore the anti-oligomeric activity follows this order: monocarbonyl Cur5<Cur5<monocarbonyl Cur6<curcumin<Cur6.

Interestingly, as opposed to curcumin, only Cur5 and Cur6 have demonstrated anti-fibrillogenic properties. This activity was confirmed also *in vivo* on AD mutated *C. elegans*: in a concentration dependent manner Cur6 and Cur5

rescue the mobility of worms paralyzed because of the deposition of amyloid fibrils.

Taken together, these results make us to hypothesize that the prenyloxy substituent may play a role in the anti-aggregation activity of these compounds, by modulating both anti-oligomeric and anti-fibrillogenic activity of Cur6 and Cur5, in a different fashion. A confirmation of this hypothesis may come from molecular docking and molecular dynamic simulation studies.

The availability of a reliable and reproducible analytical strategy to evaluate the effect of compounds on soluble Aß42 oligomers was also successfully exploited in coincubation studies with SET2. Molecules of this set were already reported in literature: RC10 showed only anti-oxidant activity, whereas GS29 was described as a good anti-oxidant compound and as a very active anti-aggregating molecule. Indeed GS29 inhibited almost completely the formation of fibrils by hindering the depletion of Aß monomers as demonstrated by ThT fluorescence assay and ESI-IT MS [27].

Based on CE analyses, we found that GS29 has a strong effect on the inhibition of the formation of large oligomers, whereas also RC10, which in our intent was used as negative control, exhibits anti-oligomeric activity in contrast with the published results.

This work demonstrates how CE can play alternative and unique role in aggregation studies of Aß peptides to evaluate the effect of compounds on those soluble oligomers which are here demonstrated to be toxic.

Cur6 is characterized by a good biological profile in terms of toxicity and anti-inflammatory properties. The interest in this compound is increasing because of its ability to modulate both oligomerization and fibrillogenesis. Therefore, Cur6 seems to respond to more than one of the features requested for a MTDL [54]. For all these reasons, Cur6 is worthy further investigations.

Supplementary material

Compounds belonging to the small library synthesized by Federica Belluti and co-workers (unpublished data).

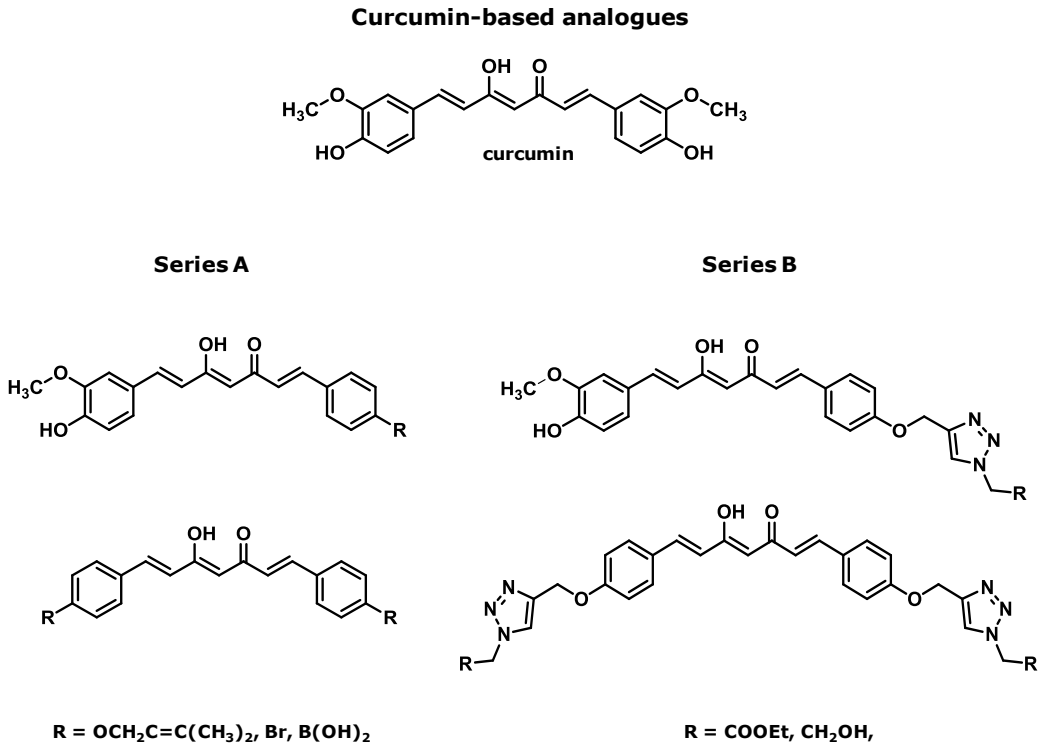

Figure S1. Design strategy of the small library of curcumin-based analogues from which SET1 was selected.

The toxic effect of curcumin, Cur6 and Cur5 at decreasing concentrations (40, 20, 10, 5 and 1 μM) was evaluated on microglia cells and reported in F**igure S2**. Cell viability assay was performed according to Mercanti *et al*. [29].

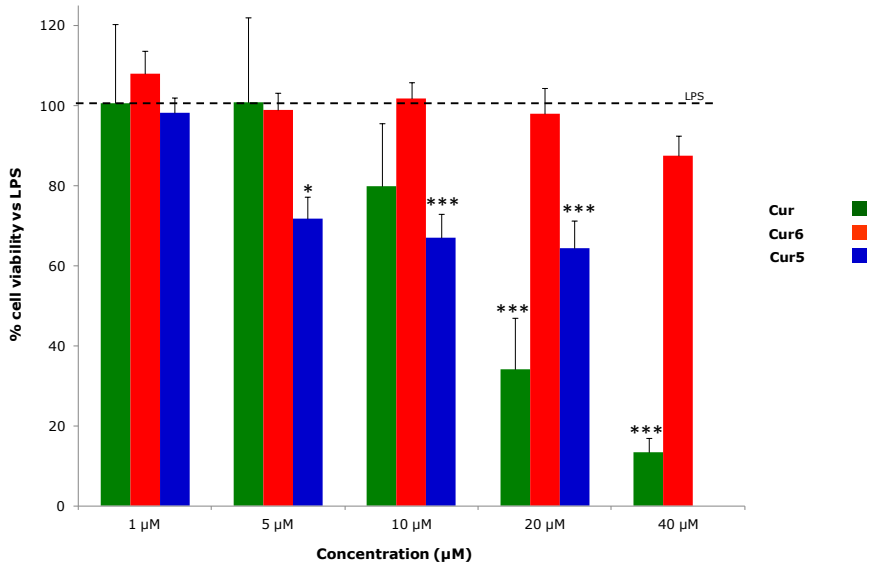

Figure S2. Analysis of microglia cell viability following exposure of increasing concentrations of Cur, Cur6 and Cur5. Data are mean of % cell viability *vs* LPS (dashed line) ± SEM (n=6 for each of three independent experiments). * $p<0.05$, ** $p<0.01$, *** $p<0.001$ *vs* LPS-stimulated cultures, ANOVA + post-hoc Dunnett's test.

The levels of IL-1ß and TNF-α released by microglia into the culture medium were measured after the incubation with curcumin and Cur6. Analyses were performed by using a commercially available enzyme-linked immunosorbent assay (ELISA) kit. Cytokine concentration in the medium was determined by reference to standard curves obtained with known amounts of IL-1ß and TNF-α according to [29].

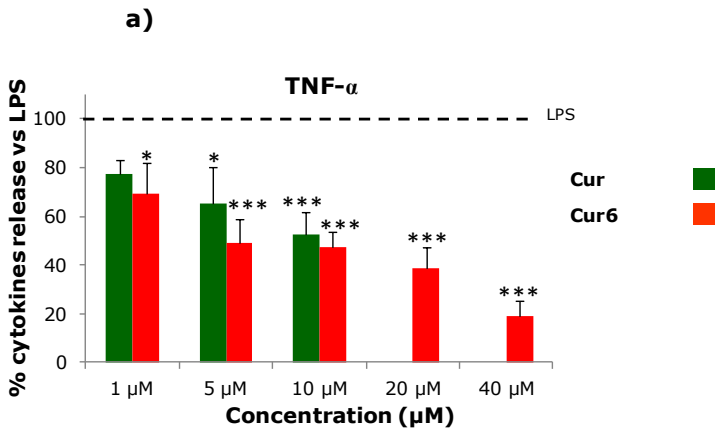

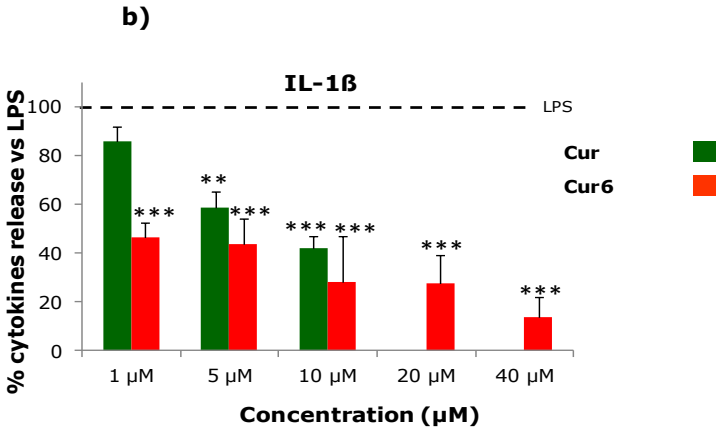

Figure S3. Inhibitory effect of Cur and Cur6 on the release of proinflammatory cytokines: a) TNF-α and b) IL-1ß. The inhibition is expressed as percentage *vs* LPS stimulus. Data are mean ± SEM (n=4 for each of three independent experiments). * $p<0.05$, ** $p<0.01$, *** $p<0.001$ *vs* LPS-stimulated cultures, ANOVA + post-hoc Dunnett's test.

To perform coincubation studies, the effect of EtOH on the aggregation process of Aß42 was evaluated. The highest concentration of EtOH present in samples coinbubated with compounds is 3,26%. It is demonstrated that this percentage does not affect the electrophoretic pattern of Aß42 and consequently the kinetics of the aggregation process is unvaried.

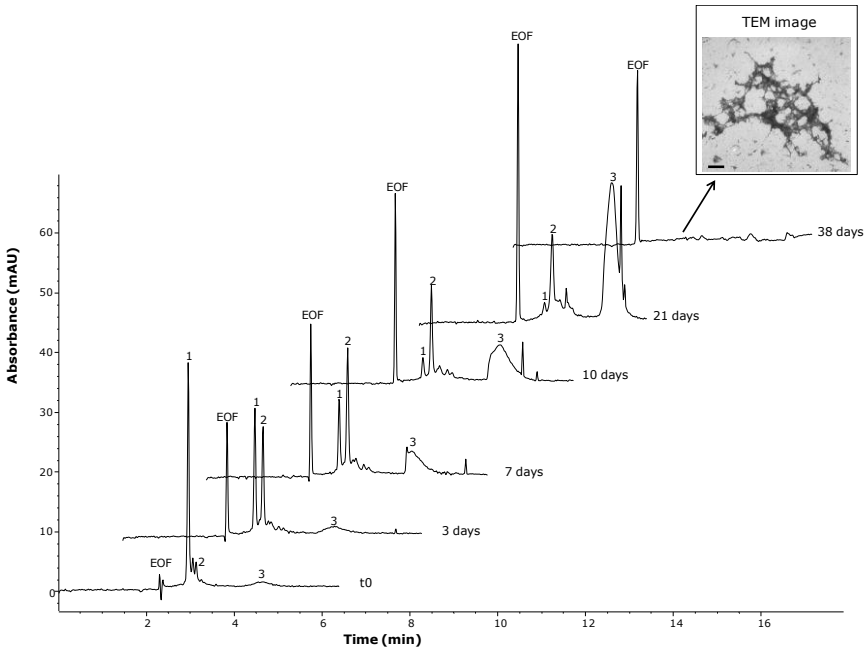

Figure S4. Effect of 3.26% EtOH on the aggregation process of 100µM Aß42.

6 References

1 Chiti, F. and Dobson, C.M. (2017) Protein Misfolding, Amyloid Formation, and Human Disease: A Summary of Progress Over the Last Decade. *Annu Rev Biochem* 86, 35.1-35.42

2 Walsh, D.M. and Selkoe, D.J. (2007) A beta oligomers - a decade of discovery. *J Neurochem* 101 (5), 1172-1184

3 Cheng, B. et al. (2013) Inhibiting toxic aggregation of amyloidogenic proteins: a therapeutic strategy for protein misfolding diseases. *Biochim Biophys Acta* 1830 (10), 4860-4871

4 Lee, S.J. et al. (2017) Towards an understanding of amyloid-beta oligomers: characterization, toxicity mechanisms, and inhibitors. *Chem Soc Rev* 46 (2), 310-323

5 Brinet, D. et al. (2017) In vitro monitoring of amyloid beta-peptide oligomerization by Electrospray differential mobility analysis: An alternative tool to evaluate Alzheimer's disease drug candidates. *Talanta* 165, 84-91.

6 Bartolini, M. et al. (2007) Insight into the kinetic of amyloid beta (1-42) peptide self-aggregation: elucidation of inhibitors' mechanism of action. *Chembiochem* 8 (17), 2152-2161

7 Bartolini, M. et al. (2011) Kinetic characterization of amyloid-beta 1-42 aggregation with a multimethodological approach. *Anal Biochem* 414 (2), 215-225

8 Sabella, S. et al. (2004) Capillary electrophoresis studies on the aggregation process of beta-amyloid 1-42 and 1-40 peptides. *Electrophoresis* 25 (18-19), 3186-3194

9 Colombo, R. et al. (2009) CE can identify small molecules that selectively target soluble oligomers of amyloid beta protein and display antifibrillogenic activity. *Electrophoresis* 30 (8), 1418-1429

10 Brogi, S. et al. (2014) Disease-modifying anti-Alzheimer's drugs: inhibitors of human cholinesterases interfering with beta-amyloid aggregation. *CNS Neurosci Ther* 20 (7), 624-632

11 Butini, S. et al. (2013) Multifunctional cholinesterase and amyloid Beta fibrillization modulators. Synthesis and biological investigation. *ACS Med Chem Lett* 4 (12), 1178-1182

12 Kaffy, J. et al. (2014) Structure-activity relationships of sugar-based peptidomimetics as modulators of amyloid beta-peptide early oligomerization and fibrillization. *Eur J Med Chem* 86, 752-758

13 Kaffy, J. et al. (2016) Designed Glycopeptidomimetics Disrupt Protein-Protein Interactions Mediating Amyloid beta-Peptide Aggregation and Restore Neuroblastoma Cell Viability. *J Med Chem* 59 (5), 2025-2040

14 Pellegrino, S. et al. (2017) beta-Hairpin mimics containing a piperidine-pyrrolidine scaffold modulate the beta-amyloid aggregation process preserving the monomer species. *Chem Sci* 8 (2), 1295-1302

15 Esatbeyoglu, T. et al. (2012) Curcumin--from molecule to biological function. *Angew Chem Int Ed Engl* 51 (22), 5308-5332

16 Payton, F. et al. (2007) NMR study of the solution structure of curcumin. *J Nat Prod* 70 (2), 143-146

17 Di Martino, R.M. et al. (2016) Versatility of the Curcumin Scaffold: Discovery of Potent and Balanced Dual BACE-1 and GSK-3beta Inhibitors. *J Med Chem* 59 (2), 531-544
18 Prasad, S. et al. (2014) Curcumin, a component of golden spice: from bedside to bench and back. *Biotechnol Adv* 32,1053-1064
19 Nelson, K.M. et al. (2017) The Essential Medicinal Chemistry of Curcumin. *J Med Chem* 60 (5), 1620-1637
20 Necula, M. et al. (2007) Small molecule inhibitors of aggregation indicate that amyloid beta oligomerization and fibrillization pathways are independent and distinct. *J Biol Chem* 282 (14), 10311-10324
21 Thapa, A. et al. (2016) Curcumin Attenuates Amyloid-beta Aggregate Toxicity and Modulates Amyloid-beta Aggregation Pathway. *ACS Chem Neurosci* 7 (1), 56-68
22 Zhao, L.N. et al. (2012) The effect of curcumin on the stability of Abeta dimers. *J Phys Chem B* 116 (25), 7428-7435
23 Konno, H. et al. (2014) Synthesis and evaluation of curcumin derivatives toward an inhibitor of beta-site amyloid precursor protein cleaving enzyme 1. *Bioorg Med Chem Lett* 24,685-690
24 Orlando, R.A. et al. (2012) A chemical analog of curcumin as an improved inhibitor of amyloid Abeta oligomerization. *PLoS One* 7 (3), e31869
25 Reinke, A.A. and Gestwicki, J.E. (2007) Structure-activity relationships of amyloid beta-aggregation inhibitors based on curcumin: influence of linker length and flexibility. *Chem Biol Drug Des* 70, 206-215
26 Masuda, Y. et al. (2011) Solid-state NMR analysis of interaction sites of curcumin and 42-residue amyloid beta-protein fibrils. *Bioorg Med Chem* 19 (20), 5967-5974
27 Simoni, E. et al. (2016) Nature-Inspired Multifunctional Ligands: Focusing on Amyloid-Based Molecular Mechanisms of Alzheimer's Disease. *ChemMedChem* 11 (12), 1309-1317
28 Lublin, A.L. and Link, C.D. (2013) Alzheimer's disease drug discovery: in vivo screening using Caenorhabditis elegans as a model for beta-amyloid peptide-induced toxicity. *Drug Discov Today Technol* 10 (1), e115-119
29 Mercanti, G. et al. (2014) Phosphatidylserine and curcumin act synergistically to down-regulate release of interleukin-1beta from lipopolysaccharide-stimulated cortical primary microglial cells. *CNS Neurol Disord Drug Targets* 13 (5), 792-800
30 Brenner, S. (1974) The genetics of Caenorhabditis elegans. *Genetics* 77 (1), 71-94
31 Casey, P.J. (1992) Biochemistry of protein prenylation. *J Lipid Res* 33 (12), 1731-1740
32 Kuzuyama, T. et al. (2005) Structural basis for the promiscuous biosynthetic prenylation of aromatic natural products. *Nature* 435 (7044), 983-987
33 Yazaki, K. et al. (2009) Prenylation of aromatic compounds, a key diversification of plant secondary metabolites. *Phytochemistry* 70,1739-1745

34 Calsolaro, V. and Edison, P. (2016) Neuroinflammation in Alzheimer's disease: Current evidence and future directions. *Alzheimers Dement* 12, 719-732
35 Querfurth, H.W. and LaFerla, F.M. (2010) Alzheimer's disease. *N Engl J Med* 362 (4), 329-344
36 Stefani, M. and Rigacci, S. (2013) Protein folding and aggregation into amyloid: the interference by natural phenolic compounds. *Int J Mol Sci* 14 (6), 12411-12457
37 Pocernich, C.B. et al. (2011) Nutritional approaches to modulate oxidative stress in Alzheimer's disease. *Curr Alzheimer Res* 8, 452-469
38 Kim, S. et al. (2014) Keap1 cysteine 288 as a potential target for diallyl trisulfide-induced Nrf2 activation. *PLoS One* 9 (1), e85984
39 Hudson, S.A. et al. (2009) The thioflavin T fluorescence assay for amyloid fibril detection can be biased by the presence of exogenous compounds. *FEBS J* 276, 5960-5972
40 Merlini, G. and Bellotti, V. (2003) Molecular mechanisms of amyloidosis. *N Engl J Med* 349 (6), 583-596
41 Kokkoni, N. et al. (2006) N-Methylated peptide inhibitors of beta-amyloid aggregation and toxicity. Optimization of the inhibitor structure. *Biochemistry* 45 (32), 9906-9918
42 Cohen, S.I. et al. (2013) Proliferation of amyloid-beta42 aggregates occurs through a secondary nucleation mechanism. *Proc Natl Acad Sci U S A* 110 (24), 9758-9763
43 Alexander, A.G. et al. (2014) Use of Caenorhabditis elegans as a model to study Alzheimer's disease and other neurodegenerative diseases. *Front Genet* 5, 279
44 Mhatre, S.D. et al. (2013) Invertebrate models of Alzheimer's disease. *J Alzheimers Dis* 33, 3-16
45 Shaye, D.D. and Greenwald, I. (2011) OrthoList: a compendium of C. elegans genes with human orthologs. *PLoS One* 6 (5), e20085
46 Link, C.D. (1995) Expression of human beta-amyloid peptide in transgenic Caenorhabditis elegans. *Proc Natl Acad Sci U S A* 92 (20), 9368-9372
47 McColl, G. et al. (2012) Utility of an improved model of amyloid-beta (Abeta(1)(-)(4)(2)) toxicity in Caenorhabditis elegans for drug screening for Alzheimer's disease. *Mol Neurodegener* 7, 57
48 Diomede, L. et al. (2012) C. elegans expressing human beta2-microglobulin: a novel model for studying the relationship between the molecular assembly and the toxic phenotype. *PLoS One* 7 (12), e52314
49 Diomede, L. et al. (2016) The new beta amyloid-derived peptide Abeta1-6A2V-TAT(D) prevents Abeta oligomer formation and protects transgenic C. elegans from Abeta toxicity. *Neurobiol Dis* 88, 75-84
50 Liu, W. et al. (2016) Development of a neuroprotective potential algorithm for medicinal plants. *Neurochem Int* 100, 164-177
51 Yuan, T. et al. (2016) Pomegranate's Neuroprotective Effects against Alzheimer's Disease Are Mediated by Urolithins, Its Ellagitannin-Gut Microbial Derived Metabolites. *ACS Chem Neurosci* 7 (1), 26-33
52 Liao, V.H. et al. (2011) Curcumin-mediated lifespan extension in Caenorhabditis elegans. *Mech Ageing Dev* 132, 480-487

53 Alavez, S. et al. (2011) Amyloid-binding compounds maintain protein homeostasis during ageing and extend lifespan. *Nature* 472 (7342), 226-229
54 Leon, R. et al. (2013) Recent advances in the multitarget-directed ligands approach for the treatment of Alzheimer's disease. *Med Res Rev* 33 (1), 139-189
55 Winblad, B. et al. (2016) Defeating Alzheimer's disease and other dementias: a priority for European science and society. *Lancet Neurol* 15, 455-532
56 Huang, Y. and Mucke, L. (2012) Alzheimer mechanisms and therapeutic strategies. *Cell* 148 (6), 1204-1222
57 Haass, C. and Selkoe, D.J. (2007) Soluble protein oligomers in neurodegeneration: lessons from the Alzheimer's amyloid beta-peptide. *Nat Rev Mol Cell Biol* 8 (2), 101-112
58 Simoni, E. et al. (2017) Multitarget drug design strategy in Alzheimer's disease: focus on cholinergic transmission and amyloid-beta aggregation. *Future Med Chem* 9 (10), 953-963

Chapter III

Evidence that the human innate immune peptide LL-37 may be a binding partner of amyloid-ß and inhibitor of fibril assembly

De Lorenzi E., Chiari M., Colombo R., Cretich M., Sola L., Vanna R., Gagni P., Bisceglia F., Morasso C., Lin J.S., Lee M., McGeer P.L., Barron A.E.

Journal of Alzheimer's disease 59, 1213-1226, 2017

1 Introduction

In the last century, a huge amount of information regarding AD has been achieved. From these studies, it emerges that AD is a neurodegenerative amyloidosis with a pronounced multifactorial nature [1]. AD is classified as amyloidosis because the aggregation and deposition of Aß peptides plays a key role in the onset and progression of AD. Both the Aß soluble oligomeric forms and the insoluble fibrils exert toxic effect on several targets, resulting in a diffuse and non specific toxicity [2,3]. In this way, Aß oligomers and fibrils can induce neurodegeneration.
Aß can directly or indirectly establish a large variety of molecular interactions with a number of natural proteins. Some of these interactions were demonstrated (**Table 1**) whereas others were only hypothesized [4]. In the same fashion, the biological significance of these bindings is not completely disclosed, also because of the difficulties in the assessment of the binding and of its role in AD [4,5].

Biomolecule	Method of Discovery/Evidence
Aβ-Binding Alcohol Dehydrogenase	Yeast two-hybrid screen using a human brain cDNA library
Aβ-Related Death-Inducing Protein	Yeast two-hybrid screen using a human brain cDNA library
Activity-Dependent Neuroprotective Protein	Isolated from a cDNA library from mouse embryonic carcinoma cells induced to differentiate into neurons using retinoic acid
α_1-Antichymotrypsin	Antigen maturation of a cDNA library
α-7 Nicotinic Acetylcholine Receptor	Co-immunoprecipitation from human brain tissue
α-Ketoglutarate	Enzyme activity in isolated rat brain mitochondria
β_2-Macroglobin	Yeast two-hybrid screen using a HeLa cDNA library
Amyloid Precursor Protein	Co-precipitation with Aβ in rat hippocampal cultures
Apolipoprotein E4	Amyloid deposition in a mice model correlated to Apo E4 expression
Apolipoprotein J	Affinity purification from cerebral spinal fluid by immobilized Aβ
Casein Kinase I and II	In vitro phosphorylation assay using casein
Catalase	In vitro binding assay to monitor catalase binding
Collagen-like Alzheimer Amyloid Plaque Component	Isolation of an Aβ-associated antigen further fractionation and identification using proteolytic cleavage and protein sequencing
Cytochrome Oxidase	Enzyme activity in isolated rat brain mitochondria
Formyl Peptide Receptor Like-1	Chemotaxis of monocytes and Ca^{2+} mobilization
Gelsolin	ELISA assay for Aβ-binding to immobilized gelsolin
Heat Shock Proteins 70 and 90	*In vitro* inhibition of Aβ assembly
Insulin Receptor	Competes with insulin for binding to the insulin receptor
Integrins	Inhibition of cell adhesion, of human neuroblastoma cells, to fibronectin by Aβ
N-Methyl-D-Aspartate Receptors	Internalization of Aβ in cultured hippocampal slices
p75 Neurotrophin Receptor	Co-immunoprecipitation, using NIH-3T3 cells, of radiolabeled Aβ
Protein Kinase C	Tissue culture phosphorylation assay
Pyruvate Dehydrogenase	Enzyme activity in isolated rat brain mitochondria
Receptor for Advanced Glycation End Products	Isolation of a Aβ-binding activity and protein sequencing
Scavenger Receptors	Microglial uptake
Serpin-Enzyme Complex Receptor	Competitive inhibition of a radiolabeled ligand binding by Aβ in human hepatoma cells
Tau	Production of antibodies, using fibrils, which recognize tau
Transthryetin	Isolation of an Aβ-binding activity from cerebral spinal fluid and protein sequencing

Table 1.Some biomolecules that bind Aß peptides [4].

The identification of natural binding partners of Aß peptides may shed light on the physiological role of Aß, as well as on alterations of its homeostasis which trigger the pathological cascade. Additionally, these biomolecules could also modulate *in vivo* the Aß fibrillogenesis, thus representing a further important tool for the development of an efficient treatment for AD.

In this chapter, by using complementary methodologies, it is demonstrated for the first time that the human innate LL-37 peptide binds Aß peptides and modulates its fibrillogenesis. The results obtained are reported in a published paper, that follows this Introduction Section.

As largely discussed in the thesis, Aß peptides are the main neurotoxic mediators linked to neurodegeneration typical of AD, whereas LL-37 is a mediator of the immune system, also endowed with antimicrobial activity [6,7].

LL-37 is the only human member of the cathelicidin family of antimicrobial peptides (AMP), for this reason since its discovery it has been largely studied [8]. LL-37 exerts a wide range of bioactivities including antibacterial, antimicrobial and also antifungal properties; furthermore, numerous immunomodulatory activities have been reported for LL-37, and it has also been classified as an Antimicrobial ImmunoModulatory Peptide (AIMOP) [7]. Considering the vast and growing issue of bacterial resistance, these properties make LL-37 an ideal starting point for the development of new therapeutic agents for infections.

Our work arises from the observation of the strong apparent complementarity and of the interconnection of different molecular pathways between Aß peptides and LL-37.

Aß peptides and LL-37 share some biophysical properties in terms of

- size: LL-37 is constituted of 37 amino acids whereas Aß peptides range from 38 to 43 amino acid residues [2,7];
- molecular weight: the MW of LL-37 is 4493 Da, i.e. very similar to that of the most amyloidogenic peptide (Aß42= 4514 Da) [2,7];
- hydrophobicity: LL-37 has nine hydrophobic and aliphatic residues, Aß peptides have ten and Aß42 has eleven [2,7];
- number of aromatic residues: in the primary structure of all peptides there are 4 aromatic amino acids, including the binary "FF" motif. In Aß peptides the pentapeptide LVFFA, in which is present the FF motif, is necessary for Aß assembly [2,7,9];
- self-aggregating tendency. While Aß self-assembles into oligomers and fibrils because of its amyloidogenic nature, for LL-37 the oligomerization is functional to its activity [7,10-12].

Despite similarities, Aß and LL-37 differ for important features such as the net charge. Aß has a net negative charge of -3 (discounting the charge of histidines), while LL-37 has a positive charge of +6. The opposite net charge may provide a strong electrostatic attraction between Aß and LL-37.
As said above, also LL-37 forms oligomers, but unlike Aß, LL-37 assumes a stable random coil conformation in aqueous solutions. The native conformation

is replaced by a secondary α-helix structure in the presence of salts and bacterial membranes. Therefore, LL-37 oligomers are not characterized by ß-sheet structures (typical of amyloidogenic proteins like Aß), but instead by an α-helix conformation [7,10,13,14].
Positively charged oligomers of LL-37 with α-helix structure interact with and disrupts negative microbial membranes. Two modes of action have been described: LL-37 can exert a detergent effect via a carpet-like mechanism, or it can form pores on the cellular surface [7,10,15]. As discussed in the "General remarks" (see General remarks "Toxicity of Aß peptides") for Aß oligomers the same mechanisms of membrane permeabilization have been proposed [15].
According to these overlapped features, in 2010 Soscia *et al.* demonstrated that Aß42 exerts an antimicrobial activity even higher than that of LL-37 [16].

The hypothesis that Aß and LL-37 may be binding partners has been prompted by these biochemical and physical overlays and also by the observation of the links between the molecular pathways of Aß and LL-37.

LL-37 is also expressed in the brain [17]. As immunomodulator, LL-37 triggers different biochemical pathways, of which some also intersect Aß-related signalling functions. Therefore, LL-37 may be directly or indirectly involved in the homeostatis of Aß42 *in vivo*.
For example, the formyl-like peptide receptor 1 (FPRL1) involved in neuroinflammation is activated by both Aß and LL-37; moreover the activation of microglia by Aß requires the expression of the G-protein coupled receptor (GPCR) P2X7R [18], while LL-37 is an activator of P2X7R [19]. The internalization of LL-37 into macrophages, where it plays a role in autophagy, is regulated by P2X7R. Recently it was reported that a human P2X7R polymorphism may fulfill a protective role in AD [20].
It has been demonstrated that vitamin D and phenylbutyrate represent neuroprotective agents in animal models of AD, furthermore they also are LL-37-inducers, as indeed Vitamin D increases the expression levels of *CAMP* gene that encodes for LL-37. Vitamin D also reduces Aß accumulation and induces autophagy in human monocyte and macrophages *via* LL-37 [21,22]. This is important in the metabolism of Aß aggregates, since the clearance of amyloid plaques can be carried out also through this mechanism [23].
The retinoid X receptor, together with vitamin D, up-regulates the expression of *CAMP* gene and, alike vitamin D, it determines an increase of cognition in mouse model of AD [23,24].
Further, LL-37 may be linked to Aß because it binds ApoA-1 in HDL particles. In turn, ApoA1 interacts with APP and modulates Aß aggregation and toxicity [25].

Inspired by these observations, we here investigate the binding between LL-37 and Aß40 (the most abundant amyloid peptide) and Aß42 (the most amyloidogenic and toxic one) [26]. The binding and its effect on Aß amyloid

process is assessed by an array of different techniques (SPR-imaging (SPRi), CD, TEM, CE).

SPRi, a very recent evolution of SPR technique, has been used to evaluate the molecular interaction between LL-37 and Aß40 or Aß42. By means of the analytical platform described in Chapter I, Aß40 and Aß42 were spotted on the SPRi chip. In this way, differently to other reports [27-29], we can define which type of oligomeric population have been spotted on the chip, since oligomers have been analytically separated and characterized by CE and UF.

In SPRi a charge-coupled device (CCD) provides a real-time imaging of the whole surface for signal detection [30]. This is useful to verify the quality and the optical properties of different ligands after immobilization. Further, it is possible to monitor more than 100 samples at the same time. Consequently, by taking advantage of this SPR mode and of the analytical platform described in Chapter I, it was possible to simultaneously evaluate the interaction of LL-37 with Aß40 and Aß42 at different states of oligomerization. By monitoring the aggregation process by CE, we selected two aggregation states of Aß peptides: immediately after solubilization, when small oligomers are the most abundant species and at later times, when also large assemblies are predominant.
This difference in the distribution of size and MW was detected by SPRi, indeed we demonstrated that the amount of Aß bound to the chip increases together with the increase of MW of oligomers spotted. This was in agreement with the presence of oligomeric populations with higher MW, as assessed by UF and CE experiments.

Based on our results, we demonstrate for the first time that LL-37 is a binding partner of Aß peptides and a modulator of Aß aggregation process: LL-37 inhibits fibril formation by shifting the equilibrium towards non toxic small oligomers and by hindering the organization of Aß42 into highly structured ß-sheets (as verifired by CD analyses). These *in vitro* proofs of the interaction between Aß and LL-37 are mirrored also in cell-based assays: LL-37 reduces Aß42-induced neuroinflammation and neurotoxicity.

The data presented here constitute a starting point for further investigations on the ability of LL-37 to modulate *in vivo* the aggregation of Aß, as well as to verify if factors that affect the production of LL-37 *in vivo* may have a role in triggering of pathological cascade that eventually leads to neurodegeneration.

2 References

1 Winblad, B. et al. (2016) Defeating Alzheimer's disease and other dementias: a priority for European science and society. *Lancet Neurol* 15, 455-532

2 Walsh, D.M. and Selkoe, D.J. (2007) A beta oligomers - a decade of discovery. *J Neurochem* 101 (5), 1172-1184

3 Lee, S.J. et al. (2017) Towards an understanding of amyloid-beta oligomers: characterization, toxicity mechanisms, and inhibitors. *Chem Soc Rev* 46 (2), 310-323

4 Stains, C.I. et al. (2007) Molecules that target beta-amyloid. *ChemMedChem* 2 (12), 1674-1692

5 Huang, Y. and Mucke, L. (2012) Alzheimer mechanisms and therapeutic strategies. *Cell* 148 (6), 1204-1222

6 Sood, R. et al. (2008) Binding of LL-37 to model biomembranes: insight into target vs host cell recognition. *Biochim Biophys Acta* 1778, 983-996

7 Burton, M.F. and Steel, P.G. (2009) The chemistry and biology of LL-37. *Nat Prod Rep* 26 (12), 1572-1584

8 Durr, U.H. et al. (2006) LL-37, the only human member of the cathelicidin family of antimicrobial peptides. *Biochim Biophys Acta* 1758, 1408-1425

9 Masuda, Y. et al. (2011) Solid-state NMR analysis of interaction sites of curcumin and 42-residue amyloid beta-protein fibrils. *Bioorg Med Chem* 19 (20), 5967-5974

10 Oren, Z. et al. (1999) Structure and organization of the human antimicrobial peptide LL-37 in phospholipid membranes: relevance to the molecular basis for its non-cell-selective activity. *Biochem J* 341 (Pt 3), 501-513

11 Chiti, F. and Dobson, C.M. (2017) Protein Misfolding, Amyloid Formation, and Human Disease: A Summary of Progress Over the Last Decade. *Annu Rev Biochem* 86, 35.1-35-42

12 Merlini, G. and Bellotti, V. (2003) Molecular mechanisms of amyloidosis. *N Engl J Med* 349 (6), 583-596

13 Bonucci, A. et al. (2015) A Spectroscopic Study of the Aggregation State of the Human Antimicrobial Peptide LL-37 in Bacterial versus Host Cell Model Membranes. *Biochemistry* 54 (45), 6760-6768

14 Xhindoli, D. et al. (2014) Native oligomerization determines the mode of action and biological activities of human cathelicidin LL-37. In *Biochem J* 457, 263-275

15 Cheng, B. et al. (2013) Inhibiting toxic aggregation of amyloidogenic proteins: a therapeutic strategy for protein misfolding diseases. *Biochim Biophys Acta* 1830 (10), 4860-4871

16 Soscia, S.J. et al. (2010) The Alzheimer's disease-associated amyloid beta-protein is an antimicrobial peptide. *PLoS One* 5 (3), e9505

17 Lee, M. et al. (2015) Human antimicrobial peptide LL-37 induces glial-mediated neuroinflammation. In *Biochem Pharmacol* 94, 130-141

18 Sanz, J.M. et al. (2009) Activation of microglia by amyloid {beta} requires P2X7 receptor expression. *J Immunol* 182, 4378-4385

19 Elssner, A. et al. (2004) A novel P2X7 receptor activator, the human cathelicidin-derived peptide LL37, induces IL-1 beta processing and release. *J Immunol* 172 (8), 4987-4994
20 Sanz, J.M. et al. (2014) Possible protective role of the 489C>T P2X7R polymorphism in Alzheimer's disease. *Exp Gerontol* 60, 117-119
21 Mookherjee, N. et al. (2009) Systems biology evaluation of immune responses induced by human host defence peptide LL-37 in mononuclear cells. *Mol Biosyst* 5 (5), 483-496
22 Yuk, J.M. et al. (2009) Vitamin D3 induces autophagy in human monocytes/macrophages via cathelicidin. *Cell Host Microbe* 6, 231-243
23 Durk, M.R. et al. (2014) 1alpha,25-Dihydroxyvitamin D3 reduces cerebral amyloid-beta accumulation and improves cognition in mouse models of Alzheimer's disease. *J Neurosci* 34, 7091-7101
24 Mariani, M.M. et al. (2017) Neuronally-directed effects of RXR activation in a mouse model of Alzheimer's disease. *Sci Rep* 7, 42270
25 Koldamova, R.P. et al. (2001) Apolipoprotein A-I directly interacts with amyloid precursor protein and inhibits A beta aggregation and toxicity. *Biochemistry* 40, 3553-3560
26 Bitan, G. et al. (2003) Amyloid beta -protein (Abeta) assembly: Abeta 40 and Abeta 42 oligomerize through distinct pathways. *Proc Natl Acad Sci U S A* 100 (1), 330-335
27 Barr, R.K. et al. (2016) Validation and Characterization of a Novel Peptide That Binds Monomeric and Aggregated beta-Amyloid and Inhibits the Formation of Neurotoxic Oligomers. *J Biol Chem* 291 (2), 547-559
28 Yi, X. et al. (2016) Surface plasmon resonance biosensors for simultaneous monitoring of amyloid-beta oligomers and fibrils and screening of select modulators. *Analyst* 141 (1), 331-336
29 Kai, T. et al. (2015) Tabersonine inhibits amyloid fibril formation and cytotoxicity of Abeta(1-42). *ACS Chem Neurosci* 6 (6), 879-888
30 Scarano, S. et al. (2010) Surface plasmon resonance imaging for affinity-based biosensors. *Biosens Bioelectron* 25, 957-966

Journal of Alzheimer's Disease 59 (2017) 1213–1226
DOI 10.3233/JAD-170223
IOS Press

Evidence that the Human Innate Immune Peptide LL-37 may be a Binding Partner of Amyloid-β and Inhibitor of Fibril Assembly

Ersilia De Lorenzi[a], Marcella Chiari[b,*], Raffaella Colombo[a], Marina Cretich[b], Laura Sola[b], Renzo Vanna[c], Paola Gagni[b], Federica Bisceglia[a], Carlo Morasso[c], Jennifer S. Lin[e], Moonhee Lee[d], Patrick L. McGeer[d] and Annelise E. Barron[e,*]
[a]*Department of Drug Sciences, University of Pavia, Pavia, Italy*
[b]*National Research Council of Italy, Institute of Chemistry of Molecular Recognition, Milan, Italy*
[c]*Laboratory of Nanomedicine and Clinical Biophotonics (LABION), Fondazione Don Carlo Gnocchi ONLUS, Milano, Italy*
[d]*Kinsmen Laboratory of Neurological Research, University of British Columbia, Vancouver, Canada*
[e]*Department of Bioengineering, Stanford University, School of Medicine, Stanford, CA, USA*

Handling Associate Editor: Benedetta Nacmias

Accepted 9 June 2017

Abstract.
Background: Identifying physiologically relevant binding partners of amyloid-β (Aβ) that modulate *in vivo* fibril formation may yield new insights into Alzheimer's disease (AD) etiology. Human cathelicidin peptide, LL-37, is an innate immune effector and modulator, ubiquitous in human tissues and expressed in myriad cell types.
Objective: We present *in vitro* experimental evidence and discuss findings supporting a novel hypothesis that LL-37 binds to $A\beta_{42}$ and can modulate Aβ fibril formation.
Methods: Specific interactions between LL-37 and Aβ (with Aβ in different aggregation states, assessed by capillary electrophoresis) were demonstrated by surface plasmon resonance imaging (SPRi). Morphological and structural changes were investigated by transmission electron microscopy (TEM) and circular dichroism (CD) spectroscopy. Neuroinflammatory and cytotoxic effects of LL-37 alone, $A\beta_{42}$ alone, and LL-37/Aβ complexes were evaluated in human microglia and neuroblastoma cell lines (SH-SY5Y).
Results: SPRi shows binding specificity between LL-37 and Aβ, while TEM shows that LL-37 inhibits $A\beta_{42}$ fibril formation, particularly Aβ's ability to form long, straight fibrils characteristic of AD. CD reveals that LL-37 prevents $A\beta_{42}$ from adopting its typical β-type secondary structure. Microglia-mediated toxicities of LL-37 and $A\beta_{42}$ to neurons are greatly attenuated when the two peptides are co-incubated prior to addition. We discuss the complementary biophysical characteristics and AD-related biological activities of these two peptides.
Conclusion: Based on this body of evidence, we propose that LL-37 and $A\beta_{42}$ may be natural binding partners, which implies that balanced (or unbalanced) spatiotemporal expression of the two peptides could impact AD initiation and progression.

Keywords: Alzheimer's disease, amyloid-β peptide, cathelicidin, innate immunity, LL-37, microglia

*Correspondence to: Marcella Chiari, National Research Council of Italy, Institute of Chemistry of Molecular Recognition, Via Mario Bianco 9, 20131 Milan, Italy. E-mail: marcella.chiari@icrm.cnr.it and Annelise E. Barron, Department of Bioengineering, Stanford University, School of Medicine, 443 Via Ortega, Stanford, CA 94305, USA. E-mail: aebarron@stanford.edu.

INTRODUCTION

Alzheimer's disease (AD) involves the assembly of amyloid-β (Aβ) peptides from soluble monomers into oligomers, fibrils, and plaques [1]. Studies of the spatiotemporal interplay between diffusible Aβ oligomers and fibrillar deposits as well as intracellular tau tangles are aimed at investigating drivers of neuronal dysfunction [2, 3]. However, root physiological causes of sporadic AD—most common—remain unspecified, preventing the development of effective therapies to prevent, halt, or reverse the disease [4].

Identification of physiologically relevant binding partners of Aβ that modulate fibril formation *in vivo* might yield new insights into causes of AD and help identify early instigators of Aβ accumulation and neurotoxic effects. A number of natural proteins that can bind to or interact with Aβ were identified by various assays [5]; however, their roles in sporadic AD are often challenging to assess. Recent, extensive *in vitro* and *in vivo* studies of Aβ interactions with the human Brichos domain, a molecular chaperone, exemplify how a discovery of this sort can yield intriguing mechanistic insights [6].

Numerous literature reports suggest that biophysical activities and signaling functions of Aβ peptides and LL-37, the only cathelicidin-derived innate immune system peptide found in humans, are related *in vivo.* For instance, the vitamin D receptor and retinoid X receptor (RXR) are both connected with AD, as well as with expression levels of LL-37. Vitamin D3 treatment was shown to reduce cerebral Aβ accumulation and improve cognition in a mouse model of AD [7], while RXR activation reduced neuronal loss and improved cognition in an aggressive mouse model of AD [8]. Expression levels of the CAMP gene that encodes hCAP-18, the precursor for LL-37 [9], are upregulated by activation of the vitamin D receptor [10], with an obligate involvement of RXR [11].

Another connection is the hypothesis that sporadic AD is essentially 'type 3 diabetes' occurring in brain tissue [12, 13]. In a recent study [14], it is shown that intraperitoneal administration of the murine cathelicidin peptide, CRAMP (which like LL-37 for humans, is unique in the mouse proteome) protects Non-Obese Diabetic (NOD) mice against the development of autoimmune diabetes. This treatment was motivated by the authors' discovery that the genetic defect of NOD mice that creates susceptibility to autoimmune diabetes is a deficit in their ability to express cathelicidin; and this defect is more pronounced in female NOD mice, who have a higher incidence of disease as compared with males. In this animal model, immunomodulatory effects of the cathelicidin peptide, including effects on the phenotypes of white blood cells including macrophages, dendritic cells, T and B cells, reduced risks of inflammatory disease [14].

To date, most approaches to AD have relied on the supposition that pathological overexpression or hindered degradation of Aβ lays the primary foundation for disease [1]. What if chronic *underexpression* of another biomolecule, which normally opposes fibril formation, plays a key role? It is of course difficult for researchers to identify a systemic element that *should* be present, or perhaps should be better regulated, but is not.

Here we report a multifaceted approach to confirm and characterize, *in vitro,* both the interactions between Aβ and LL-37 and inhibitory effects of LL-37 on Aβ oligomer/fibril formation. We also demonstrate that LL-37 and $A\beta_{42}$, both individually toxic and proinflammatory to neuroblastoma cell line SH-SY5Y via the stimulation of microglial production of inflammatory cytokines, lose most of their cytotoxicity to neurons if the two peptides are co-incubated prior to being added to the cell culture media.

The interactions between LL-37 and Aβ peptides were investigated by surface plasmon resonance imaging (SPRi), a recent evolution of traditional SPR, which couples the label-free monitoring of molecular interactions by scanning angle SPR measurements with simultaneous charge-coupled device (CCD)-based imaging of the whole surface for signal detection [15]. The multi-array SPRi configuration improves the overall accuracy of the study by allowing simultaneous detection of signals originating from both positive and negative control ligands immobilized on the same chip. In addition, the real-time imaging of the entire SPR-biochip allows for verification of the quality and the optical properties of different ligands after their immobilization on the chip surface. To evaluate the aggregation state and the presence of soluble oligomers in the Aβ samples used for SPRi, capillary electrophoresis (CE) analysis was carried out. The inhibitory effect on fibril formation was demonstrated through transmission electron microscopy (TEM) by investigating fibril formation in quasi-physiological conditions. Conformational analyses of $A\beta_{42}$ peptide in solution, in the absence and presence of LL-37, were carried out by circular dichroism (CD) spectroscopy.

In this work, we demonstrate that Aβ and LL-37 bind to each other specifically, and that LL-37 inhibits the adoption by Aβ of ordered β-type secondary structure. We discuss a variety of different published findings that suggest a physiological interplay between, and potential co-regulation of these two peptides, as an aspect of human innate immunity that may affect the initiation and progression of AD-related pathology.

MATERIALS AND METHODS

Materials

$A\beta_{40}$, $A\beta_{42}$ free base, and 1% NH_4OH were from AnaSpec (Fremont, CA). LL-37 was from Innovagen (Lund, Sweden). An unrelated peptide to serve as a binding study control (sequence SYSVQDQYQALL QQHAQYK) was kindly gifted by Dr. Alessandro Gori from the Peptide Synthesis Lab, ICRM, CNR, Milan. "Scrambled sequence" LL-37 peptide was from AnaSpec, and has the same amino acid composition as natural LL-37, but with the following sequence: GLKLRFEFSKIKGEFLKTPEVRFRDIK LKDNRISVQR. 1,1,1, 3,3,3-Hexafluoro-2-propanol (HFIP), acetonitrile, sodium carbonate, sodium hydroxide as well as NaH_2PO_4 and Na_2HPO_4 were from Sigma-Aldrich (Stenheim, Germany). Buffer solutions were prepared daily using Millipore Direct-Q™-deionized water, filtered with 0.45 μm Millipore membrane filters (Bedford, MA) and degassed by sonication.

In SPRi and CE experiments, 1 mg/mL stock solutions of $A\beta_{40}$ and unrelated peptide or scrambled-sequence LL-37 in PBS were diluted to the desired concentration. $A\beta_{42}$ was prepared as described by Bartolini et al. [16]. Briefly, 0.5 mg of lyophilized $A\beta_{42}$ powder was dissolved in HFIP (149 μM) and kept overnight at room temperature. After 12 h, the solution was aliquoted and the HFIP was left to evaporate overnight at room temperature. The $A\beta_{42}$ film was redissolved in CH_3CN/300 μM Na_2CO_3/ 250 mM NaOH (48.3:48.3:3.4, v/v/v). The obtained 500 μM $A\beta_{42}$ solution was diluted to the desired concentration with 20 mM phosphate buffer, pH 7.4 (SPRi: 20 μM; CE: 100 μM).

For TEM and CD analysis, the samples were prepared as described previously [17], and analyzed at 50 and/or 100 μM concentrations. Briefly, to 1 mg lyophilized $A\beta_{42}$ powder (AnaSpec) 80 μL of 1% NH_4OH solution was added. After 1 min sonication, the solution was diluted with 20 mM phosphate buffer, pH 7.4, to the desired concentration, and divided into aliquots, which were freeze-dried and stored at –80°C. Each lyophilized peptide aliquot was resuspended in 20 mM phosphate buffer, pH 7.4 immediately before use. Samples were sonicated 3 min in an ultrasonic bath, to break down pre-formed aggregates and increase the peptide's effective concentration [18]. For samples incubated with LL-37, lyophilized peptide was re-suspended in appropriately diluted LL-37 solutions, so as to keep the peptides at the desired molar concentrations and obtain proper $A\beta_{42}$/LL-37 molar ratios. Samples were analyzed either immediately after solubilization, or after different lengths of incubation time, as noted in figure legends.

Surface plasmon resonance imaging

Bare gold SPRi-biochips (HORIBA Jobin Yvon SAS, France) were treated for 10 min with an Oxygen Plasma Generator (Harrick Plasma Cleaner), then coated using a solution of co-poly(DMA-NAS-MAPS) (MCP-2, Lucidant Polymers, Sunnyvale, CA) via surface immersion for 30 min (MCP-2 copolymer was dissolved at 1% w/v in aqueous 20% ammonium-sulfate). Coated SPRi-biochips were then washed with distilled water and dried at 80°C for 15 min. Residual reactive groups were then reacted with 50 mM ethanolamine/0.1M Tris pH 9.0 for 1 h, washed with water, and dried with nitrogen.

The SPRi-biochip surface coated with the copolymer was functionalized by spotting the following 20 μM solutions: 1) $A\beta_{40}$ (t = 0 days); 2) $A\beta_{42}$ (t = 0 days); 3) $A\beta_{42}$ (t = 24 days, i.e., spotted after 24 days of incubation at room temperature); and 4) an unrelated peptide used as reference. These peptides were spotted in replicate (8 spots, around 190 μm diameter each) using a piezoelectric spotter (SciFLEXARAYER S5; Scienion) at 20°C and 50% humidity. After spotting, the SPRi-biochip was incubated overnight in a sealed chamber saturated with sodium chloride at room temperature.

The binding analysis was performed using a Horiba XelPleX SPRi imaging instrumentation (HORIBA Jobin Yvon SAS, France) after an overnight instrument equilibration with HBS-ET (10 mM HEPES, 150 mM NaCl, 3 mM EDTA, 0.05% Tween) used also as running buffer. Thereafter increasing concentrations of LL-37 peptide solution (1.0; 2.5; 5.0; 10; 25; 50; 100 μM in phosphate buffer 20 mM; pH 7.4) were injected onto the chip at 50 μL/min for 10 min, at 25°C, in order to reach a binding equilibrium

for all the responses. Ovalbumin (Sigma-Aldrich, A5503) was used as the negative control sample. After each injection, the chip surface was regenerated by injecting 50 mM glycine at pH 2.0, 50 μL/min for 4 min, thus obtaining a complete regeneration of the chip surface without significant loss of binding capacity. The results were preprocessed using EzSuite (HORIBA Jobin Yvon SAS, France), then equilibrium-binding constants (K_D and K_A (1/ K_D) values were calculated using Scrubbergen2 (licensed by HORIBA Jobin Yvon SAS)). Additional binding analysis experiments were performed using the same procedures and conditions, but by injecting a control scrambled-sequence LL-37 peptide.

Capillary electrophoresis

All CE experiments were carried out by slightly modifying the method reported by Brogi et al. [17]. Briefly, an Agilent Technologies 3D CE system with built-in diode-array detector (Waldbronn, Germany) was used and data were collected using Chemstation A.10.02 software. The fused-silica capillary (50 μm id, 360 μm od, total length 33 cm, effective length 24.5 cm) was from Polymicro Technologies (Phoenix, AZ). A new capillary was flushed at 1 bar with 1 M NaOH and water for 60 min each and background electrolyte (BGE, 80 mM sodium phosphate buffer, pH 7.4) for 90 min. The between-run rinsing cycle consisted of 50 mM SDS (1.5 min), water (1.5 min), and BGE (2 min). Sample injection (100 μM) was carried out by applying a pressure of 30 mbar for 3 s. Separations were carried out at 25°C and +12 kV (current 75–80 μA). The acquisition wavelength was 200 nm.

Transmission electron microscopy

For each TEM sample, a 10-μL droplet of suspension or solution was applied to a carbon-coated Formvar nickel grid (200 mesh) (Electron Microscopy Sciences, Washington, PA, USA). Each sample was allowed to sediment onto the carbon film for 15 min, then negative staining was performed with 10 μL of 2% w/v uranyl acetate solution (Electron Microscopy Sciences). After carefully draining off excess staining solution using filter paper, the specimen was transferred to a Philips CM12 TEM for examination, operating the TEM at 80 kV. Electron micrographs of negatively stained samples were photographed using Kodak film.

Circular dichroism

CD spectra were collected at 20°C using a Jasco-810 spectrophotometer and a quartz cuvette with a 0.1 cm path length. All experiments were performed with an $A\beta_{42}$ concentration of 50 μM. Spectra were registered from 190 to 250 nm and run at a scan speed of 20 nm/min, with a time response of 2 s and data pitch of 0.2 nm. All spectra were baseline-corrected. Molar mean residue ellipticity [θ] is expressed in degrees cm^2 $dmol^{-1}$, and calculated as $[\theta] = \theta_{obs}$ MWR/(10 l c), where θ is observed ellipticity in degrees; MWR, peptide mean residue molar weight; l, the optical path length in cm; and c, peptide concentration in g/mL.

SH-SY5Y cells – microglia co-culture

The human neuroblastoma SH-SY5Y cell line was a gift from Dr. R. Ross, Fordham University, NY. The cells were grown in DMEM/F12 medium containing 10% fetal bovine serum (FBS, Invitrogen, Carlsbad, CA) and 100 IU/mL penicillin and 100 μg/mL streptomycin (Invitrogen, Carlsbad, CA) under humidified 5% CO_2 and 95% air.

Human microglial cells were isolated from surgically resected temporal lobe tissue as described earlier [19]. Briefly, tissues were rinsed with a PBS solution and chopped into small pieces (<2 mm^3) with a sterile scalpel. They were treated with 10 mL of a 0.25% trypsin solution at 37°C for 20 min. Subsequently DNase I (from bovine pancreas, Pharmacia Biotech, Baie d'Urfé, PQ, Canada) was added to reach a final concentration of 50 μg/mL. Tissues were incubated for an additional 10 min at 37°C. After centrifugation at 275 g for 10 min, the cell pellet was re-suspended in the serum-containing medium and passed through a 100 μm nylon cell strainer (Becton Dickinson, Franklin Lakes, NJ). The cell suspension was centrifuged again (275 g for 10 min) and re-suspended in 10 mL of DMEM/F12 medium with 10% FBS containing gentamicin (50 μg/mL), and plated onto tissue culture plates (Becton Dickinson) in a humidified 5% CO_2, 95% air atmosphere at 37°C for 2 h. This achieved adherence of microglial cells. Cells were allowed to grow by replacing the medium once per week.

For estimating the purity of microglial cell cultures, aliquots of the cultures were placed on glass slides at 37°C for 48 h. The attached cells were then fixed with 4% paraformaldehyde for 1 h at 4°C, and made permeable with 0.1% Triton X-100 for 1 h at

room temperature. After washing twice with PBS, the culture slides were treated with the monoclonal anti-GFAP antibody (1/4,000, DAKO) for astrocytic staining and polyclonal anti-Iba-1 antibody (1/500, Wako Chemicals, Richmond, VA) for microglial staining for 3 h at room temperature. The slides were then incubated with Alexa Fluor 488-conjugated goat anti-mouse IgG antibody (Invitrogen, 1:500) and Alexa Fluor 546-conjugated goat anti-rabbit IgG antibody (Invitrogen, 1:500) in the dark for 3 h at room temperature to yield a positive red fluorescence. To visualize all cells, the slides were washed twice with PBS and counterstained with the nuclear dye DAPI (100 μg/mL, Sigma) to give a blue fluorescent color. Images were acquired using an Olympus BX51 microscope and a digital camera (Olympus DP71). Fluorescent images were co-localized with Image-Pro software (Improvision Inc., Waltham, MA). The purity of microglia was more than 99% (1.93 ± 0.54 astrocytes in 500 total cells in microglial culture, $n = 30$).

To achieve SH-SY5Y differentiation, the undifferentiated cells were treated for 4 days with 5 μM retinoic acid (RA) in DMEM/F12 medium containing 5% FBS, 100 IU/mL penicillin, and 100 μg/mL streptomycin [20]. The RA-containing medium was changed every two days. Differentiated SH-SY5Y cells demonstrated neurite extension, indicative of their differentiation [21].

Cell culture treatment with Aβ and LL-37 peptides

Human microglial cells (5×10^4 cells per well) or human neuroblastoma SH-SY5Y cells (5×10^5 cells per well) or their mixture were seeded into 24-well plates in 1 mL of DMEM/F12 medium containing 5% FBS. $A\beta_{42}$ peptide (AnaSpec, Fremont, CA) was dissolved in mixture of 1% NH_4OH and 0.1% Thioflavin S (Sigma, St. Louis, MO) in water to make 30 mM stock solution. Further dilution was made with water to reach 30 μM. Similar methods were used to prepare LL-37 peptide solutions (AnaSpec, Fremont, CA). Cultured cells were exposed to either 30 μM $A\beta_{42}$ or 30 μM LL-37; or to a combined 1:1 equimolar mixture of the two peptides at 30 μM each. After incubation for 72 h cell free medium was collected to measure levels of proinflammatory cytokines such as TNFα and IL-6. For SH-SY5Y cell viability, MTT assays were performed [22].

SH-SY5Y-microglial cell viability assays

The viability of SH-SY5Y cells following incubation with glial cell supernatants was evaluated by MTT assays as previously described [22]. Briefly, the viability was determined by adding MTT to the cell cultures to reach a final concentration of 1 mg/mL. Following 1 h incubation at 37°C, the dark crystals formed were dissolved by adding a SDS/DMF extraction buffer (300 μL, 20% sodium dodecyl sulfate, 50% N, N-dimethylformamide, pH 4.7). Subsequently plates were incubated overnight at 37°C and optical densities at 570 nm were measured by transferring 100 μL aliquots to 96-well plates and using a plate reader with a corresponding filter. Data are presented as a percentage of the values obtained from cells incubated in fresh medium only.

Measurement of TNFα and IL-6 release

Cytokine levels were measured in cell-free supernatants after 72 h. Quantitation was performed with ELISA detection kits (Peprotech, NJ) following protocols described by the manufacturer.

Statistical data analysis for cell culture assays

The significance of differences between data sets was analyzed by one-way ANOVA tests. Multiple group comparisons were followed by a *post-hoc* Bonferroni test, e.g., cell viability in control condition versus cells treated with LL-37 alone; cell viability in control condition versus cells treated with $A\beta_{42}$ alone; and viability in control condition versus cells treated with mixed LL-37 + $A\beta_{42}$. *P* values are given in the figure legends.

RESULTS

SPRi analysis of LL-37 binding to immobilized Aβ and CE analysis

To demonstrate interaction between LL-37 and $A\beta_{42}$, an SPRi biochip was functionalized with copoly(DMA-NAS-MAPS), a polydimethylacrylamide-based copolymer, widely used to immobilize biomolecules on microarray slides [23]. Three different solutions of 20 μM Aβ-peptides, in different states of aggregation, were spotted onto the SPRi-chip surface. The aggregation state and the presence of soluble oligomers were determined by CE analysis [17, 24]. $A\beta_{40}$ (a)

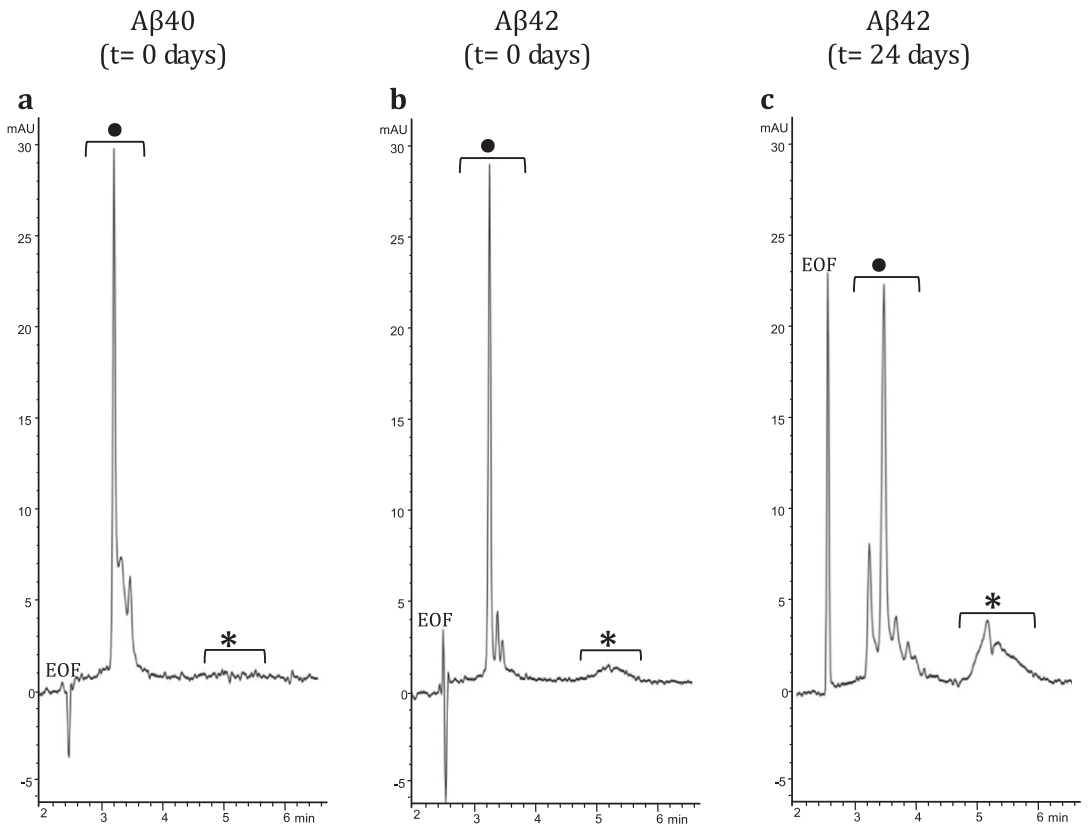

Fig. 1. CE electropherograms: a) $A\beta_{40}$ (t = 0 days); b) $A\beta_{42}$ (t = 0 days); and c) $A\beta_{42}$ (t = 24 days). In the CE traces: • low MW-oligomers, *high MW-oligomers.

dissolved in PBS, $A\beta_{42}$ (b) prepared as in [16], both solubilized immediately before spotting (t = 0 days), and $A\beta_{42}$ (c) prepared as sample (b), but stored in the buffer for 24 days (t = 24 days) were spotted in different subarrays. $A\beta_{42}$ was dissolved following the protocol detailed in the Material and Methods section. The solubilization buffer consisted of i) HFIP, a low-polarity solvent that stabilizes the α-helix and disrupts the interstrand hydrogen bonds of the β-sheets and ii) a mixture of acetonitrile/Na_2CO_3/NaOH. While acetonitrile stabilizes the unordered/α-helix structure, the basic pH increases the solubility of Aβ peptide. Overall, this procedure disfavors aggregation and provides a time window long enough to appreciate the prevailing formation of low-molecular weight (MW) oligomers at early stages (t = 0 days) and the building up of high-MW oligomers at late-stages (t = 24 days) of the *in vitro* fibrillogenesis process. Indeed, this was confirmed by analyzing in CE the three samples at 100 μM concentration using a method slightly modified from Sabella et al. [24]. Figure 1 shows CE electropherograms of the same Aβ peptide solutions spotted on the SPRi chip; consistent with what has been reported previously in literature [17, 24, 25], the fast-migrating group of peaks can be attributed to low MW-oligomers whereas the slow-migrating broad band corresponds to high MW-oligomers. In particular, in the $A\beta_{42}$ sample, the high MW-oligomers build up over time, as evident in Fig. 1b and c.

The interaction of Aβ in different aggregation states with LL-37 was investigated by SPRi. The CCD image of the chip surface, and the plasmonic curves acquired before the injection of LL-37 (Supplementary Figure 1), show the three Aβ forms conjugated to the surface. Specifically, the plasmonic curves of the different samples indicate that the sample containing a higher amount of $A\beta_{42}$ high-MW oligomers (t = 24 days) binds to the surface more, compared to $A\beta_{42}$ low-MW oligomers (t = 0 days) which, in turn, binds more than $A\beta_{40}$ low-MW oligomers (t = 0 days).

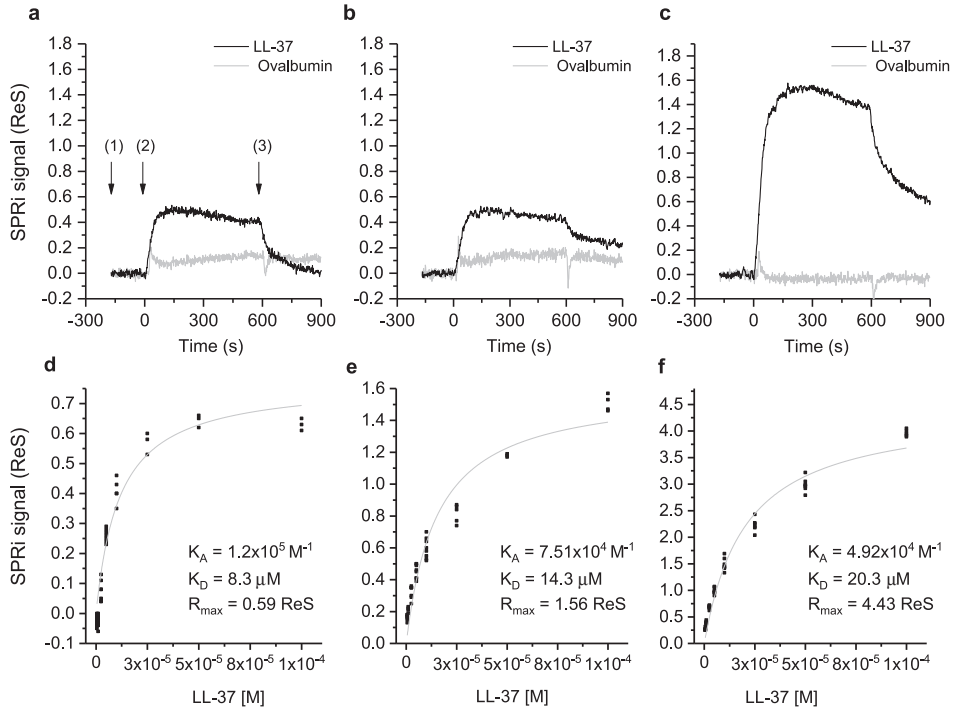

Fig. 2. Binding studies performed by SPRi. The SPRi-chip was functionalized with $A\beta_{40}$ (t = 0 days) (a, d); $A\beta_{42}$ (t = 0 days) (b, e); and $A\beta_{42}$ (*t* = 24 days) (c, f). All the Aβ peptides were immobilized in replicate (*n* = 8) on the same SPRi chip at the same concentration (20 µM). SPRi reference-corrected responses related to LL-37 (10 µM) (black) and ovalbumin (10 µM) (gray) (negative control) flowed on the SPRi-chip functionalized with different Aβ forms (a, b, c). The three SPRi sensograms show the injection of running buffer (baseline) (1), the injection of the analyte (association phase) (2), and the subsequent injection of buffer (dissociation phase) (3). Calibration curve of LL-37 flowed onto different Aβ forms immobilized on the SPRi-chip $A\beta_{40}$ (t = 0 days, d) $A\beta_{42}$ (t = 0 days, e), $A\beta_{42}$ (t = 24 days, f). The equilibrium binding constants (K_A and K_D) values were calculated using a nonlinear curve fit of the SPRi response at equilibrium (see Supplementary Figure 2).

Differences in the immobilized mass could result from the increased MW of the samples in different aggregation states from low to high MW-oligomers [16, 17]. The sensograms taken after flowing a solution of LL-37 onto the SPRi chip for 10 min, revealed specific and reversible interactions with all the three Aβ forms (Fig. 2, top part). The injection of ovalbumin, a non-correlated protein, did not produce interaction signals. Analogously, the amount of LL-37 captured by non-correlated peptides (negative controls), spotted in parallel on the same SPRi chip, was significantly lower compared to that of positive signals. In a follow-up experiment, seven serial dilutions of LL-37, ranging from 1 to 100 µM, were injected to investigate the dependency of the SPR signal on ligand concentration for affinity studies (Supplementary Figure 2). An equilibrium analysis (steady-state analysis) was performed by fitting the SPRi response at the equilibrium state for each concentration (Fig. 2, bottom part). It is noteworthy that the system reached the equilibrium state at each LL-37 concentration and a complete regeneration of the SPRi chip surface was obtained after each injection. As expected, the maximal response value, or maximum binding capacity (R_{max}), which is related to the maximum number of LL-37 peptides that can bind the Aβ peptides at a certain time, decreases in the following order: $A\beta_{42}$ (t = 24 days) $\gg$ $A\beta_{42}$ (t = 0 days) > $A\beta_{40}$ (t = 0 days) (Fig. 2, Table 1). This is in agreement with the amount of Aβ peptide immobilized on the SPRi chip, which increased with Aβ aggregation. To the contrary, as shown in Table 1, the affinity of LL-37 for the different Aβ forms shows the opposite trend, i.e., LL-37 binds to low-MW Aβ oligomers more strongly than to high-MW Aβ oligomers. The binding specificity of LL-37 was verified by performing the same equilibrium analysis with a control scrambled-sequence LL-37. For this experiment, it was difficult to extract adequate calibration curves (see Supplementary Figure 3), mostly due to non-specific and irregular interactions. For this reason, the binding affinities constants could

Table 1
Values of the maximal response (R_{max}), (related to the absolute number of LL-37 molecules bound on the Aβ peptides at a certain time) and equilibrium binding constants ($K_A(1/K_D)$ and K_D), calculated using a nonlinear curve fit of the SPRi response at equilibrium

Peptide	R_{max}	K_A (M^{-1})	K_D (μM)
$A\beta_{40}$ (t = 0 days)	0.59	1.20×10^5	8.3
$A\beta_{42}$ (t = 0 days)	1.56	7.51×10^4	13.3
$A\beta_{42}$ (t = 24 days)	4.43	4.92×10^4	20.3

not be calculated for experiments using scrambled LL-37.

Transmission electron microscopy

An inhibitory effect of LL-37 peptide binding on fibril formation was demonstrated by TEM. For these experiments (see Methods), samples were prepared according to a more aggregating protocol [17], to mimic quasi-physiological conditions and to better verify LL-37 anti-fibrillogenic activity. $A\beta_{42}$ reproducibly forms a dense network of interpenetrating, μm-long, straight, unbranched filaments with a diameter of about 10 nm (Fig. 3a, $n = 3$), corresponding to known features of classic, mature amyloid fibrils [26]. This network of long, straight, interconnected fibrils covered the TEM plate uniformly. On the other hand, LL-37 alone in solution produced globular, amorphous aggregates (Fig. 3b, $n = 3$). To assess the influence of LL-37 on Aβ fibril formation, 50 μM $A\beta_{42}$ was co-incubated with an equimolar amount of LL-37 peptide. Mixtures of $A\beta_{42}$ and LL-37, prepared as described in Methods, were analyzed by TEM, either immediately after solubilization or after 3 or 9 days of incubation. In the equimolar solution of the two peptides at t = 0, shortened, less defined, more sparsely represented fibrils (as compared to Fig. 3a) were observed, in mixture with clumps of amorphous material (Fig. 3c, $n = 2$). These evolved into (as compared to Fig. 3a) sparser clumps of shorter and more curved fibrils at t = 3 days (Fig. 3d, $n = 2$), and then into globular amorphous aggregates at t = 9 days, with no visible fibrils present (Fig. 3e, $n = 2$). As reported in literature, molecules with a similar time-dependent antifibrillogenic effect are considered inhibitors of $A\beta_{42}$ fibril formation [27, 28], thus from these data it can be deduced that LL-37 inhibits $A\beta_{42}$ fibril formation.

Conformational analysis by circular dichroism spectroscopy

Conformational analyses of $A\beta_{42}$ peptide in solution, in the absence and presence of LL-37, were carried out by CD spectroscopy. As in TEM analysis, spectra were recorded immediately after dissolving

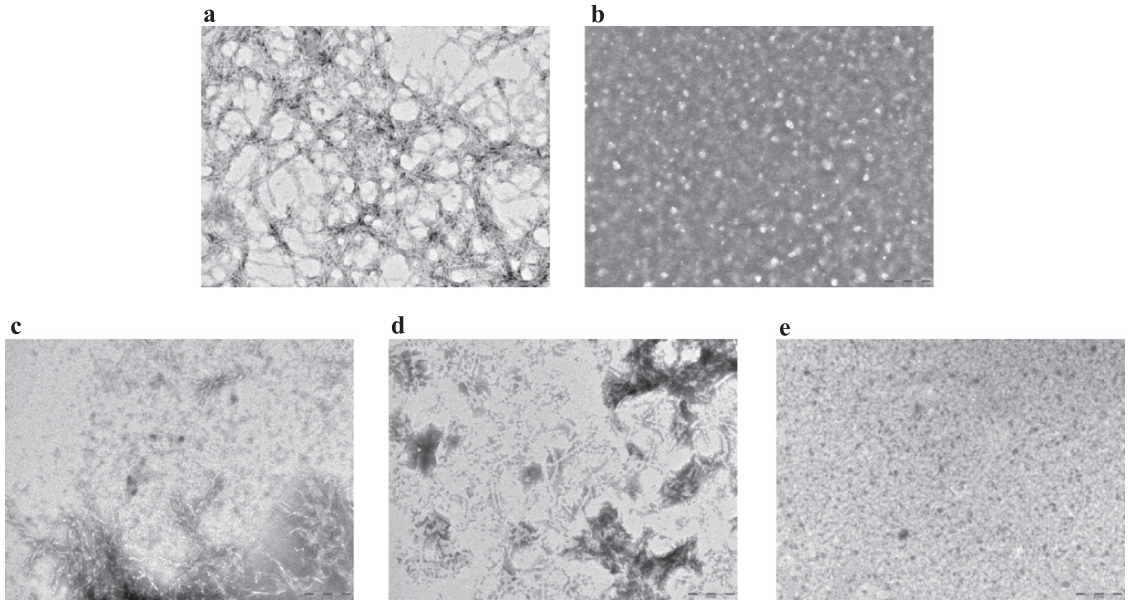

Fig. 3. Transmission electron microscopy images for (a) 50 μM $A\beta_{42}$ at t = 0; (b) 100 μM LL-37 at t = 10 days; (c) equimolar mixtures of 50 μM $A\beta_{42}$ and LL-37 at t = 0; (d) t = 3 days; (e) t = 9 days. Scale bar: 200 nm, magnification 60,000x.

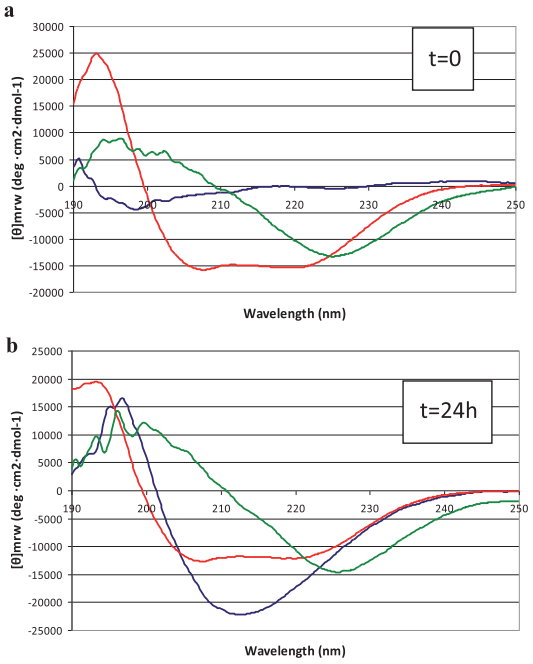

Fig. 4. Circular dichroism spectra of peptide solutions, recorded at (a) t = 0 min and (b) t = 24 hours. Blue line: 50 μM $A\beta_{42}$; red line: 50 μM LL-37; green line: 1:1 mixture.

peptide according to [17] (Fig. 4a) and again after 24 h (Fig. 4b). We found that at t = 0, $A\beta_{42}$ assumed an unordered conformation (Fig. 4a, blue line) whereas over 24 h, adoption of β-type conformations was observed (Fig. 4b, blue line), with a characteristic positive band at 195 nm and negative band at 215 nm. On the other hand, 50 μM LL-37 at t = 0, immediately adopted α-helical conformations and maintained this secondary structure over 24 h (Fig. 4a,b, red lines). Remarkably, in the presence of LL-37, the $A\beta_{42}$ peptide in solution seemed to be prevented, to a large degree, from forming typical β structure (Fig. 4a,b, green lines).

While CD is essentially an "averaging" spectroscopic method, the spectra of 1:1 mixed $A\beta_{42}$ and LL-37 peptides do not show ordered β structure of the type that predominates in pure $A\beta_{42}$ solutions. No time-dependence, within 24 h, of peptide secondary structure was observed in the mixed solutions, in contrast to the behavior of $A\beta_{42}$ solutions. As discussed below, this interaction between the peptides makes sense, considering their opposite charges and mutually high and similar proportions of aromatic and aliphatic amino acids (Fig. 5). We can only conclude, definitively, that, in the presence of LL-37 we do not

LL-37 cathelicidin peptide:
LLGDFFRKSKEKIGKEFKRIVQRIKDFLRNLVPRTES

$A\beta_{42}$ pro-amyloid peptide:
DAEFRHDSGYEVHHQKLVFFAEDVGSNKGAIIGLMVGGVVIA

Blue: positively charged; Red: negatively charged; Purple: aromatic hydrophobic; Green: aliphatic hydrophobic

Fig. 5. Amino acid sequences: human cathelicidin peptide LL-37 (so named because it comprises 37 amino acids) and the human amyloid-β peptide, $A\beta_{42}$.

observe the typical CD spectrum of self-associated $A\beta_{42}$.

Effects of $A\beta_{42}$, LL-37, and $A\beta_{42}$/LL-37 complexes on human microglia, SH-SY5Y neuronal cells, and microglia-mediated cytotoxicity to SH-SY5Y neuronal cells

We studied the effects of $A\beta_{42}$ alone, LL-37 alone, and $A\beta_{42}$/LL-37 complexes on SH-SY5Y neuroblastoma cells, human microglia, and on cytokine release from microglia that impact SH-SY5Y cells. Specifically, we exploited a simplified model that reproduces the cross-talk between the major players involved in neuronal damage by looking at the effect of cell-free supernatant from microglial cell culture, on cultured neuronal cells. Cultured cells were exposed to either $A\beta_{42}$ alone or LL-37 alone (each at 30 μM concentration). After incubation for 72 h, MTT assays were performed and the cell-free medium was collected to measure levels of proinflammatory cytokines TNFα and IL-6. Note, as shown in the control experiments (Supplementary Figure 4), neither Aβ nor LL-37 peptide was toxic to SH-SY5Y cells alone, nor to human microglia alone, at any concentration.

However, we find evidence for microglia-mediated neuroinflammation, for both peptides. Human microglia were exposed to either Aβ alone, LL-37 alone, or an equimolar LL-37/Aβ mixture for 2 days. Then cell-free supernatants from microglia cultures were transferred to differentiated SH-SY5Y cells. SH-SY5Y cell viability was measured after 72 h. We also measured TNFα and IL-6 levels in microglial cell-free supernatants after 2 days' incubation with the peptides. Data are presented in Fig. 6a-c. Treatment of microglia with Aβ or LL-37 induced release of toxic microglial cytokines TNFα and IL-6 (Fig. 6b, c) and resulted in a reduction in SH-SY5Y cell viability (down to 70% after 3 days, Fig. 6a). However, when microglia were exposed to an equimolar Aβ:LL-37 mixture (30 μM each), the

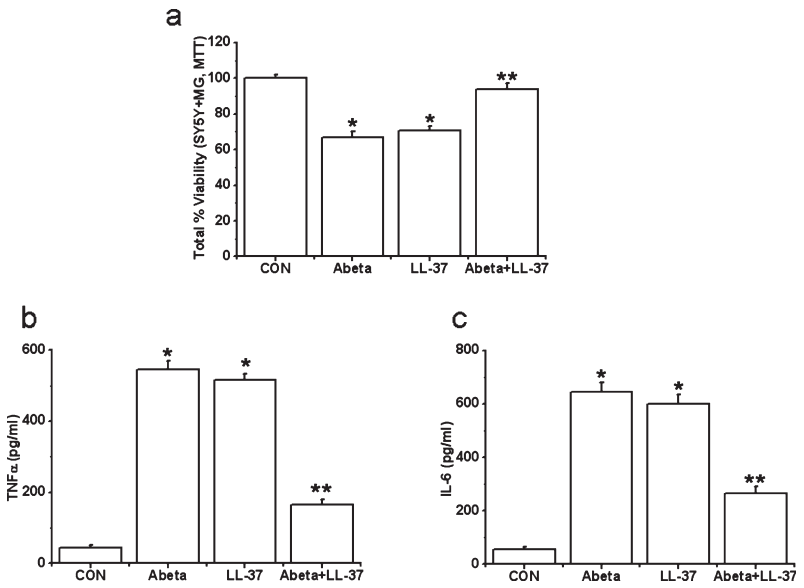

Fig. 6. Effects of treatment with Aβ, LL-37, or their mixture on the viability changes of SH-SY5Y cells induced by microglial-mediated toxicity in 72 h (a) and levels of cytokines, TNFα (b) and IL-6 (c) in microglial toxic supernatant. Values are mean ± SEM, $n = 4$. One-way ANOVA was carried out to test significance. Multiple group comparisons were followed by a *post-hoc* Bonferroni test where necessary. *$p < 0.01$ for Aβ-treated cells and LL-37-exposed cells compared with control (CON) group and **$p < 0.01$ for Aβ-LL-37-treated groups compared with Aβ-treated cells and LL-37-exposed cells. Note that Aβ and LL-37 inhibit the microglial activation of each other.

complexation of these two peptides reduced TNFα and IL-6 release, and attenuated SH-SY5Y cell viability loss by more than 90%, which is a major reduction in the deleterious impacts of either peptide, i.e., their complex is non-toxic.

DISCUSSION

Among the many inhibitors of Aβ aggregation and neurotoxicity that have been identified previously by various assays, or designed, synthesized, and/or selected [5, 6], no naturally occurring peptides that match Aβ in size were ever identified. The cathelicidin LL-37 is a pleiotropic, 37-residue innate immune effector that corresponds to residues 134–170 of the human cationic antimicrobial protein [9]. It is one of a kind in the human proteome and is expressed in many organs, including the brain [9, 29]. It fulfills myriad systemic roles as an immune system effector and modulator [30], links the endocrine and immune systems [31], and plays a central role in Vitamin D3-stimulated monocyte/macrophage autophagy [32].

This study aims at investigating a potential molecular binding interaction between Aβ and LL-37, as a step toward exploring a hypothesis that these two peptides may be natural binding partners. If so, dynamics of the spatiotemporal expression of LL-37 and Aβ could have major significance to human health. While there are myriad well-studied functions of LL-37 as an antimicrobial and antiviral weapon of immune cells [9, 30, 32], the physiological functions of Aβ are not yet fully elucidated [33]. Recently published work suggests that Aβ may itself be an antimicrobial and antiviral peptide [34–36].

Our study was initially inspired by an observation of a strong, apparent complementarity between the peptides' amino acid (aa) sequences (Fig. 5). They are similar in size and molecular weight (Aβ: 39–42 aa, $Aβ_{42}$ is 4493 g/mol; and LL-37:37 aa, 4514 g/mol). $Aβ_{42}$ has a net negative charge of -3 (discounting the charge of histidines), while LL-37 has a positive charge of +6, providing for strong electrostatic attraction. Aβ has four aromatic residues (F or Y) with a binary "FF" motif within the KLVFF sequence known to be necessary for Aβ's assembly [5], while LL-37 has four aromatic residues as well, and comprises the same "FF" motif within residues 4–8 (DFFRK). LL-37 has nine hydrophobic, aliphatic residues (L, V, I) while Aβ has eleven, again making them biophysically similar. And like Aβ, LL-37 associates into homo-oligomers when alone in solution [16, 37, 38], which remain helical in character, unlike Aβ which slowly self-assembles via adoption of

β-type secondary structure when alone in solution. In our prior publication [29], we reported that the human cathelicidin precursor protein hCAP18 and its downstream cleavage product, the peptide LL-37, are both expressed in many organs of the human body, with the highest basic levels of LL-37 being expressed in the GI tract and the brain. Prior to that publication, LL-37's expression and functional role in the human central nerve system had not been reported. Thus, LL-37 is known to be expressed in brain tissue in the human body, as is the Aβ peptide.

SPRi interaction study

The physical interaction and binding specificity between LL-37 and different Aβ forms was demonstrated by SPRi, taking advantage of the simultaneous monitoring of different interactions on the same chip enabled by the imaging configuration of the technique. CCD images and related plasmonic curves (Fig. 2) correlated to the amount of molecules adsorbed on the surface, showed an increasing immobilization density from low-MW oligomers to high-MW oligomers [16, 39]. While SPR measurements revealed higher absolute SPRi signals (R_{max}) for Aβ with oligomeric features, the affinity for LL-37 was higher for the low-MW oligomeric forms present at the early stage of aggregation (i.e., $A\beta_{40}$ (t = 0 days) and $A\beta_{42}$ (t = 0 days)) [16, 24].

Several studies have reported the use of conventional SPR approaches to study Aβ potential interactors. Kai et al. reported the inhibition of Aβ fibril formation by tabersonine and demonstrated the binding between this small molecule and $A\beta_{42}$ monomers and oligomers immobilized on the SPR chip surface [40]. Equilibrium binding studies yield K_D values of 69 and 535 μM for $A\beta_{42}$ monomers and oligomers, respectively. In a similar study, Barr et al. verified the inhibition of Aβ fibril formation by a 15-amino acid peptide [41]. SPR surfaces functionalized with monomeric, oligomeric, and fibrillar $A\beta_{42}$ revealed a stronger affinity of the polypeptide toward the fibrillar form, although only a K_D value of 11 μM was measured by injecting $A\beta_{42}$ onto immobilized peptides and no affinity constant was given. Here we found kinetic constants in the range between 8 to 20 μM, similar to what is published for other Aβ fibrils inhibitors, as noted above. On the other hand, as mentioned earlier (and differently to what was previously shown) [40, 41], LL-37 shows higher affinity for low-MW Aβ oligomers. This strongly supports the ability of LL-37 to inhibit fibril formation by shifting the equilibrium toward smaller species of Aβ, according to the fibrillization mechanisms proposed by Cohen et al. [42] and previously studied in our laboratories [25, 39].

Effects of LL-37 and Aβ on cytotoxicity and inflammatory cytokine release

The results of the MTT assays showed that $A\beta_{42}$ and LL-37 both induced microglial-mediated toxicity to SH-SY5Y cells. At the same time, the results of quantitative ELISA assays on IL-6 and TNFα showed that the levels of these proinflammatory markers released from microglia were markedly elevated compared with that of the untreated control group, when each peptide was added alone. However, the effects of each peptide on cell viability and inflammatory marker production were largely mitigated when the two peptides were co-incubated prior to being added to the culture medium. These data support the hypothesis that $A\beta_{42}$ interacts with LL-37 as seen by the considerable attenuation of the toxicity of the peptides when they are in complexation.

Certain aspects of our results are not surprising, as previously we have shown that microglia, upon stimulation by LL-37, release pro-inflammatory factors that are toxic to human neurons [29]. Similarly, Aβ has been shown to activate microglia to produce neurotoxic factors [43]. However, an attenuation of the release of pro-inflammatory factors (IL-6 and TNFα) upon treatment of microglia with equimolar LL-37 and Aβ peptide mixtures is a novel finding, which lends support to a new hypothesis that these two peptides may be natural binding partners, which perhaps the body seeks to maintain in balance over the longer term (after an acute innate immune response). Unlike either peptide alone, which causes human microglia to release pro-inflammatory and neurotoxic cytokines, the complex of the two peptides lacks that neurotoxic effect.

Correlation of biophysical activities of Aβ-peptides and LL-37

No one has yet established a correlation between cathelicidin expression levels and AD. However, in addition to those mentioned in the introduction, other literature reports suggest that the biophysical activities and signaling functions of Aβ peptides and LL-37 are related *in vivo*. For instance, the Formyl-like Peptide Receptor 1 (FPRL1) is activated by both Aβ [44] and LL-37 [45]. This receptor is reportedly involved

in inflammatory aspects of AD [46] *via* its effects on phagocyte responses [47]; and a decreased phagocyte clearance of central nervous system Aβ is a hallmark of AD [48]. As mentioned above, LL-37 itself is involved in monocyte and macrophage autophagy; its expression, stimulated by vitamin D3 [10], engenders enhanced autophagy [32]. Thus, a dearth of LL-37 generally would reduce phagocytic activity. Phenylbutyrate and vitamin D3 have both been shown to be neuroprotective in AD mouse models [7, 49], and these same two compounds are known cathelicidin inducers [50]. Finally, there is mounting evidence that innate immunity plays a larger role in AD than previously thought, and that Aβ's normal function may be as an antimicrobial and antiviral peptide [34, 36, 51]. Kumar et al. showed that Aβ expression protects against fungal and bacterial infections in mouse, nematode, and cell culture models of AD [35]. And, part of the body's natural response to infection is, of course, to upregulate cathelicidin [9].

Conclusions

This work demonstrates that these two peptides, the cathelicidin peptide LL-37 and Aβ, both ubiquitous in human tissues, interact *in vitro* with each other in different aggregation states, with affinity constants typical of protein-protein interactions and close to values reported in the literature for the binding of Aβ with optimized synthetic peptides. The addition of LL-37 to $A\beta_{42}$, in a buffer that mimics quasi-physiological conditions, strongly inhibits fibril formation. The protective effect of LL-37's presence against microglia-mediated $A\beta_{42}$ toxicity to SH-SY5Y neuroblastoma cells is an important new finding, revealing that in combination the two peptides are 90% less pro-inflammatory than either peptide alone. Literature reports suggest that numerous biophysical activities and signaling functions of Aβ peptides and LL-37 are related *in vivo*. The *in vitro* data presented here constitute a starting point from which to investigate whether factors that affect cathelicidin gene CAMP regulation, which will in turn control the production of LL-37 *in vivo*, modulate Aβ aggregation and/or microglia-induced neuroinflammation.

DISCLOSURE STATEMENT

Authors' disclosures available online (http://j-alz.com/manuscript-disclosures/17-0223r1).

SUPPLEMENTARY MATERIAL

The supplementary material is available in the electronic version of this article: http://dx.doi.org/10.3233/JAD-170223.

REFERENCES

[1] Huang Y, Mucke L (2012) Alzheimer mechanisms and therapeutic strategies. *Cell* **148**, 1204-1222.
[2] Goedert M (2015) Neurodegeneration. Alzheimer's and Parkinson's diseases: The prion concept in relation to assembled Abeta, tau, and alpha-synuclein. *Science* **349**, 1255555.
[3] Soejitno A, Tjan A, Purwata TE (2015) Alzheimer's disease: Lessons learned from amyloidocentric clinical trials. *CNS Drugs* **29**, 487-502.
[4] Andrieu S, Coley N, Lovestone S, Aisen PS, Vellas B (2015) Prevention of sporadic Alzheimer's disease: Lessons learned from clinical trials and future directions. *Lancet Neurol* **14**, 926-944.
[5] Stains CI, Mondal K, Ghosh I (2007) Molecules that target beta-amyloid. *Chem Med Chem* **2**, 1674-1692.
[6] Cohen SI, Arosio P, Presto J, Kurudenkandy FR, Biverstal H, Dolfe L, Dunning C, Yang X, Frohm B, Vendruscolo M, Johansson J, Dobson CM, Fisahn A, Knowles TP, Linse S (2015) A molecular chaperone breaks the catalytic cycle that generates toxic Abeta oligomers. *Nat Struct Mol Biol* **22**, 207-213.
[7] Durk MR, Han K, Chow EC, Ahrens R, Henderson JT, Fraser PE, Pang KS (2014) 1alpha,25-Dihydroxyvitamin D3 reduces cerebral amyloid-beta accumulation and improves cognition in mouse models of Alzheimer's disease. *J Neurosci* **34**, 7091-7101.
[8] Mariani MM, Malm T, Lamb R, Jay TR, Neilson L, Casali B, Medarametla L, Landreth GE (2017) Neuronally-directed effects of RXR activation in a mouse model of Alzheimer's disease. *Sci Rep* **7**, 42270.
[9] Burton MF, Steel PG (2009) The chemistry and biology of LL-37. *Nat Prod Rep* **26**, 1572-1584.
[10] Gombart AF, Borregaard N, Koeffler HP (2005) Human cathelicidin antimicrobial peptide (CAMP) gene is a direct target of the vitamin D receptor and is strongly up-regulated in myeloid cells by 1,25-dihydroxyvitamin D3. *FASEB J* **19**, 1067-1077.
[11] Cederlund A, Nylen F, Miraglia E, Bergman P, Gudmundsson GH, Agerberth B (2014) Label-free quantitative mass spectrometry reveals novel pathways involved in LL-37 expression. *J Innate Immun* **6**, 365-376.
[12] de la Monte SM (2014) Type 3 diabetes is sporadic Alzheimers disease: Mini-review. *Eur Neuropsychopharmacol* **24**, 1954-1960.
[13] de la Monte SM, Wands JR (2008) Alzheimer's disease is type 3 diabetes-evidence reviewed. *J Diabetes Sci Technol* **2**, 1101-1113.
[14] Sun J, Furio L, Mecheri R, van der Does AM, Lundeberg E, Saveanu L, Chen Y, van Endert P, Agerberth B, Diana J (2015) Pancreatic beta-cells limit autoimmune diabetes via an immunoregulatory antimicrobial peptide expressed under the influence of the gut microbiota. *Immunity* **43**, 304-317.
[15] Scarano S, Mascini M, Turner AP, Minunni M (2010) Surface plasmon resonance imaging for affinity-based biosensors. *Biosens Bioelectron* **25**, 957-966.

[16] Bartolini M, Naldi M, Fiori J, Valle F, Biscarini F, Nicolau DV, Andrisano V (2011) Kinetic characterization of amyloid-beta 1-42 aggregation with a multimethodological approach. *Anal Biochem* **414**, 215-225.

[17] Brogi S, Butini S, Maramai S, Colombo R, Verga L, Lanni C, De Lorenzi E, Lamponi S, Andreassi M, Bartolini M, Andrisano V, Novellino E, Campiani G, Brindisi M, Gemma S (2014) Disease-modifying anti-Alzheimer's drugs: Inhibitors of human cholinesterases interfering with beta-amyloid aggregation. *CNS Neurosci Ther* **20**, 624-632.

[18] Stathopulos PB, Scholz GA, Hwang YM, Rumfeldt JA, Lepock JR, Meiering EM (2004) Sonication of proteins causes formation of aggregates that resemble amyloid. *Protein Sci* **13**, 3017-3027.

[19] Lee M, Cho T, Jantaratnotai N, Wang YT, McGeer E, McGeer PL (2010) Depletion of GSH in glial cells induces neurotoxicity: Relevance to aging and degenerative neurological diseases. *FASEB J* **24**, 2533-2545.

[20] Singh US, Pan J, Kao YL, Joshi S, Young KL, Baker KM (2003) Tissue transglutaminase mediates activation of RhoA and MAP kinase pathways during retinoic acid-induced neuronal differentiation of SH-SY5Y cells. *J Biol Chem* **278**, 391-399.

[21] Lee M, McGeer E, McGeer PL (2013) Neurotoxins released from interferon-gamma-stimulated human astrocytes. *Neuroscience* **229**, 164-175.

[22] Lee M, Kang Y, Suk K, Schwab C, Yu S, McGeer PL (2011) Acidic fibroblast growth factor (FGF) potentiates glial-mediated neurotoxicity by activating FGFR2 IIIb protein. *J Biol Chem* **286**, 41230-41245.

[23] Cretich M, Bagnati M, Damin F, Sola L, Chiari M (2011) Overcoming mass transport limitations to achieve femtomolar detection limits on silicon protein microarrays. *Anal Biochem* **418**, 164-166.

[24] Sabella S, Quaglia M, Lanni C, Racchi M, Govoni S, Caccialanza G, Calligaro A, Bellotti V, De Lorenzi E (2004) Capillary electrophoresis studies on the aggregation process of beta-amyloid 1-42 and 1-40 peptides. *Electrophoresis* **25**, 3186-3194.

[25] Colombo R, Carotti A, Catto M, Racchi M, Lanni C, Verga L, Caccialanza G, De Lorenzi E (2009) CE can identify small molecules that selectively target soluble oligomers of amyloid beta protein and display antifibrillogenic activity. *Electrophoresis* **30**, 1418-1429.

[26] Merlini G, Bellotti V (2003) Molecular mechanisms of amyloidosis. *N Engl J Med* **349**, 583-596.

[27] Kokkoni N, Stott K, Amijee H, Mason JM, Doig AJ (2006) N-Methylated peptide inhibitors of beta-amyloid aggregation and toxicity. Optimization of the inhibitor structure. *Biochemistry* **45**, 9906-9918.

[28] Kroth H, Ansaloni A, Varisco Y, Jan A, Sreenivasachary N, Rezaei-Ghaleh N, Giriens V, Lohmann S, Lopez-Deber MP, Adolfsson O, Pihlgren M, Paganetti P, Froestl W, Nagel-Steger L, Willbold D, Schrader T, Zweckstetter M, Pfeifer A, Lashuel HA, Muhs A (2012) Discovery and structure activity relationship of small molecule inhibitors of toxic beta-amyloid-42 fibril formation. *J Biol Chem* **287**, 34786-34800.

[29] Lee M, Shi X, Barron AE, McGeer E, McGeer PL (2015) Human antimicrobial peptide LL-37 induces glial-mediated neuroinflammation. *Biochem Pharmacol* **94**, 130-141.

[30] Mookherjee N, Hamill P, Gardy J, Blimkie D, Falsafi R, Chikatamarla A, Arenillas DJ, Doria S, Kollmann TR, Hancock RE (2009) Systems biology evaluation of immune responses induced by human host defence peptide LL-37 in mononuclear cells. *Mol Biosyst* **5**, 483-496.

[31] Mayer ML, Hancock RE (2010) Cathelicidins link the endocrine and immune systems. *Cell Host Microbe* **7**, 257-259.

[32] Yuk JM, Shin DM, Lee HM, Yang CS, Jin HS, Kim KK, Lee ZW, Lee SH, Kim JM, Jo EK (2009) Vitamin D3 induces autophagy in human monocytes/macrophages via cathelicidin. *Cell Host Microbe* **6**, 231-243.

[33] Pearson HA, Peers C (2006) Physiological roles for amyloid beta peptides. *J Physiol* **575**, 5-10.

[34] Soscia SJ, Kirby JE, Washicosky KJ, Tucker SM, Ingelsson M, Hyman B, Burton MA, Goldstein LE, Duong S, Tanzi RE, Moir RD (2010) The Alzheimer's disease-associated amyloid beta-protein is an antimicrobial peptide. *PLoS One* **5**, e9505.

[35] Kumar DK, Choi SH, Washicosky KJ, Eimer WA, Tucker S, Ghofrani J, Lefkowitz A, McColl G, Goldstein LE, Tanzi RE, Moir RD (2016) Amyloid-beta peptide protects against microbial infection in mouse and worm models of Alzheimer's disease. *Sci Transl Med* **8**, 340ra372.

[36] Bourgade K, Garneau H, Giroux G, Le Page AY, Bocti C, Dupuis G, Frost EH, Fulop T Jr (2015) beta-Amyloid peptides display protective activity against the human Alzheimer's disease-associated herpes simplex virus-1. *Biogerontology* **16**, 85-98.

[37] Oren Z, Lerman JC, Gudmundsson GH, Agerberth B, Shai Y (1999) Structure and organization of the human antimicrobial peptide LL-37 in phospholipid membranes: Relevance to the molecular basis for its non-cell-selective activity. *Biochem J* **341**(Pt 3), 501-513.

[38] Xhindoli D, Morgera F, Zinth U, Rizzo R, Pacor S, Tossi A (2015) New aspects of the structure and mode of action of the human cathelicidin LL-37 revealed by the intrinsic probe p-cyanophenylalanine. *Biochem J* **465**, 443-457.

[39] Butini S, Brindisi M, Brogi S, Maramai S, Guarino E, Panico A, Saxena A, Chauhan V, Colombo R, Verga L, De Lorenzi E, Bartolini M, Andrisano V, Novellino E, Campiani G, Gemma S (2013) Multifunctional cholinesterase and amyloid Beta fibrillization modulators. Synthesis and biological investigation. *ACS Med Chem Lett* **4**, 1178-1182.

[40] Kai T, Zhang L, Wang X, Jing A, Zhao B, Yu X, Zheng J, Zhou F (2015) Tabersonine inhibits amyloid fibril formation and cytotoxicity of Abeta(1-42). *ACS Chem Neurosci* **6**, 879-888.

[41] Barr RK, Verdile G, Wijaya LK, Morici M, Taddei K, Gupta VB, Pedrini S, Jin L, Nicolazzo JA, Knock E, Fraser PE, Martins RN (2016) Validation and characterization of a novel peptide that binds monomeric and aggregated beta-amyloid and inhibits the formation of neurotoxic oligomers. *J Biol Chem* **291**, 547-559.

[42] Cohen SI, Linse S, Luheshi LM, Hellstrand E, White DA, Rajah L, Otzen DE, Vendruscolo M, Dobson CM, Knowles TP (2013) Proliferation of amyloid-beta42 aggregates occurs through a secondary nucleation mechanism. *Proc Natl Acad Sci U S A* **110**, 9758-9763.

[43] Block ML, Zecca L, Hong JS (2007) Microglia-mediated neurotoxicity: Uncovering the molecular mechanisms. *Nat Rev Neurosci* **8**, 57-69.

[44] Le Y, Gong W, Tiffany HL, Tumanov A, Nedospasov S, Shen W, Dunlop NM, Gao JL, Murphy PM, Oppenheim JJ, Wang JM (2001) Amyloid (beta)42 activates a G-protein-coupled chemoattractant receptor, FPR-like-1. *J Neurosci* **21**, RC123.

[45] Yang D, Chen Q, Schmidt AP, Anderson GM, Wang JM, Wooters J, Oppenheim JJ, Chertov O (2000) LL-37, the neutrophil granule- and epithelial cell-derived cathelicidin, utilizes formyl peptide receptor-like 1 (FPRL1) as a receptor to chemoattract human peripheral blood neutrophils, monocytes, and T cells. *J Exp Med* **192**, 1069-1074.

[46] Cui Y, Le Y, Yazawa H, Gong W, Wang JM (2002) Potential role of the formyl peptide receptor-like 1 (FPRL1) in inflammatory aspects of Alzheimer's disease. *J Leukoc Biol* **72**, 628-635.

[47] Iribarren P, Zhou Y, Hu J, Le Y, Wang JM (2005) Role of formyl peptide receptor-like 1 (FPRL1/FPR2) in mononuclear phagocyte responses in Alzheimer disease. *Immunol Res* **31**, 165-176.

[48] Mawuenyega KG, Sigurdson W, Ovod V, Munsell L, Kasten T, Morris JC, Yarasheski KE, Bateman RJ (2010) Decreased clearance of CNS beta-amyloid in Alzheimer's disease. *Science* **330**, 1774.

[49] Cuadrado-Tejedor M, Ricobaraza AL, Torrijo R, Franco R, Garcia-Osta A (2013) Phenylbutyrate is a multifaceted drug that exerts neuroprotective effects and reverses the Alzheimer's disease-like phenotype of a commonly used mouse model. *Curr Pharm Des* **19**, 5076-5084.

[50] Steinmann J, Halldorsson S, Agerberth B, Gudmundsson GH (2009) Phenylbutyrate induces antimicrobial peptide expression. *Antimicrob Agents Chemother* **53**, 5127-5133.

[51] Vijaya Kumar DK, Moir RD (2017) The emerging role of innate immunity in Alzheimer's disease. *Neuropsychopharmacology* **42**, 362.

Evidence that the human innate immune peptide LL-37 may be a binding partner of Aβ and inhibitor of fibril assembly: SUPPORTING INFORMATION

a (plasmonic curve)

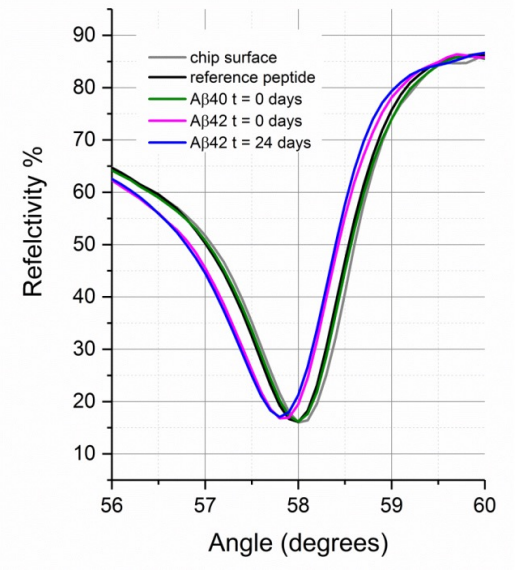

b (CCD image)

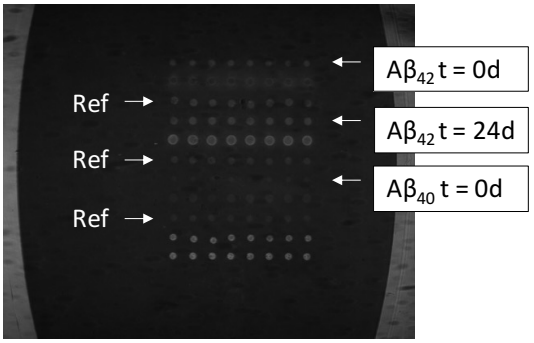

Figure Supp. 1: a) Plasmonic curves acquired before the injection of LL-37 peptide. The shift between these curves is related to the amount of molecules immobilized on the SPRi chip surface. In particular, the plasmonic curves related to both $A\beta_{40}$ (t = 0 days) and $A\beta_{42}$ (t = 24 days) show a significant shift from that related to $A\beta_{40}$ solubilized in PBS (t = 0) and from that of the reference peptide (negative) and to the chip (no molecules adsorbed); b) CCD image of the chip surface, the size of spots measured directly by this type of images was around 190 µm. The spots used in this study are described in the figure.

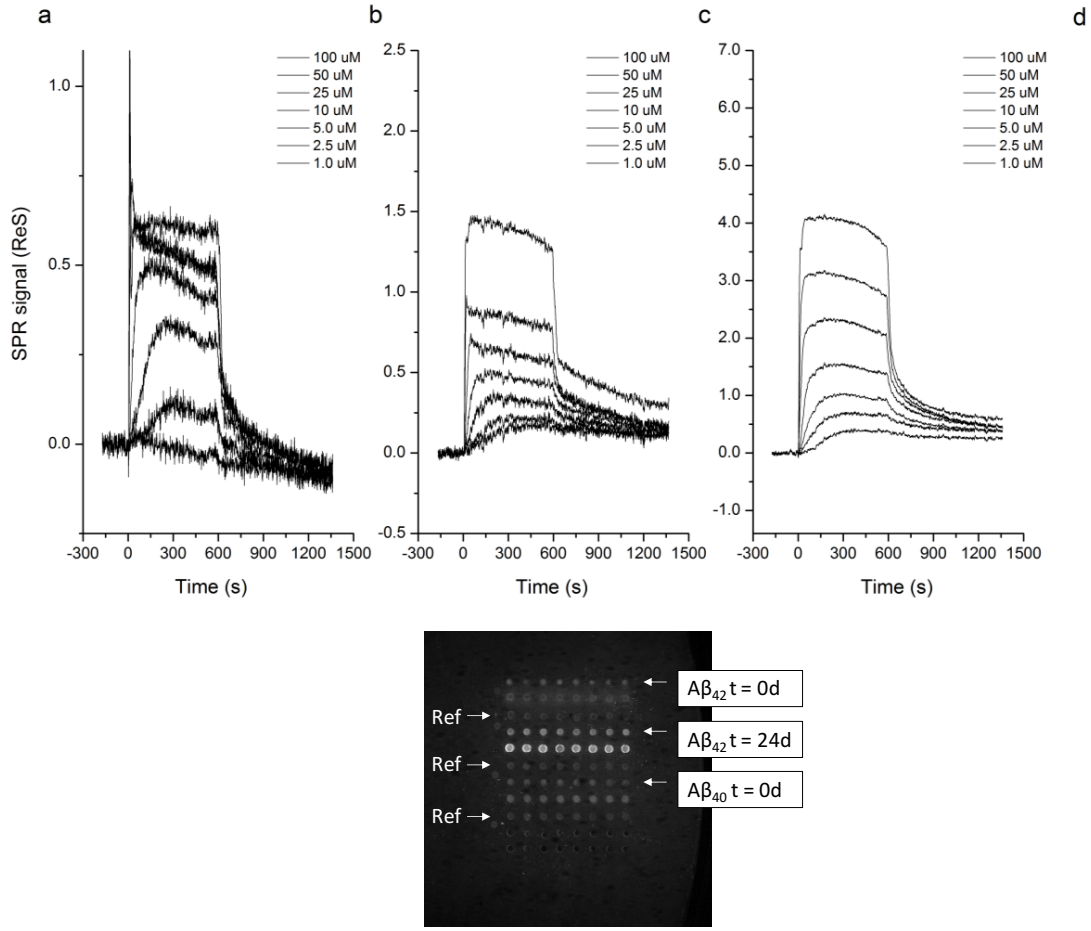

Figure Supp. 2: Reference-corrected responses related to seven dilutions of LL-37 injected on the SPRi-chip functionalized with **a**) Aβ(1–40) solubilized in PBS; **b**) Aβ(1–42) t = 0 days and **c**) Aβ(1–42) t = 24 days, used to calculate the equilibrium binding constants (K_D) in Figure 2. All the responses reached the equilibrium (plateau) before the end of the injection (500 s); **d**) CCD differential image of the SPRi-biochip during the late association phase (500 s) of LL-37 injected at concentration 25 μM. "Ref" is the reference peptide used as negative control on the chip surface.

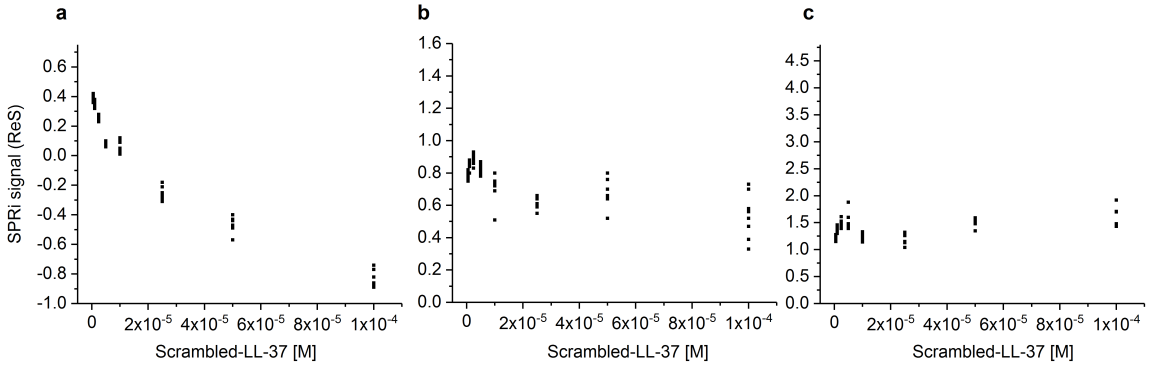

Figure Supp. 3: Equilibrium-binding analysis of the control scrambled LL-37 peptide, performed by surface plasmon resonance imaging (SPRi) using the same procedures and conditions used to study LL-37 (compare with Fig.2, bottom). The SPRi-chip was functionalized with Aβ40 (t = 0 days) (**a**); Aβ42 (t = 0 days) (**b**) and Aβ42 (t = 24 days) (**c**). The equilibrium binding constants and the fitting curves could not be calculated, due to the irregular and negative dose-response trend.

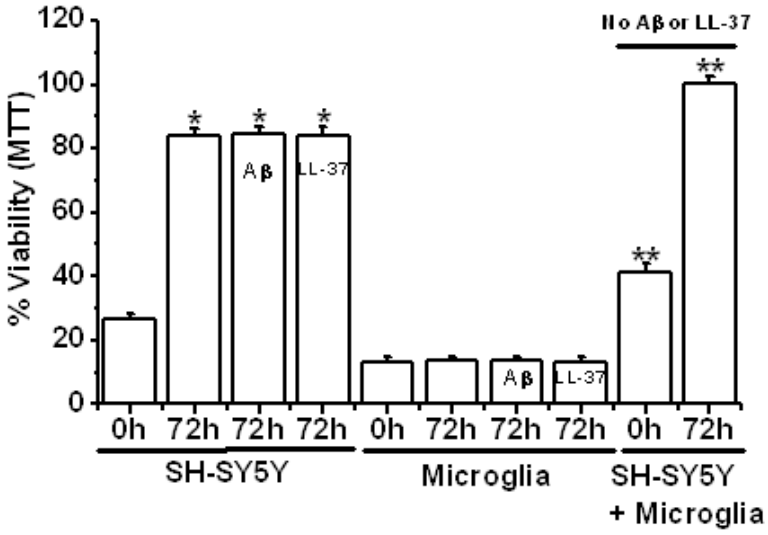

Figure Supp. 4: A) SH-SY5Y, Microglia and SH-SY5Y/Microglia viability changes induced by Aβ peptide and LL-37 peptide (30 μM each). Reductions in numbers of live cells are indicated by the MTT assay. Values are mean±SEM, n=4. One-way ANOVA was carried out to test significance. Multiple group comparisons were followed by a post-hoc Bonferroni test where necessary. * $P<0.01$ for cells in 72 h compared with the ones in 0 h and ** $P<0.01$ for SH-SY5Y plus microglia without Aβ or LL-37 peptides group compared with SH-SY5Y cells or microglial cells in the same incubation time. Note that the cell viability of SH-SY5Y and microglia co-culture is nearly equal to the sum of two cell culture group in 72 h, and that treatment with Aβ or LL-37 did not change viability of either cell type over the course of 72 h.

Conclusions and perspectives

The peculiar nature of Aß peptides and their high aggregation tendency makes it difficult the assessment of which particular oligomeric populations represent the main neurotoxic mediators in AD. This contributes to the lack of effective disease-modifying treatments for the disease.

In this Ph.D thesis, it is shown how a micro-separative technique like CE can play an alternative and unique role in the *in vitro* aggregation studies of Aß oligomers and consequently in the testing of molecules active on the amyloidogenic process.

The analytical platform developed has been successfully applied to overcome one of the most important challenges in Aß aggregation studies: the univocal identification and characterization of different Aß aggregates. Indeed, the evaluation of potential modulators of the amyloid process can be considered reliable only if it is based on standardized preparation procedures and analytical methods, as well as if it is based on as much information as possible on the oligomers obtained.

Based on the literature, Aß42 solutions are difficult to handle and prepare. This is mainly due to the high aggregation tendency and to the high variability of synthetic peptides. Nevertheless in this work, the analytical separation and identification of different Aß42 oligomeric populations have been achieved in a highly reproducible manner. As an added value, the electrophoretic pattern of Aß42 samples can be also exploited to identify potential differences in the peptide aggregation, due to lot-to-lot or suppler-to-supplier variability of the Aß42 powder.

In order to obtain as many oligomeric populations as possible, Aß42 was prepared by following different solubilisation protocols, as described in Chapter I. In the conditions applied, it has been found that solvents used for the preparation can modulate the aggregation process in terms of timing and of size of the oligomers obtained. By monitoring over time the aggregation process of oligomers we found that for the most aggregating process, small oligomers (trimers-decamers) contribute to the formation of large aggregates already at early times from solubilization. Conversely, with the less aggregating procedures, the process is slower and oligomers are kept in solution for about one month. To our knowledge no reports declare the presence of characterized soluble oligomers after such a long period of time. This is extremely important since to study the effect of molecules a wide time window in which oligomers are soluble and at dynamic equilibrium should be ensured, before precipitation into amyloid fibrils.

The small oligomers obtained by the protocols explored slightly differ in the electrophoretic profiles. Based on the UF investigations, this mirrors a

difference in MW of assemblies. Indeed, with the less aggregating protocol the smallest species formed are monomers and dimers. On the other hand, the peak relative to large oligomers corresponds to aggregates bigger than decamers.

The possibility to physically separate by UF aggregates of different MW has important implications in the toxicity assessment, in structural investigations as well as in the evaluation of the effect of compounds on the aggregation process.
Indeed, to our knowledge, for the first time ATR-FTIR investigations were performed on separated oligomers: the differences found in secondary structure are in agreement with the different oligomeric size distribution of small and large aggregates. Further, neuroblastoma cell toxicity studies carried out on filtrated and retained oligomeric solutions revealed that only the large oligomers result to be neurotoxic. Therefore, aggregates bigger then decamers represent important targets for potential inhibitors of the amyloidogenic process.
The standardization of the analytical platform is mandatory for coincubation studies. In this contex, the analytical tool has been applied to evaluate the potential anti-amyloidogenic activity of modulators. In particular with the intent to hit the aggregation process from different fronts, two different categories of inhibitors have been taken into account: small molecules and an endogenous peptide.

For small compounds, the starting point was curcumin. The strategy applied was to modify curcumin structure, to enhance properties of interest, to reduce or abrogate those associated to its limitations. Moreover, in order to modulate the antiaggregation properties of curcumin its pharmacophore has been dissected and rationally modified. In this way, a very promising curcumin-based analogue (Cur6) also endowed with anti-inflammatory activity has been identified. This compound hinders the formation of large toxic oligomers by shifting the equilibrium towards smaller species, in particular it stabilizes dimers alike what was reported for curcumin. Cur 6 resulted to have an antioligomeric activity higher than that of curcumin. Interestingly, Cur6 inhibits the formation of amyloid fibrils also in *in vivo* investigations. We hypothesized that the substitution of one 4-hydroxy-3-methoxy group (related to the activity of curcumin) with a prenyloxy functional group may have a positive effect on the modulation of antiamyloidogenic properties of the compound: the prenyloxy function may enhance the feature of ß-sheet breaker described for the curcumin scaffold. These considerations support the feasibility of SAR studies starting from a molecule of natural origin.

The analytical platform developed allows the discrimination of the effect on soluble toxic oligomers from the effect on the amyloid fibrils. Since oligomers and fibrils can be formed through different pathways, such as on-pathway or

off-pathway, to define an amyloidogenic modulator it is necessary to involve a multimethodological approach. Following this rationale, it is demonstrated that a compound without antifibrillogenic properties, was able to inhibit the formation of toxic soluble oligomers. This platform could be successfully applied to re-evaluate and to rescue molecules discarded during the search of amyloid inhibitors at the preliminary phase, when tests specific for fibrils only, such as ThT fluorescence assay, are commonly carried out.

The search of natural binders of Aß peptides has relied on the premises that alterations in the expression of these biomolecules can play a key role in the onset and progression of AD. We identified a novel natural binding partner of Aß40 and Aß42. It is an endogenous peptide named LL37 which is expressed in the brain and it is involved in the homeostasis of Aß peptides by way of a fine co-regulation of several molecular pathways. LL37 has a high affinity for the small oligomers identified by CE and it inhibits the formation of amyloid fibrils.
To date, no information has been produced on the potential antioligomeric activity of this peptide in coincubation with Aß. Therefore, CE analyses can be carried out also to verify these properties.

For both the interesting modulators identified by the analytical platform, namely Cur6 and LL-37, molecular docking and molecular dynamic simulation studies may prove useful to unveil the molecular interactions between the compound (or the biomolecule) and Aß peptides.
Finally, the promising albeit very preliminary results obtained on an animal model alternative to classical animal models such as AD-mutated *C. elegans*, open an avenue in a field which to date is still fairly unexplored. Type and set up of experiments to be carried out, number of data to be acquired, adequate statistical elaboration are still an issue and this prompts us to investigate further in this direction.

Acknowledgements

First I would like to thank my supervisor Professor Ersilia De Lorenzi for being a willing tutor always open to dialogue. You taught me so much, you gave me your intellectual rigor and you supported me even when "I was in a black hole".

My warm thanks for help with the experimental work and fruitful discussion and are due to:

Prof. Cristina Lanni and collaborators (University of Pavia) and Dr. Morena Zusso (University of Padua) for the studies on neuroblastoma and microglia cells;

Dr. Laura Verga (Policlinico San Matteo) for the TEM analyses;

Dr. Sofia Giorgetti and collaborators (University of Pavia) for the studies on C. elegans;

Dr. Marcella Chiari and co-workers (CNR Milan) and Dr. Renzo Vanna and Dr. Carlo Morasso (Don Gnocchi Foundation) for SPRimaging studies;

Prof. Annelise Barron (Standford University) and Prof. McGeer (University of British Columbia) and collaborators for the studies on LL37;

Dr. Antonino Natalello (University of Milano Bicocca) for ATR-FTIR experiments;

Dr. Federica Belluti and Prof. Michela Rosini (University of Bologna) for providing the compounds belonging to SET1 and SET2.